Analytical Configuration of Wheeled Robotic Locomotion

Article · June 2001
Source: CiteSeer

1 author:

Dimitrios Apostolopoulos
Carnegie Mellon University
44 PUBLICATIONS   **615** CITATIONS

Some of the authors of this publication are also working on these related projects:

Project   Broad-impact topic View project

Project   Inflatable Robotic Rovers View project

Analytical Configuration
of Wheeled Robotic Locomotion

Dimitrios S. Apostolopoulos

CMU-RI-TR-01-08

Submitted in partial fulfillment of the
Requirements for the degree of
Doctor of Philosophy in Robotics

The Robotics Institute
Carnegie Mellon University
Pittsburgh, Pennsylvania 15213

April 2001

Abstract

Through their ability to navigate and perform tasks in unstructured environments, robots have made their way into applications like farming, earth moving, waste clean-up and exploration. All mobile robots use locomotion that generates traction, negotiates terrain and carries payload. Well-designed robotic locomotion also stabilizes a robot's frame, smooths the motion of sensors and accommodates the deployment and manipulation of work tools. Because locomotion is the physical interface between a robot and its environment, it is the means by which it reacts to gravitational, inertial and work loads. Locomotion is the literal basis of a mobile robot's performance.

Despite its significance, locomotion design and its implications to robotic function have not been addressed. In fact, with the exception of a handful of case studies, the issue of *how to synthesize robotic locomotion configurations* remains a topic of ad hoc speculation and is commonly pursued in a way that lacks rationalization. This thesis focuses on the configuration of wheeled robotic locomotion through the formulation and systematic evaluation of analytical expressions called *configuration equations*. These are mathematical functions which capture quantitative relationships among *configuration parameters* (e.g., wheel diameter, chassis articulation location), *performance parameters* (e.g. drawbar pull, maximum gradeable slope) and *environmental/task parameters* (e.g. soil geophysical properties, density and size of obstacles). Solutions to the configuration equations are obtained in parametric form to allow for comprehensive characterization of variant locomotion concepts as opposed to searching for point designs. Optimal configuration parameters are sought in the context of three indices of performance: *trafficability*, *maneuverability* and *terrainability*.

The derivation of configuration equations, the estimation and optimization of configuration parameters and predictions of performance are performed in a computational framework called Locomotion Synthesis (LocSyn). LocSyn offers a practical approach to rationalizing configuration design of robotic locomotion through quantitative studies.

The configuration of Nomad, a planetary prototype robot for exploration of barren terrain is a case illustrating the implementation and evaluation of the Locomotion Synthesis (LocSyn) framework put forth by this thesis.

Acknowledgments

A number of great people have contributed to this thesis work. First and foremost, the work presented here is founded in the guidance of Red Whittaker. Your ground breaking vision and uncompromising commitment to pushing the frontiers of robotics has made this and many other great things possible.

I wish to thank John Bares, Kenneth Waldron and Eric Krotkov for serving on my thesis committee. Your insights and advice have been invaluable.

I also wish to express my appreciation to all my teammates on the Atacama Desert Trek and Robotic Search for Antarctic Meteorite projects. Your thoughts on robotic locomotion, technical contributions and most of all friendships are truly appreciated. I will never forget the great times we have spent together over the past few years. I would especially like to thank Benjamin Shamah, Michael Wagner and David Wettergreen for their utterly invaluable support in our endeavors and in the completion of this dissertation.

Dedicated to the memory of my beloved grandmother Lilika Soulioti.

TABLE OF CONTENTS

Chapter 1

INTRODUCTION

Through their ability to navigate and perform tasks in unstructured environments, robots have made their way into applications like farming, earth moving, waste clean-up and exploration. All mobile robots use locomotion that generates traction, negotiates terrain and carries payload. Well-designed robotic locomotion also stabilizes a robot's frame, smooths the motion of sensors and accommodates the deployment and manipulation of worktools. Because locomotion is the physical interface between a robot and its environment, it is the means by which it reacts to gravitational, inertial and work loads. Locomotion is the literal basis of a mobile robot's performance.

Despite its significance, locomotion design and its implications to robotic function execution have not been addressed. In fact, with the exception of a handful of case studies, the issue of *how to design robotic locomotion* remains a topic of ad hoc speculation and is commonly pursued in a way that lacks rationalization. This thesis ventures to shed light on how to synthesize robotic locomotion from engineering analysis. Towards this goal, a fundamental hypothesis is made that the level of performance achieved by a mobile robot depends on the thoroughness of locomotion configuration.

The core of this thesis is a practical analytical framework for synthesis and optimization of wheeled robotic locomotion configurations. The decision to study wheeled robotic locomotion configuration is motivated by the fact that wheels are the most commonly used means of robotic mobility and that their design is amenable to generalized analyses and widely accepted metrics of performance. The configuration of Nomad, a planetary prototype robot for exploration of barren terrain is a case illustrating the implementation and evaluation of the Locomotion Synthesis (LocSyn) framework put forth by this thesis.

1.1 Motivation

Locomotion makes a vehicle move, negotiate terrain, reach its goals and react to forces created during the execution of its task. Robotic locomotion is distinct from traditional forms of locomotion in that, not only must it fulfill those roles, but it must perform in a controlled and reliable manner without the aid of a human operator. Moreover, robotic locomotion must facilitate onboard perception and guidance sensors, planning and navigation computing, and real-time motion control. This discussion leads to two fundamental observations. First, it is evident that robotic locomotion is critical to the successful execution of a mobile robot's tasks. Second, because the level of achieved performance depends on the interoperability of classical electromechanical, mechatronic and advanced robotic components, the design of robotic locomotion is a complex task.

The current state-of-practice in robotic locomotion design draws on knowledge of precedent robotic and conventional vehicles, intuition and experience, but rarely involves analysis and quantitative rationalization. Especially when a new robot design is pursued, empirical approaches may result in ill-conceived designs that require redesign or reworks to achieve desired functionality. Moreover, using current practices it is difficult to predict how much the paper design will grow in physical and control complexity during development. Concurrent prototyping and testing is insufficient to address this challenge because a detailed performance evaluation is possible only after system-level tests have been carried out.

Another deficiency is that analytical models governing the relationships between classical electromechanical and robotic subsystems are not well understood. For instance, it is not clear how to design robotic locomotion to achieve superior terrain negotiation while minimizing requirements of perception. The lack of quantitative methods to aid robotic locomotion design makes it difficult to identify the engineering traits of significance to a specific design. In many cases traits such as the optimal disposition of locomotion elements around the chassis frame are not recognized until the robot is fully developed and tested. Because of very poor understanding of the underlying principles, the effect of robotic functions, such as autonomous navigation, on the design are commonly deferred until after the robot is complete. Most frequently the resulting robot performance is below expectations either because the robot design defies accurate models needed for planning and control or simply because the design does not meet robotic requirements.

As yet, there exists no theory, methodology or metrics for the systematic design of wheeled robotic locomotion. A design phase that is practically unexplored and often neglected is that of *configuration* during which locomotion concepts are synthesized and evaluated and a decision regarding which concept to carry into full design is made. The aforementioned deficiencies of the current state-of-practice also pertain heavily to configuration. What is not widely realized is that configuration is the foundation to design and to successful mobile robot development.

Despite its significance, the process of configuration and design of locomotion for mobile robot performance has not been sufficiently addressed. As a result, robotic locomotion is a product of *ad hoc* efforts lacking rationalization and method, and ultimately performance. This thesis is motivated by the need to improve this practice by systematizing the synthesis of locomotion configurations through the use of analytical methods and parametric optimization. The scope of the research undertaken has been to make explicit *physics-based mathematical relationships* that capture the relationships between configuration parameters and performance, and devise them in the context of a computational framework which is practical and is applicable to a generic class of robot designs.

The focus of this thesis is on the configuration of wheeled robotic locomotion, the most commonly used means for robotic mobility. An additional motivation is that a body of research exists on classical vehicle-terrain systems but no one has attempted to apply it to mobile robots. This thesis embarks to bridge this gap and through the implementation of a

systematic framework to make explicit how classical models of vehicle-terrain interaction affect robotic locomotion configuration.

1.2 Thesis Statement

The success of a mobile robot depends on performance of its locomotion system. Despite a great deal of wheeled robot development, the current state-of-practice does not offer a practical approach to configuration of robotic locomotion. The purpose of this research is to formulate, implement and validate a computational framework for synthesizing wheeled configurations from analytical models of performance. The goal is to improve the state-of-practice and offer robot designers and researchers an aid to pursue new designs with rationale and method.

In response to the need to improve the current state of practice this work ventures to prove the thesis that:

Analytical relationships for all-terrain traversability and the mechanics of interaction between classical mobility and robotic functionality are essential to generating robotic locomotion configurations with rational and predictable performance.

1.3 Scope

Configuration is an early design phase during which concepts are synthesized from engineering principles and creative brainstorming, and then evaluated against design and performance criteria. In general, configuration occurs after requirements have been identified and analyzed, and before detailed design commences. Configuration is therefore a critical phase since it involves the selection of the best one or two candidates for detailed design. The scope of this thesis is to formulate and implement quantitative techniques applicable to configuration of wheeled robotic locomotion. It has become apparent through the course of this work that the developed techniques also apply to detailed design if improving the fidelity of the design is sought before physical prototyping.

Robotic locomotion configuration deals with the synthesis of a robot's propulsion (drive), steering, suspension and chassis subsystems (Figure 1). More precisely, *configuration synthesis is the derivation and selection of the various subsystems' geometric parameters that are essential to initiate detailed design*. Such parameters can be estimated from analytical models of the mechanics of robot-terrain interaction. The bulk of this research has been in the investigation of analytical formulations of classical vehicle-terrain systems and their applicability and implications to robotic locomotion. Because of unique issues pertaining to mobile robot performance such as the ability to safely and autonomously navigate in an unknown environment, robotic locomotion configuration must also take into account the accommodation of robotic hardware and execution of computational functions. This work addresses critical configuration issues and illustrates how they are pursued in the context of configuration using a novel computational framework known as LocSyn.
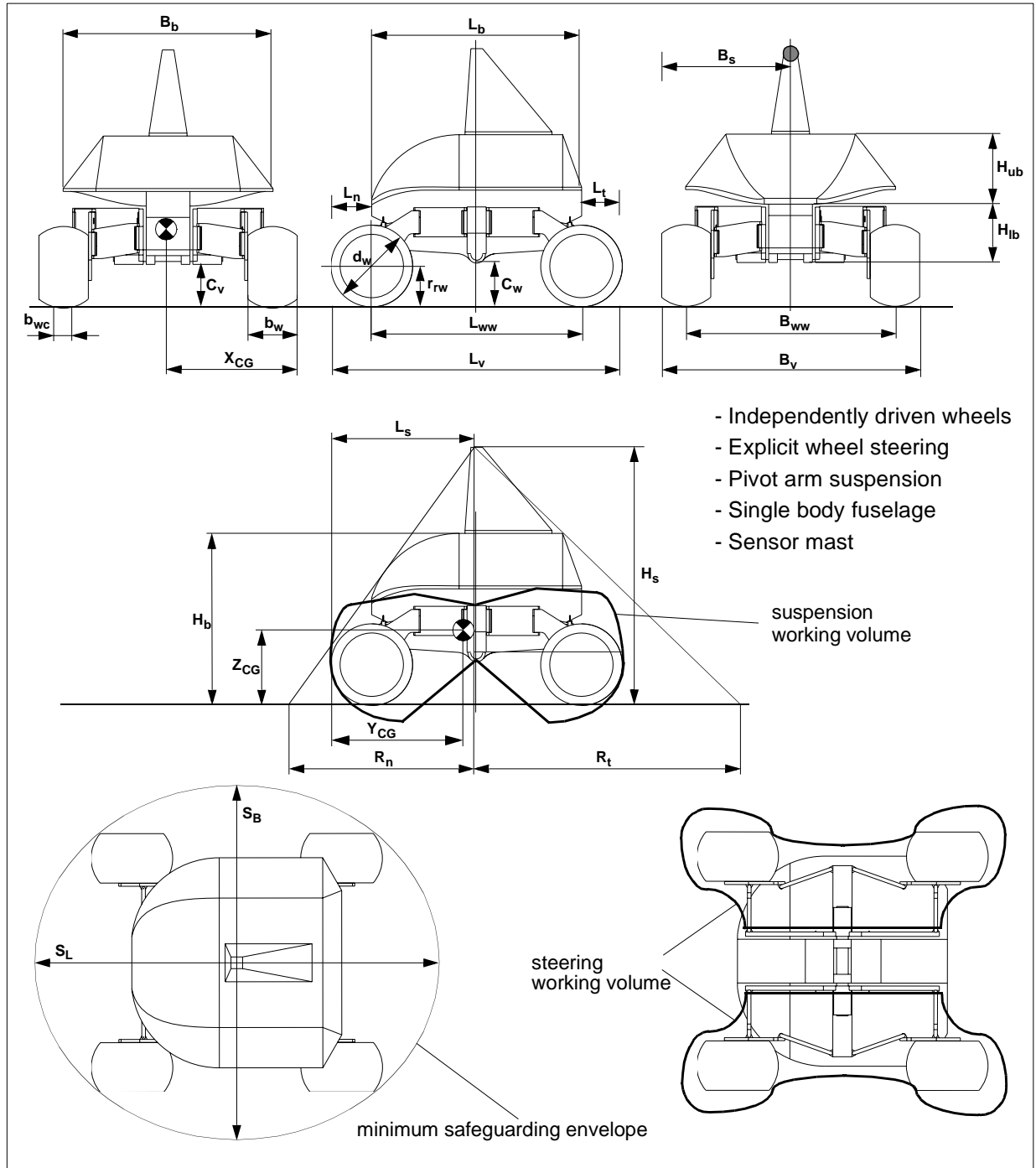
Figure 1: Example of a four-wheel robotic locomotion configuration. Such a representation is commonly referred to as *configuration design* because it contains enough information to pursue detailed design. As can be inferred from the various section views the configuration process must not only estimate optimal values of geometric parameters, but should also facilitate general configuration features such as the number and disposition of powered and steered wheels, type of suspension, actuation, etc.

LocSyn uses analytical models of performance and parametric optimization to estimate configuration parameters such as the number and type of wheels, geometry of the locomotion chassis, method of steering, etc. The selection of optimal values for configuration parameters is based on optimization with regard to performance criteria. There are three general indices of performance considered:

- Trafficability, which is a robot's ability to traverse soft soils or hard ground without loss of traction.
- Maneuverability, which addresses a robot's ability to navigate through an environment.
- Terrainability, which captures a robot's ability to negotiate terrain irregularities.

To maximize the information gained from each analytical formulation, LocSyn implements optimization on individual equations, rather than formulating multi-variable systems of equations and then solving for the critical configuration parameters. LocSyn outputs parametric graphs that allow for in-depth interpretation of the quantitative relationships between configuration parameters and predicted performance.

LocSyn's is structured in a way that allows for incorporation of additional configuration studies without the need to redesign its architecture. LocSyn's configurations are applicable to any type of wheeled locomotion configuration. This is in response to the main motivation of the thesis which is to impact the general state of practice. Emphasis has also been placed in carrying out the various analytical studies in a manner which is as general as possible. Even though not all possibilities of subsystem configurations are examined, the reader can learn from the work presented the appropriate engineering methods and how to use them.

LocSyn was used to configure the locomotion of Nomad, a robotic rover for long range exploration of barren environments such as deserts and polar icefields. To verify some of the performance predictions made by LocSyn, this research has conducted an extensive experimental program, first using a single wheel testbed and then the Nomad robot.

1.4   Approach

This approach of this thesis towards the configuration of wheeled robotic locomotion is to:

- Identify and formulate *configuration equations* which are analytical expressions with merit to configuration.
- Assemble a framework that systematically utilizes configuration equations to estimate configuration parameters.
- Realize the applicability and limitations of such equations through in depth research and incremental implementation.
- Exercise the framework on the locomotion configuration of a novel robot.
- Critique the results and identify improvements and additional configuration studies.

A great deal of effort is devoted in creating or adapting *terramechanical* models of wheel/ soil interaction to derive wheel and chassis parameters and quantify the expected tractive performance of a configuration. Quasi-static models of maneuverability, obstacle

negotiation and slope climbing are then used to acquire configuration equations for the steering and suspension subsystems. Emphasis is placed on studies that are applicable to any type of wheeled robot. Wherever this is not possible, a concerted effort is made to present the derivation of configuration equations in a way which is not only generic but also highlights the underlying engineering principles.

LocSyn is the computational framework that systematizes the synthesis of configurations. It carries out all the analyses, provides numerical solutions to configuration equations and outputs both text data and graphs. LocSyn solves all the configuration equations and as such captures the relationships among configuration (physical and geometric attributes such as those shown in Figure 1), performance (defined within the context of the three indices of trafficability, maneuverability, terrainability) and environmental/task parameters (constraints and requirements). LocSyn's graphical output allows for simultaneous evaluation of multiple configuration candidates and visualization of the space of acceptable solutions. LocSyn's architecture is straightforward; numerical solutions are sought for each configuration study independently and sequentially. In its current instantiation, LocSyn does not automatically evaluate candidate configurations. This is done by the designer to maximize the benefits gained from an elaborate examination of numerical results.

The derivation of configuration equations and their implementation in LocSyn and ultimately in the configuration of the Nomad robot are detailed in this thesis. Chapter 2 outlines the underlying fundamental questions of this research and summarizes related research. Chapter 3 introduces the concept of configuration equations and the framework for synthesis of locomotion configuration (LocSyn), and details LocSyn's analytical models. Chapter 4 discusses the implementation of LocSyn on Nomad's robotic locomotion and critiques the experimental results and LocSyn's theoretical predictions. Finally, Chapter 5 captures the contributions to robotics and envisions future developments.

Chapter 2

BACKGROUND

The synthesis of robotic wheeled locomotion configurations from physics-based models and the optimization of selected configurations based on metrics of ground performance are the objective of this research. The fundamental assumption of this work is the notion that both traditional ground vehicles and wheeled robots are subject to the same physical principles that govern the interaction between locomotion elements and the terrain. This hypothesis allows for a detailed examination of trafficability, maneuverability and terrainability as they pertain to wheeled robots through the use of quasi-static terramechanics, the science of vehicle-terrain interaction.

Lacking prior research on how terramechanics impacts the design of wheeled robots, it became a priority to investigate, reformulate and in some cases develop new analytical models of ground performance in a way that is suitable to robotic locomotion. Moreover this research has pursued those models and associated metrics with general applicability to any wheeled robot design. It is likely that the configuration optimization criteria would be different from application to application, but the configuration equations developed are of general use. The configuration analyses are based on the assumption of quasi-static vehicle mechanics. Notable exceptions to the class of robots whose performance conforms to that assumption include autonomous highway vehicles and a new generation of unmanned ground vehicles for defense applications.

The process by which locomotion configurations are synthesized is based on the derivation of parametric solutions to configuration equations and the interpretation of the space of feasible configuration parameters. This allows for a thorough examination of analytical expressions with merit to configuration and an efficient handling of multiple and in most cases conflicting optimization criteria. Moreover, the devised framework can be easily augmented with analytical studies that pertain to the configuration of a specific class of wheeled robots.

The works by [Bekker56/60/69] and [Wong93] have had a profound impact on the technical investigations of this thesis. [Bekker69] researched systematic approaches to the development of off-road vehicle concepts and devised semi-analytical methods for selecting vehicle configurations for a given mission and environment. His experimental programs produced a thorough characterization of the terrain performance of medium and large-size all-terrain vehicles for defense and civilian applications and a substantial body of analytical work on various aspects of tire/soil interaction [Bekker60]. Bekker also pioneered the use of terramechanics in the configuration and performance prediction of lunar rover designs [Bekker64]. This work also investigated the relative merits of wheels and legs in the context of planetary exploration. Wong's comprehensive work on the theory and practice of ground vehicles is an invaluable resource in understanding the mechanics of locomotion based on the theory of plastic equilibrium of soils.

The role, scope and approach to address the configuration of robotic locomotion is a subject that has received little attention from the robotics community. Notable exceptions include the works by [Bares97/91], [Hirose91/95] and [Waldron84/85/95], and to a lesser degree the works of commercial aerospace and NASA teams that have pursued the design of planetary rovers [MMSSC88][Lindemann92][Littmann92][Wallace92/93].

[Todd85] in his book *"Walking Machines: An Introduction to Legged Robots"* presents a comparative evaluation of wheels and legs based on simplified soil mechanics and a study of energetics of locomotion. Even though Todd's work focuses on the configuration of legged robots, the discussion of foot work energetics reveals the significance of terramechanics in characterizing the ground performance of a robot and demonstrates mobility studies of impact to robot design.

[Bares91] represents a systematic approach to configuration of autonomous walking robots for exploration of extreme terrains. His work distinguishes the role and scope of locomotion configuration of legged robots and details the metrics and techniques for synthesizing such systems. Using geometric analysis of gaits, vehicles kinematics and power expenditure studies, Bares characterized the expected extreme-terrain performance of a small number of configurations.

[Waldron85a] differentiates between the configuration of mobile robots and traditional ground vehicles. The primary distinction of robotic configuration is that it is driven by metrics of superior mobility, power efficiency and robust motion control. Additionally, because most robots are confined to remote or hazardous environments subject to infrequent human control, they must possess locomotion features that enhance their ability to avoid immobilization, accommodate degraded performance and even self-recover. Waldron also addresses the synergy among the mechanics, control and sensing of a mobile robot and its impact on configuration through metrics of mobility, actuation and motion coordination [Waldron85b]. Waldron's work is of great significance in that not only did it formulate practical metrics for configuration, but proved their applicability on the configuration design of a high-performance actively articulated wheeled robot [Waldron95].

Although the main product of this thesis is a computational framework for wheeled robotic locomotion configuration, it does not attempt to automate the configuration process. It is therefore quite distinct from other approaches, which through the use of knowledge-based systems and optimization such as dynamic programming and genetic algorithms have pursued the automation of robot design synthesis and optimization. A discussion of such approaches can be found in [Roston94], [Katragadda98] and [Leger99].

Chapter 3

CONFIGURATION FRAMEWORK

This chapter deals with the study of *configuration equations* for synthesis of robotic locomotion configurations. Configuration equations are functions that capture the quantitative relationships among *environmental/task parameters* (e.g. geophysical soil properties, density and size of obstacles) configuration *parameters* (e.g., wheel diameter, chassis articulation location) and *performance parameters* (e.g. drawbar pull, maximum gradeable slope). Solutions to the configuration equations are obtained in parametric form to allow for comprehensive characterization of variant locomotion concepts as opposed to searching for point designs. Optimal configuration parameters are sought in the context of three indices of performance: *trafficability*, *maneuverability* and *terrainability*.

The derivation of configuration equations, the estimation and optimization of configuration parameters and predictions of performance are performed in Locomotion Synthesis (LocSyn), a framework that combines computation, simulation and design to configure wheeled robotic locomotion. LocSyn offers a practical approach to rationalizing the configuration design of robotic locomotion through quantitative studies. LocSyn's general architecture can easily be modified to accommodate case-based studies. The following sections present the derivation of configuration equations of merit to configuration of wheeled robotic locomotion and discuss their limitations.

3.1 Locomotion Synthesis (LocSyn)

LocSyn is a computational framework for the quantified derivation of robotic locomotion configurations. It carries out all the analyses, provides numerical solutions to configuration and outputs both text data and graphs. LocSyn's architecture is straightforward; numerical solutions are sought for each configuration study independently and sequentially. Analysis of trafficability is treated first, followed by maneuverability and terrainability. LocSyn presents the designer with its results graphically to enable understanding of trends and trade offs.

LocSyn utilizes information on a robot's mission and environment of operation as input to compute dimensional and functional features of the robot's locomotion. The impact of "environment" and "mission" to configuration is captured by environmental/task parameters, which are input entities to the configuration process. Environmental/task parameters are the constraints and specifications derived from requirements, such as the geophysical properties of the terrain to be traversed by the robot or the maximum available transport-stowage volume. LocSyn does not require that environmental/task parameters are deterministic but can be expressed in any mathematical form including statistical functions. This is necessary if environmental/task parameters can only be derived probabilistically.

LocSyn estimates the dimensions and other functional features of locomotion by solving configuration equations. These mathematical expressions are derived from physics or geometry-based analytical models, and encode the relationships between the physical configuration of locomotion and its performance, expressed as configuration and performance parameters, respectively. Configuration equations also incorporate environmental/task parameters. A fundamental assumption is made that configuration from analytical models can benefit most if a quantitative relationship between *the physical configuration* and *performance* is utilized. To illustrate the concept of configuration equations, consider the following equation of the theoretical static sinkage of a solid, low compliance, powered wheel rolling in soft soil:

$$d_w(k_\phi b_w + k_c)^2 = \frac{9W_w^2 cos^2\theta}{(3-n)^2(z_{rw})^{2n+1}}$$

This expression captures the relationship between the diameter d_w and width b_w of the wheel (configuration parameters) and sinkage z_{rw} (performance parameter). k_ϕ, k_c, n and θ are soil and terrain environmental/task parameters. It is evident that this formulation allows for the quantitative evaluation of the effect of wheel dimensions on sinkage performance. Configuration equations can be used in different ways depending on what kind of information is available to the designer. For instance, one can estimate wheel dimensions if the maximum allowable wheel sinkage is defined for a variety of soils. Conversely, one can estimate the expected sinkage if the lower and upper bounds of wheel dimensions have already been determined by another configuration study or simply are defined based on commercially available tire designs. This information is useful not just for the purposes of configuration but also in the detailed design of the robot's propulsion control system.

Configuration equations are solved one by one rather than as systems of equations. The reason for doing so is threefold: First, most configuration equations are non-linear and any attempt to examine them as systems of equations would have required linearization and approximations that would have defeated the purpose of LocSyn as a practical tool for early configuration synthesis. Second, it is essential that one must exploit each configuration equation to the fullest to adequately characterize the relationships between configuration and performance parameters. One way to achieve this is through parametric evaluation of the relationships of configuration and performance parameters as they are captured through each equation. Finally, independent treatment of each equation enables sensitivity analysis of the relative effect of configuration parameters on performance.

LocSyn considers three indices of performance: trafficability, maneuverability and terrainability. These relate to any form of wheeled robotic locomotion independently of the environment of operation or task. Each performance index entails a fair number of engineering studies as illustrated in Table 1.

Trafficability	Maneuverability	Terrainability
Sinkage Ground Pressure	Axial/ Lateral Resistance	Downhill/Crosshill Grade Negotiation Stability/Traction/ Torque/Power
Traction/Slip Braking/Skid	Turning Radius/Range	Combined-Grade Negotiation Stability/Traction/ Torque/Power
Motion Resistance	Steering Torque/Energy/Power	Discrete Obstacle Negotiation Stability/Traction/Torque/ Power
Drawbar Pull	Steering Efficiency	Combined-Obstacle Negotiation Stability/Traction Torque/Power
Drive Torque/Energy/Power	Steering Resolution/Accuracy	Tipover Static/Dynamic Resistance
Traction/Torque/Power Efficiency	Steering Kinematics (skid/wagon/ackermann)	Rollover Static/Dynamic Resistance
Drive Resolution/Accuracy	Steering Geometry (linkages, motion range, working volume)	Suspension Geometry (linkages, motion range, working volume)
Propulsion Actuation (all v some wheel drive)	Steering Actuation (all v some wheel steer)	Suspension Actuation (all v some linkage actuation)
Locomotion & Chassis Geometry		Hang-up Failure Avoidance
Locomotion Element Disposition		Nose-in Failure Avoidance
Immobilization Resistance		Wedging Avoidance
Axial Impact Resistance		Obstacle Impact Resistance

Table 1: **Performance indices and engineering studies of merit to any type of wheeled robotic locomotion. In some cases more than one configuration equations can be derived from a single study. For example, an investigation of steering kinematics yields various configuration equations, depending on the type of steering scheme deployed.**

The formulation of engineering studies for configuration leverage-off the theory and practice of:

- Terramechanics
- Kinematics
- Mechanics
- Physics of sensing

3.2 Configuration for Trafficability

The fundamental functions of locomotion are to generate traction and move the robot. Traction is the result of forward thrust developed at the interface of a drive wheel with the ground. Impediments to forward motion are various forms of resistance, most notably resistance due to compaction and bulldozing of the soil, rolling resistance caused by internal losses and non-linear phenomena at the tire-soil interface, and resistance due to obstacle and slope negotiation.

Known as drawbar pull, the difference between traction and motion resistance is a pivotal metric for robotic locomotion performance, because it expresses whether or not a robot can drive without loss of traction independently of how it is controlled. Configuration for trafficability should select configurations that maximize soil thrust while minimizing motion resistance. Maximizing drawbar pull also improves the slope and obstacle climbing capabilities of a robot as well as its response to immobilization. If a robot is expected to operate in a variety of terrain conditions, configuration parameters should be selected to optimize the average tractive performance. The selected locomotion configurations should possess the implicit attributes to improve traction control and minimize dead reckoning errors by limiting wheel slip.

Finally, configuration for trafficability should minimize power expenditure due to losses from soil compaction or other phenomena associated with motion resistance. This optimization criterion has far reaching effects in that it ultimately impacts the selection of the size and type of propulsion actuators and electronics for closed-loop control.

3.2.1 Sinkage

A wheeled robot traversing off-road terrain is subject to sinkage. The amount of sinkage depends on the geophysical properties of the soil and the dimensions, shape, stiffness and loading of the wheel. Wheels can be classified as *rigid or flexible* based on how much they deflect under static loading. Rigid wheels retain a constant rolling diameter and cross-section shape under any loading, and include hard metallic wheels or wheels with solid non-metallic tires. Flexible wheels deflect by at least 10% of the rolling diameter; their tires are constructed of thin wall metallic or non-metallic materials and include low- to medium-pressure pneumatic tires.

Pneumatic tires are commonly used on mobile robots. When a high-pressure pneumatic tire operates in weak soil, it behaves in a way similar to a rigid wheel. This is known as the rigid mode of operation of the wheel. Conversely, if the maximum contact pressure that the terrain can support is greater than the combined inflation pressure of the tire and the pressure due to the stiffness of the carcass, then the tire flattens at the contact patch with the terrain. This is known as the flexible mode of operation [Wong93].

Consider [McCullough89] model of sinkage of an flexible wheel shown in Figure 2. This is a generic case, in which the wheel initially sinks into soft soil while rolling. In addition to sinking, the wheel deflects when the normal pressure that the terrain can sustain is greater than the wheel loading over the contact patch with the soil.
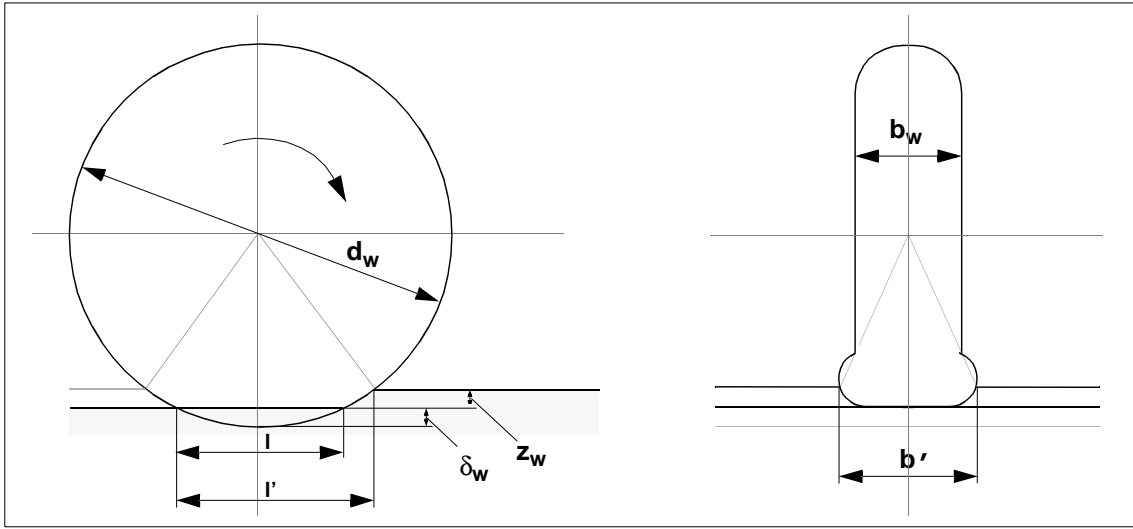
Figure 2: **Sinkage model of a flexible wheel rolling in soft soil.**

The relationship between contact pressure and wheel sinkage for a given soil and wheel loading provides a parametric equation of wheel sinkage as a function of the width of the loading area. Independent of the type of tire or the mode of operation, for locomotion configuration purposes the width of the contact area b_w is the nominal tire width:

$$p = \left(\frac{k_c}{b_w} + k_\phi \right) z^n \qquad [1]$$

The cohesive k_c and frictional k_ϕ moduli of soil deformation are calculated by measuring the contact pressure per unit sinkage of two rectangular plates of different widths.

The exponent of soil deformation n is the mean of values determined for at least two measured sets of pressure and sinkage. The values of n, k_c, k_ϕ have been tabulated for various soils, organic terrain, and snow.

Soil Type	Moisture Content	n	k_c	K_ϕ	c	ϕ
Dry sand	0%	1.10	0.1	3.9	0.15	28°
Sandy loam	22%	0.20	7	3	0.2	38°
Clay	38%	0.50	12	16	0.6	13°
Heavy clay	40%	0.11	7	10	3	6°
Lean Clay	22%	0.20	45	120	10	20°
Snow	-	1.6	0.07	0.08	0.15	20°

Table 2:   Geophysical properties of soils and snow [Wong93].

In a static model of wheel sinkage the integral of the vertical component of normal pressure over the wheel-soil contact patch equals the vertical wheel loading. With the assumption that the normal pressure acting on the wheel rim in contact with the soil is equal to the contact pressure on a plate at the same depth and under the same loading, one can make use of the pressure-sinkage relationship to derive an equation for the maximum sinkage of a solid wheel in weak soil:

$$z_{rw} = \left(\frac{3W_w \cos\theta}{(3-n)(k_c + b_w k_\phi)\sqrt{d_w}} \right)^{\frac{2}{(2n+1)}} \qquad [2]$$

This equation expresses robot performance in the form of wheel sinkage as a function of soil parameters n, k_c, k_ϕ and wheel dimensions d_w, b_w. In most applications it is not possible to have the exact values of the soil parameters for the terrains that the robot will be traversing. Nevertheless, approximate values for a wide variety of soils and moisture contents can be found in the literature and can be used as good approximations of the geophysical properties of the terrain under consideration.

Equation [2] is valid for a rigid wheel or a pneumatic tire operating in a rigid mode. It is very accurate for values of the exponent of soil deformation n up to 1.3. Typical values of the exponent n are 0.20 for clay, 1.1 for dry sand and 1.6 for snow. If the wheel is operating in an flexible mode, the maximum sinkage is estimated from the fundamental pressure-sinkage relationship [1] by solving for the sinkage. This equation is very accurate for a flat wheel loading area, and can be also used to predict the sinkage of a track.

$$z_{ew} = \left(\frac{p}{\left(\frac{k_c}{b_w} + k_\phi \right)} \right)^{\frac{1}{n}} \qquad [3]$$

The contact pressure p is the sum of the tire inflation pressure and the pressure produced by the stiffness of the carcass. For commercial tires and tires with width to diameter ratios greater than 0.8, such as terra tires and rolligons, the contact pressure is expressed by the average ground pressure, which is usually provided by the tire manufacturer.

The fundamental equations of sinkage form the analytical basis for estimating the configuration parameters d_w and b_w. Solving the above equations for the geometric dimensions of the wheel leads to the following configuration equations of sinkage:

• Rigid wheel:

$$d_w(k_\phi b_w + k_c)^2 = \frac{9W_w^2 \cos^2\theta}{(3-n)^2(z_{rw})^{2n+1}}$$ [4]

• Flexible wheel:

$$b_w = \frac{k_c}{\left(\dfrac{p}{z_{ew}^n} - k_\phi\right)}$$ [5]

From the equations of sinkage it is evident that larger wheel diameters and widths result in lower sinkage. The upper bounds on wheel dimensions are set by considerations of mass, volume, and functionality [Wallace93]. For example, the wheel diameter cannot be greater than the required length of the wheelbase, in case for instance that the wheelbase is limited by stowability constraints. The sinkage of a very-low pressure pneumatic or a highly flexible metallic tire, is virtually independent of wheel diameter.

A complete analysis of the effects of wheel dimensions on sinkage should take into account the changes in motion resistance and, in particular, compaction and bulldozing resistance as the wheel sinks deeper into soil. The effects of sinkage on tractive performance and locomotion configuration are discussed in the upcoming sections.

3.2.2 Soil Thrust and Traction

Vehicle motion relevant to the terrain is produced through traction. Caused by a physical process of adhesion and deformation, traction develops at the interface of a powered wheel with the ground. Unpowered (towed) wheels cannot generate traction because there is no input torque to react to the tractive force needed to turn the wheel and propel the vehicle. The maximum produced traction is limited by the adhesion between the wheel and the ground [Gillespie92] and the torque-speed characteristics of the vehicle's prime mover and drivetrain which basically determine that maximum torque and power transmitted to the wheel.

For locomotion in soft soils traction is limited by the mechanical properties of the soil and loading at the wheel/soil interface patch. The maximum force that can be sustained by the soil before excessive slippage occurs (usually more than 20%) is known as soil thrust. The study of the mechanics of traction generation provide equations for the configuration of a

robot's wheel and overall locomotion geometry. Consider the case of towed and powered wheels rolling at slow speeds through soft terrain:
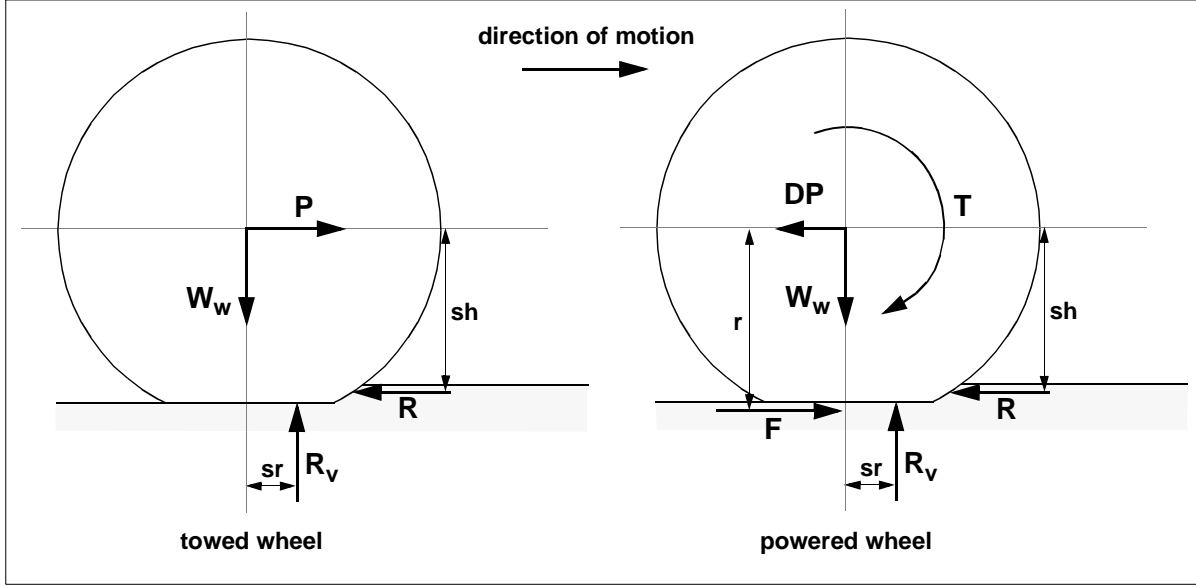

Figure 3:   Free-body diagrams of towed and powered wheels.

The towed wheel which supports a fraction of the robot weight W_w is put to motion by the towing force P. The towing force is balanced by the motion resistance R, and the weight is equal but opposite to the vertical ground reaction R_v. In the case of the powered wheel a drive torque T is required to produce the tractive force F. Traction should exceed the motion resistance force if forward motion is to be sustained.

The maximum tractive force F is limited by the thrust H produced by the soil, which in turn is proportional to mechanical strength of the soil. Data on the stress/strain relationships of disturbed soils, sand, snow, and saturated clays have verified the appropriateness of the Janosi-Hanamoto relationship to describe the shear stress-strain behavior of unprepared terrain [Wong93]:

$$\tau = (c + p \tan\phi)\left(1 - e^{\frac{-J}{K}}\right) \qquad [6]$$

τ is the shear stress, p is the normal pressure (normal stress), J is the shear displacement, and c and ϕ are the modulus of cohesion and angle of internal friction of the soil, respectively. K is the modulus of shear deformation and in theory is the magnitude of the sheared displacement required to develop the maximum shear stress. Wong proposes that K can be taken as 1/3 of the shear displacement at a stress τ that is 95% of the maximum shear stress of the soil τ_{max}. In practice, K is fitted using experimentally calculated values of τ_{max}, τ, and J. The shear displacement J is a function of the slip, contact angle, and rolling radius of the wheel.

The amount of soil thrust H is computed by integrating the shear stress over the contact patch between the wheel tread and the soil. Assuming a uniform distribution of normal pressure on the tread-soil interface:

$$H = (cA_w + W_w \cos\theta \tan\phi)\left(1 - e^{\frac{-J}{K}}\right)$$ [7]

This equation expresses the in-soil performance of the wheel in terms of the maximum developed tractive force as a function of the contact patch between the tire and the soil, and the weight distribution over the wheel. It is evident that increasing the contact area by means of wider tires, or transferring a higher portion of the robot's weight to a powered wheel, result in proportional improvements in traction.

Of critical importance to the amount of forward thrust developed at the tire-soil interface is the geometric shape of the tire. Consider the road-tire shaped wheel. The contact patch between the tire and the soil has an elliptical shape and an approximate area:

$$A \approx \left(\frac{\pi}{4}\right) l'b'$$ [8]

where l' and b' are the principal axes of the elliptically-shaped contact patch. When rolling, the size of the contact area changes continuously because of different soil properties and dynamic weight transfer due to changes in the posture of the robot traveling on uneven terrain. In the case of a flexible wheel the approximate dimensions of the contact area are:

$$l' = 2\sqrt{(d_w - \delta_w)\delta_w} + \sqrt{(\delta_w + z_w)(d_w - \delta_w(1 - z_w))}$$
$$b' = 2(\sqrt{(b_w - \delta_w)\delta_w} + \sqrt{(\delta_w + z_w)(b_w - \delta_w(1 - z_w))})$$ [9]

Assuming that the width of the contact area is practically equal to the nominal width of the tire, the equation of soil thrust can be rewritten as follows:

$$H = \left(c\left(\frac{\pi}{4}\right)(2\sqrt{(d_w - \delta_w)\delta_w} + \sqrt{(\delta_w + z_w)(d_w - \delta_w(1 - z_w))})b_w + W_w \cos\theta \tan\phi\right)\left(1 - e^{\frac{-J}{K}}\right) \geq F$$ [10]

The configuration equation for the maximum achievable traction based on the available soil thrust is:

$$F_{max,\,ew} = \left(c\left(\frac{\pi}{4}\right)(2\sqrt{(d_w - \delta_w)\delta_w} + \sqrt{(\delta_w + z_w)(d_w - \delta_w(1 - z_w))})b_w + W_w \cos\theta \tan\phi\right)\left(1 - e^{\frac{-J}{K}}\right) \Rightarrow$$

$$(2\sqrt{(d_w - \delta_w)\delta_w} + \sqrt{(\delta_w + z_w)(d_w - \delta_w(1 - z_w))})b_w = \frac{4F_{max,\,ew}}{c\pi\left(1 - e^{\frac{-J}{K}}\right)} - W_w \cos\theta \tan\phi$$ [11]

Equations [10] and [11] can be used to estimate the configuration parameters d_w, b_w, and δ_w of a flexible wheel. To optimize traction, one can compute the maxima of the function $F_{max,ew}= f(d_w, b_w, \delta_w)$ for appropriate value ranges of the configuration parameters. Alternatively, if the maximum traction has been estimated from a drawbar pull specification, there are only two independent configuration parameters and the third determined as a function of the other two. If the flexible tire is rolling on hard ground, the above equations can be simplified by eliminating the terms that involve sinkage.
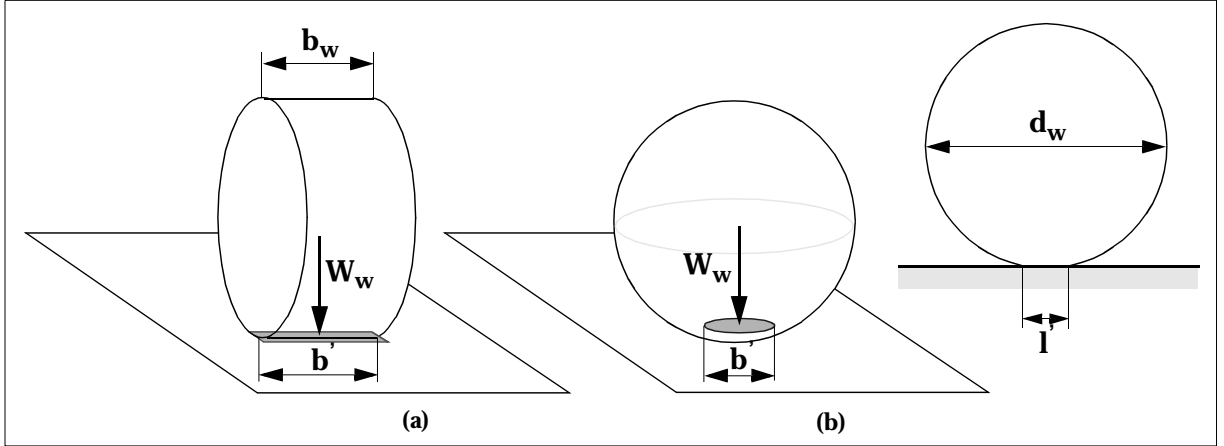
Figure 4:   **Contact patch profiles for cylindrical (a) and spherical (b) wheels.**

Now consider the case of a solid cylinder in contact with a flat planar surface. The area of the contact patch between the tire and the ground can be approximated as follows [Shigley89]:

$$l' = 1.60 \sqrt{W_w K_D \frac{C_E}{b_w}}$$
$$b' = b_w$$
$$A = l'b'$$

[12]

In the case of cylinder-plane or sphere-plane contact, the shape coefficient K_D and flexible coefficient C_E are:

$$K_D = d_w$$
$$C_E = \frac{(1 - v_w^2)}{E_w} + \frac{(1 - v_s^2)}{E_s}$$
$$E_s \approx \infty$$

[13]

v_w and E_w are the Poisson's ratio and modulus of the flexibility of the tire material, respectively. Substituting [13] into [7] results in the configuration equation of maximum traction developed by a cylindrical solid wheel on hard ground:

$$F_{max,\,rw} = \left(c1.60 b_w \sqrt{W_w d_w \frac{\left(1 - \nu_w{}^2\right)}{E_w b_w}} + W_w \cos\theta\,\tan\phi \right)\left(1 - e^{\frac{-J}{\overline{K}}} \right) \Rightarrow$$

$$b_w d_w = \left(\frac{0.4 E_w}{c^2\left(1 - \nu_w{}^2\right)} \right)\left(\frac{F_{max,\,rw}}{\left(1 - e^{\frac{-J}{\overline{K}}}\right)} - W_w \cos\theta\,\tan\phi \right)^2 \qquad [14]$$

The above configuration equations are useful in estimating the configuration parameters d_w and b_w. Because the shape of the wheel impacts the maximum traction through the dimensions of the contact patch l' and b', the above equations can be used as a metric of comparison of different wheel shapes. For example, if a spherical wheel is rolling on hard soil the dimensions of the contact patch and the maximum developed traction are:

$$l' = b' = r_c = 0.721\left(W_w K_D C_E\right)^{\frac{1}{3}}, A = \pi r_c{}^2$$

$$F_{max,\,rw} = \left(0.52\,c\pi\left(W_w d_w \frac{\left(1 - \nu_w{}^2\right)}{E_w} \right)^{\frac{2}{3}} + W_w \cos\theta\,\tan\phi \right)\left(1 - e^{\frac{-J}{\overline{K}}} \right) \Rightarrow$$

$$d_w = \left(\frac{2.67 E_w}{(c\pi)^{\frac{3}{2}} W_w\left(1 - \nu_w{}^2\right)} \right)\left(\frac{F_{max,\,rw}}{\left(1 - e^{\frac{-J}{\overline{K}}}\right)} - W_w \cos\theta\,\tan\phi \right)^{\frac{3}{2}} \qquad [15]$$

The first equation in [15] can be used to calculate the maximum wheel traction as a function of wheel diameter for given soil conditions. Wheel shape affects the tractive efficiency of a robot and its resistance to steering. The majority of commercial vehicles use tire-shaped wheels which are very effective for locomotion on hard terrain. Low section-height tires are used in off-road applications to minimize sinkage and improve traction. Tread patterns and deep grooves are common features of tires used in demanding applications, such as tillage earthmoving and excavation [Dudzinski89].

Numerous innovative wheel shapes have emerged in an effort to develop highly efficient wheel designs for planetary exploration. These designs included the wire-mesh tire-shaped wheel used for the Apollo Lunar Roving Vehicle [Burke92], the loop-spring torus-shaped wheel developed for the Russian Mars Roving Vehicle [Kemurjian92], as well as convolute cone, hemispherical, and cantilevered cleat wheels proposed for various planetary rovers.

To compute the maximum traction of a rigid wheel driving though weak soils, assume that the length of the contact area equals its projection l' on a horizontal plane and that the width of the contact area b' is the width of the wheel b_w:
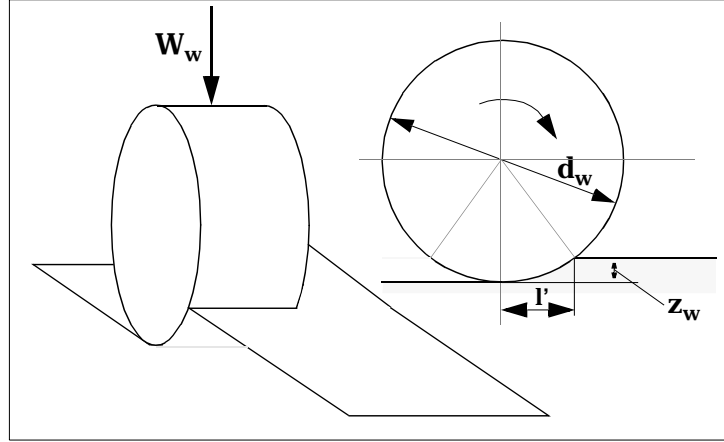

Figure 5:   Cylindrical rigid wheel rolling in soft ground.

$$A = l'b', b' = b_w, l' = \sqrt{(d_w - z_w)z_w}$$

$$F_{max, rw} = (cb_w\sqrt{(d_w - z_w)z_w} + W_w\cos\theta\tan\phi)\left(1 - e^{\frac{-J}{\overline{K}}}\right) \Rightarrow$$

$$b_w^2(d_w - z_w) = \frac{1}{c^2 z_w}\left(\frac{F_{max, rw}}{\left(1 - e^{\frac{-J}{\overline{K}}}\right)} - W_w\cos\theta\tan\phi\right)^2 \tag{16}$$

3.2.3 Motion Resistance

When a robot moves on paved surfaces and highways it consumes energy to overcome the rolling resistance between the tires and the ground, as well as gravitational and inertial forces. At speeds of more than 60 mph aerodynamic forces become the main mechanism of energy losses. The rolling resistance between the tire and the ground is attributed to tire slip, scrubbing in the contact patch, deflection of the road surface and energy losses due to tire adhesion on the road and hysteresis. Rolling resistance varies with the type and material of the tire tread, the velocity of the vehicle, and environmental parameters such as temperature and humidity [Gillespie92].

For locomotion on unprepared, off-road terrain the main mechanisms of energy losses are the wheel's compaction, bulldozing and dragging of soil. On slopes, resistance due to the gravitational component parallel to a slope is an additional impediment to forward motion.

Even more challenging are situations where the robot must climb an obstacle or a vertical step. The ability to overcome the resistance of an obstacle on a slope usually determines the extreme terrainability of the robot. The summary of such resistive forces is known as the "external motion resistance." Resistance to motion is also caused by frictional forces between drivetrain components, mechanical linkages, and hysteresis within the mechanical components of the robot, and are known as "internal motion resistance."

A study of the effects of motion resistance on the performance of a robot is accomplished by estimating configuration parameters that minimize the amount of energy dissipated into the terrain and the forces opposed to the motion of the wheel.

3.2.3.1 Soil Compaction Resistance (R_c)

Loss of soil thrust in unprepared terrains is primarily due to the compaction resistance of the soil. This form of motion resistance can be analyzed considering the mechanics of a wheel rolling into soft terrain. Compaction is equivalent to the vertical work per unit length in pressing a wheel into the ground to a depth of its maximum sinkage. Using the simplified model of wheel sinkage proposed by [Bekker69], the compaction resistance can be calculated as:

$$R_c = b_w \int_0^{z_{max}} \left(\frac{k_c}{b_w} + k_\phi \right) z^n dz \qquad [17]$$

This model assumes that the normal pressure acting on the wheel tread of width b_w is equal to normal pressure acting on a flat plate of width b_w at the same depth z, and has been successfully used to predict the resistance of wheel diameters greater than 20 inches and wheel sinkage of less than 15% of the wheel diameter. However, experimental results have shown that in practice and for a variety of soils, the maximum of the normal pressure distribution does not occur at the lowest contact point of the wheel P, but rather at the intersection of the soil flows A, as illustrated in Figure 6. Experimental work has also shown that the location of the maximum contact pressure is a function of wheel slippage [Wong93]. For low slip values there are two distinct flows of soil beneath the interface of the tire and the ground. Soil is compacted in front of the center of contact pressure, and pushed behind it. At 100% slip the wheel does not move forward, and soil is pushed from the front to the back. Finally, if the wheel is locked and is dragged forward there is a soil wedge formed in front of the tire with a significant flow accumulation.

For the purpose of this work Bekker's analytical formulations adequately describe the mechanics of wheel-soil interaction as they pertain to motion resistance and provide the analytical means for accurate estimation of the wheel configuration parameters for wheel widths greater than 15 inches, relatively low sinkage (less than 5 inches), and ground pressures of less than 10 psi.
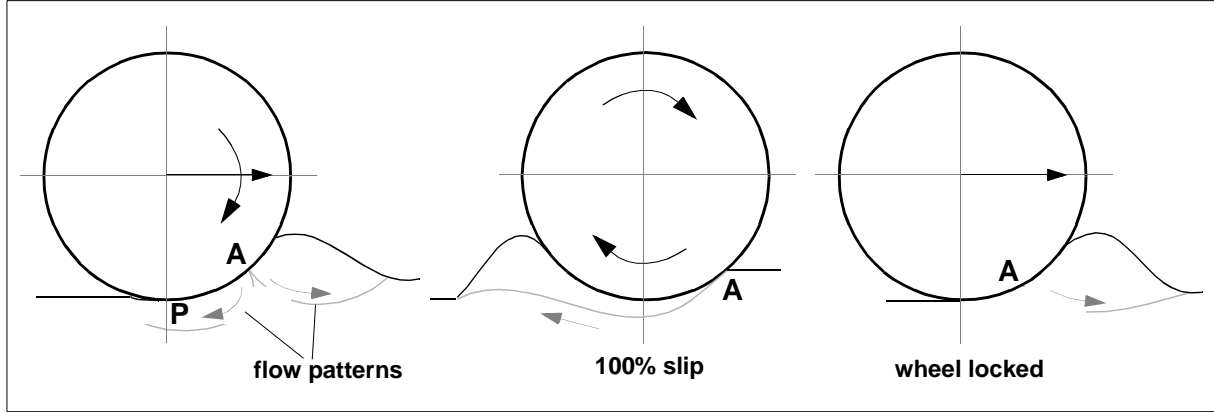
Figure 6: **Soil flow at the wheel-soil interface during sustained driving (left), 100% slip (middle) and breaking (right).**

Using the definitions of rigid and flexible wheels, and substituting the appropriate equations of sinkage into the integral of compaction resistance, we first derive an expression for the compaction resistance of a flexible wheel:

$$R_{cew} = \frac{b_w^{\left(\frac{n-1}{n}\right)} p_{gr}^{\left(\frac{n+1}{n}\right)}}{(n+1)(k_c + b_w k_\phi)^{\frac{1}{n}}} \Rightarrow$$

$$b_w^{(n-1)}\left(\frac{p_{gr}^{(n+1)}}{R_{cew}^n (n+1)^n k_\phi}\right) - b_w = \frac{k_c}{k_\phi}$$

[18]

p_{gr} is the average ground pressure which is usually provided by the tire manufacturer for a given inflation pressure and wheel loading. For configuration purposes, the compaction resistance can be approximated as a percentage of the soil thrust in response to a performance specification. For example, above a given value, the maximum compaction resistance can be estimated from the ratio of the total difference between soil thrust and compaction resistance over the gross vehicle weight. Equation [18] shows that the compaction resistance of a flexible wheel is solely a function of the width of the contact patch (the minimum width of the tire in this case) and the geophysical properties of the soil.

In a similar fashion, the compaction resistance of a rigid wheel is:

$$R_{crw} = \frac{\left(\dfrac{3W_w\cos\theta}{\sqrt{d_w}}\right)^{\frac{(2n+2)}{(2n+1)}}}{(3-n)^{\frac{(2n+2)}{(2n+1)}}(n+1)(k_c+b_wk_\phi)^{\frac{1}{(2n+1)}}} \Rightarrow$$

$$d_w^{(n+1)}(k_c+b_wk_\phi) = \frac{(3W_w\cos\theta)^{(2n+2)}}{R_{crw}^{(2n+1)}(3-n)^{(2n+2)}(n+1)^{(2n+1)}}$$

[19]

In this case both wheel diameter and width influence compaction resistance. As a result of the fact that the diameter of a solid wheel enters the compaction equation in a power higher than the width of the tire and that both configuration parameters are inverse proportional to compaction, an increase of the diameter reduces the compaction resistance by a greater rate than an equal increase of the tire width [Wallace93].

3.2.3.2 Bulldozing Resistance (R_b)

Bulldozing resistance is developed when a substantial soil mass is displaced by a wheel. This type of resistance is very common when a wheel compresses the surface layers of the soil and pushes the compacted soil fore and aft of the tire [Bekker60], [Gee-Clough79]. The soil bulldozing phenomenon is apparent in the case of a wide wheel (width greater than 10 inches) traversing very loose soils and has been estimated to cause a significant increase in total motion resistance for sinkage values greater than 0.06 of the wheel diameter.

The bulldozing resistance on narrow tires is mitigated by the fact that a portion of the soil bulk is pushed to the sides of the wheel. The bulldozing resistance can be calculated by implementing the theory of bearing capacity of soils subject to various criteria of failure.

$$R_b = \left(\frac{b_w\sin(\alpha+\phi)}{2\sin\alpha\cos\phi}\right)(2cK_cz_w+\gamma K_\gamma z_w^2) + \frac{\pi\gamma l_r^2(90-\phi)}{540} + \frac{\pi c l_r^2}{180} + c l_r^2\tan\left(45+\frac{\phi}{2}\right)$$

$$K_c = (N_c-\tan\phi)\cos^2\phi$$

$$K_\gamma = \left(\frac{2N_\gamma}{\tan\phi}+1\right)\cos^2\phi$$

[20]

$$\alpha = a\cos\left(1-\frac{2z_w}{d_w}\right)$$

$$l_r = z_w\tan^2\left(45-\frac{\phi}{2}\right)$$

The bulldozing resistance increases rapidly with the increase of the tire width. Especially in cases of robotic locomotion in high density, viscous soils is required. Soil bulldozing and in particular soil dragging become the most prominent sources of energy and traction losses. As far bulldozing resistance is concerned, large-diameter narrow wheels would develop more traction than small-diameter wide wheels with the same contact-patch area and normal loading.

3.2.3.3 Rolling Resistance (R_r)

In addition to soil compaction and bulldozing, motion resistance is caused by the deflection of the tire and the tread elements, wheel slip and scrubbing at the wheel-soil interface. The combined effect of these forms of motion resistance is known as rolling resistance. The most common definition of rolling resistance is that it is the product between the vertical load applied on the wheel and an experimental coefficient:

$$R_r = f_r W_w \qquad [21]$$

This formulation seems to deviate from the general principle of this thesis that a mathematical expression can be used as a configuration equation if it includes both configuration and performance parameters. However, the values of both the coefficient of rolling resistance f_r and the wheel loading W_w depend on configuration parameters. The calculation of the coefficient of rolling resistance is a fairly involved process that considers various factors such as: travelling speed, wheel slip, tire material, design, inflation pressure, temperature and loading, and the type of soil. The wheel diameter and tire cross section also factor in the calculation of f_r. Gravitational and inertial load distribution on the wheels depend on the geometric configuration of the chassis and mass distribution.

3.2.3.4 Gravitational Resistance (R_g)

Ground slopes add a component to the motion resistance which is proportional to the component of the total weight parallel to the slope. In the case of a robot driving on an uphill slope the gravitation resistance is:

$$R_g = W_w sin\theta \qquad [22]$$

Assuming the random location of a robot's center of gravity and that the robot is negotiating a combined crosshill/uphill slope, the gravitational resistance force on each wheel can be estimated assuming that the magnitude of the gravitational load on a wheel is inversely proportional to the distance of the wheel contact from the projection of the center of gravity to the contact plane (defined by the contact points of at least three wheels). If crosshill/uphill performance is a critical design requirement, a detailed analytical investigation of the impact of the location of the center of gravity, number and disposition of wheels on the optimal distribution of the gravitational load among the wheels is required.

3.2.3.5 Obstacle Resistance (R_o)

When a wheeled robot is climbing an obstacle, an additional component of motion resistance is developed at the tire/obstacle interface due to the change in the normal contact force. In fact, as the posture of the robot changes due to obstacle climbing, so does the weight distribution over the wheels. This is a similar situation to that of a robot climbing a slope, but in this case the "grade" is determined by the angle between the line that connects the front/rear wheel contact points and the ground level. Modeling the resistance force due to obstacle climbing in soft soils and compliant obstacles is an extremely involved process that goes beyond the scope of robotic locomotion configuration. However, a manageable configuration equation of obstacle resistance can be derived from the equations of static equilibrium of a robot climbing a discrete obstacle on a hard surface or compacted soil. Consider for instance the case of a four-wheel, all-wheel-drive robot with rigid suspension climbing a square obstacle.
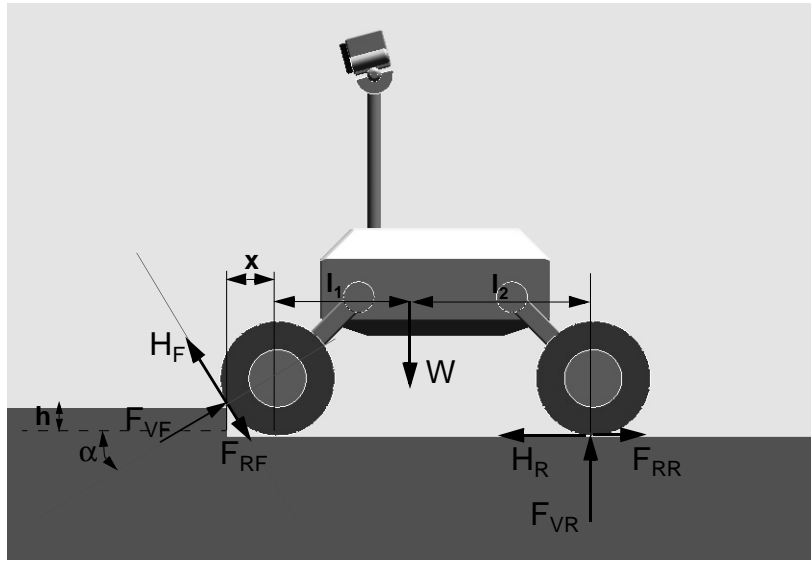
Figure 7: **Force analysis of discrete obstacle climbing with the front wheels.**

The total resistance due to obstacle climbing is:

$$R_o = F_{VF} cos\alpha + F_{RF} sin\alpha \qquad [23]$$

where F_{VF} can be calculated from solving the equations of static equilibrium:

$$\sum F_X = 0 \Rightarrow H_R - F_{RR} + H_F sin\alpha - F_{VF} cos\alpha - F_{RF} sin\alpha = 0$$

$$\sum F_Z = 0 \Rightarrow F_{VR} + H_F cos\alpha + F_{VF} sin\alpha - F_{RF} sin\alpha - W = 0 \qquad [24]$$

$$\sum M_C = 0 \Rightarrow W(l_1 + x) + H_R h - F_{RR} h - F(l_1 + l_2 + x) = 0$$

Assuming that the maximum soil thrust and rolling resistance can be approximated by:

$$H = \mu_\alpha F_V \qquad [25]$$

$$F_R = f_r F_V$$

one can obtain the following configuration equation of obstacle resistance when the front wheel is climbing an orthogonal obstacle:

$$R_{oF} = \frac{W(l_1 + x)(\mu_\alpha - f_r)(f_r sin\alpha + cos\alpha)}{(cos\alpha + f_r sin\alpha - \mu_\alpha sin\alpha)(h(-\mu_\alpha + f_r) + l_1 + l_2 + x)} \qquad [26]$$

where the contact angle α and dimension x can both be expressed in terms of the obstacle height h and wheel diameter d_w:

$$sin\alpha = \frac{d_w - 2h}{d_w} \qquad [27]$$

$$x = 0.5\sqrt{d_w^2 - (d_w^2 - 2h)^2}$$

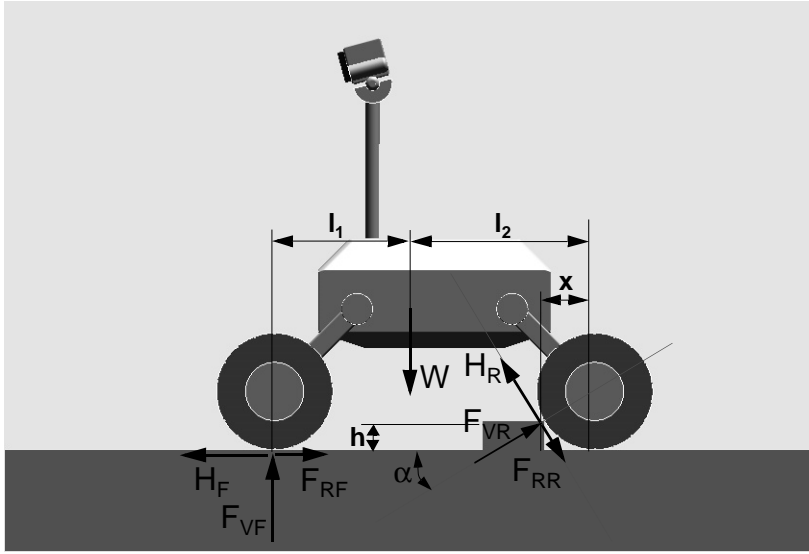**Figure 8: Force analysis of discrete obstacle climbing with the rear wheels.**

Because it is assumed that obstacles have hard surfaces, the tractive force can be approximated as the product of the a coefficient of adhesion μ_α and the wheel loading [Wong93].

Similarly, the obstacle resistance when the rear wheel is climbing the obstacle is:

$$R_{oR} = \frac{W(l_2 - x)(\mu_\alpha - f_r)(f_r sin\alpha + cos\alpha)}{(cos\alpha + f_r sin\alpha - \mu_\alpha sina)(h(\mu_\alpha - f_r) + l_1 + l_2 - x)} \qquad [28]$$

The configuration equations for R_o are significant in that they involve multiple critical

CONFIGURATION FRAMEWORK

configuration and environmental/task parameters. Assuming that the weight of the robot, geometry of the chassis and the wheels, and tire/ground properties are known, R_o can be calculated as a function of the obstacle height. It is worth noting that the (h, F_{VF}, F_{VR}) set that satisfies the equations of static equilibrium is the solution to the problem of determining the maximum negotiable obstacle (h_{max}) for a specific locomotion configuration (d_w, l_1, l_2) and tire-ground interaction (μ_α, f_r). Ultimately, the maximum climbable obstacle is the smaller of the values obtained from the analysis of R_{oF} and R_{oR}.

It is evident that the maximum climbable obstacle and obstacle resistance depend on whether all or some of the wheels are powered. If, for instance, the front wheels are not powered and the rolling resistance is negligible, then the obstacle resistance on the front wheel is:

$$R_{oF} = \frac{W(l_1 + x)\mu_\alpha}{(l_1 + l_2 + x - \mu_\alpha h)} \tag{29}$$

Under the same assumptions, in the case of the rear wheel climbing the obstacle the obstacle resistance force is:

$$R_{oR} = \frac{W l_1 \sin 2\alpha}{2(l_1 + l_2 - x)} \tag{30}$$
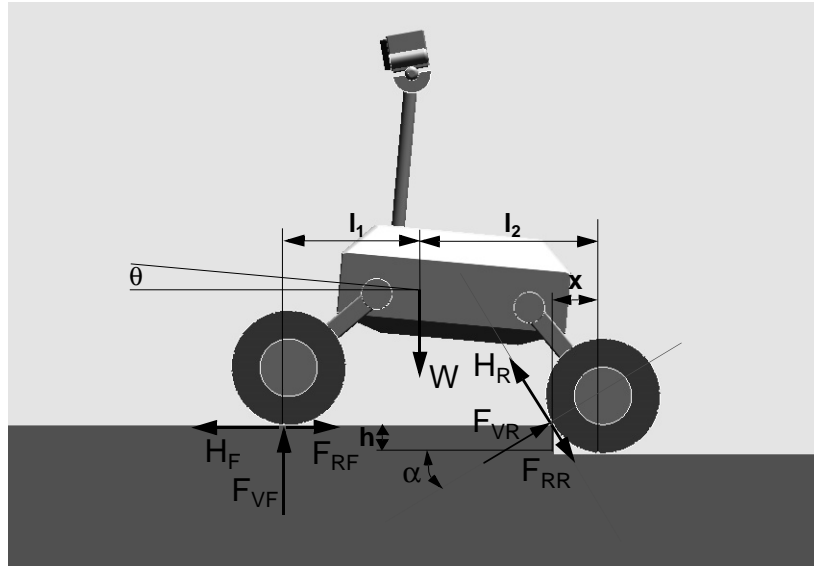
Figure 9:   Force analysis of infinitesimal obstacle climbing with the rear wheels.

Finally, if the obstacle is an infinitesimal step, the equations of static equilibrium when the rear wheel is climbing are slightly different. The resulting obstacle resistance is:

$$R_{o\infty R} = \frac{W(l_2 \cos\theta - x)(\mu_\alpha - f_r)(f_r \sin\alpha + \cos\alpha)}{(\cos\alpha + f_r \sin\alpha - \mu_\alpha \sin a)((l_1 + l_2)\cos\theta - x)} \tag{31}$$

The configuration parameters d_w, l_1 and l_2 can be estimated analytically by minimizing obstacle resistance while maximizing the height of a negotiable obstacle. The aforementioned formulations do not take into account the torque and power limitations of the robot's propulsion system and drivetrain.

3.2.4 Drawbar Pull

Drawbar pull is the difference between traction and motion resistance, and is the force which is available to pull or push an additional payload until the maximum available traction is reached.

$$DP = F - R_{ALL} \tag{32}$$

If the wheel is fitted with grousers or other tire features for increasing gripping with the terrain, the above equation is corrected as:

$$DP = F + F_g - R_{ALL} \tag{33}$$

where F_g is the additional traction produced by the grousers and the total resistance is the summary of the various forms that have been discussed in previous sections. The effects of grousers on trafficability can be found in [Bekker56/69].

$$R_{ALL} = R_c + R_b + R_r + R_g + R_o \tag{34}$$

and

$$DP = F + F_g - (R_c + R_b + R_r + R_g + R_o) \tag{35}$$

In the case of locomotion on hard ground or compacted soil the maximum tractive force F_{max} is limited by wheel/ground adhesion whereas in soft soils the limiting factor is soil thrust. In both cases wheel slip further reduces the maximum available traction. Additional limitations are imposed by the maximum tractive effort that can be delivered by the robot's prime mover to the powered axles or wheels, but for the purposes of locomotion configuration it is assumed that this is a constraint that can be handled separately during the detailed design of the robot's engine and drivetrain subsystems. Clearly, drawbar pull is a significant performance parameter as it involves practically all the configuration and environmental/task parameters that affect *trafficability*.

3.2.5 Drive Torque and Power

Losses due to motion resistance must be overcome through torque and power delivered by the robot's drivetrain. Assuming the tractive capacity of the robot's prime mover (taken to be the maximum torque that can be delivered to the powered wheel) is greater than the moment of all resistive forces about the center of the tire, then positive traction is produced and the vehicle moves forward. The torque due to resistive forces is:

$$T_{drw} = (R_c + R_b + R_r)\left(\frac{d_w}{2} - \delta\right)$$ [36]

(δ= 0.0 for a rigid wheel)

Configuration equation [36] expresses the torque required at the wheel output to sustain traction. It therefore imposes a constraint on the design of the robot's actuation and drivetrain subsystems. For this reason T_{drw} is called "drive torque." If locomotion on inclined terrain is involved, [36] must be corrected to include the additional component of gravitational resistance [37]. It must be noted that the drive torque equations capture individual wheel performance and should not be used to determine the total torque required to propel the robot. The correct approach to estimate the total required drive torque is to first compute the required drive torque per wheel and then add all the values.

$$T_{drws} = (R_c + R_b + R_r + R_g)\left(\frac{d_w}{2} - \delta\right)$$ [37]

Drive power is the power required to be transmitted to the output of the powered wheels to sustain traction. Configuration equation [38] shows that to estimate the maximum required drive power one must consider all components of resistance impeding wheel rolling and the motion of the robot, including all non-linear components such as soil compaction and rolling resistance.

$$P_{drw} = T_{drw}\left(\frac{2V}{d_w}\right)$$ [38]

3.3 Configuration for Maneuverability

Of equal importance to trafficability is the maneuverability, which is the ability to change a robot's heading, avoid obstacles and navigate through cluttered environments. The configuration of the steering system has a specific contribution to the overall locomotion configuration because of its direct impact on the positioning and navigation capabilities of the robot.

Generally, steering maneuvers require more traction and energy to perform than straight-line driving. Forces and moments developed during turning maneuvers impose significant loading on the robot's locomotion subsystems. In explicit steering schemes special configuration provisions are needed for the sweeping volume of the wheels and possible interferences between the steering mechanism and the undercarriage structure. This chapter examines the configuration equations of skid steering which serves as a representative case of the types of quasi-static analyses required to characterize maneuverability.

3.3.1 Robotic Steering Schemes

Before entering into the specifics of configuration for maneuverability, it is useful to overview some of the most common steering schemes for mobile robots. These include:

• **Skid steering** in which there is no explicit steering of the wheel axles. Skid steering is performed by controlling the direction and magnitude of the circumferential wheel velocities on the opposing sides of the chassis. As a result, steering is enabled by lateral displacement of the chassis rather than steering the wheels. The difference in velocities between the two sides defines the turning radius and affects the power draw. In the case of a symmetric chassis configuration, if the two sides are servoed to equal but opposite velocities, the center of turning coincides with the geometric center and the robot performs a point turn. This is a favorable attribute for autonomous robots operating in rugged, off-road terrain where navigation requires frequent turning maneuvers in limited space. In skid steering, one or more wheels on each side of the chassis must be powered to achieve a steering maneuver, and the wheels do not change orientation with respect to the chassis. An axisymmetric, skid-steered locomotion configuration has equal maneuverability in forward and reverse.

• **Articulated steering** in which a partition of the chassis and the wheels attached to it steer about a pivot point. The heading of the robot changes by "folding" the hinged chassis units. The articulated joint can either be actuated or passive. In a passive configuration, the steering action is achieved by locking the wheels on the one chassis unit and driving the wheels on the other. The maneuverability and efficiency of an articulated steering robot increases dramatically with the number of articulated joints, but the complexity of the steering system also increases. Articulated steering is usually combined with an additional articulation about the roll or pitch axes to mitigate the dynamic effects of steering by improving the terrain adaptability of the robot.

• **Coordinated steering** in which mechanical coupling is used to synchronize the turning of two or more wheels subject to desired kinematic geometry. Ackermann steering which is known for its extensive use in commercial transportation is a special case of coordinated steering.

• **Independent steering** in which each wheel assembly is explicitly steered. Synchronized or all-wheel explicit steering schemes can emulate any rigid-chassis steering, including skid steering. The heading change is achieved by electronically modulating the angle of steering and direction by which the heading of the wheel changes. Apart from the issues of actuation complexity and accuracy of coordination control, this scheme provides great advantages to the maneuverability of mobile robots, especially those operating in unprepared terrains. A common variation of independent all-wheel steering, not attainable by the other schemes, is "crab steering" in which all wheels turn by the same angle in the same direction. As a result, the robot moves in a sideways fashion. Coordination of driving and steering leads to low energy consumption maneuvering, reduces the danger of actuator fighting and internal losses, and simplifies automatic motion control of the robot.

The four classes of steering form a basis for generating numerous configurations. Specific requirements of an application motivate the configuration of a steering system beyond these standard forms. For instance, applications that require a variable wheelbase to meet

unique transportation or maneuverability constraints could lead to the selection of a deployable steering mechanism with some or all wheels explicitly turned.
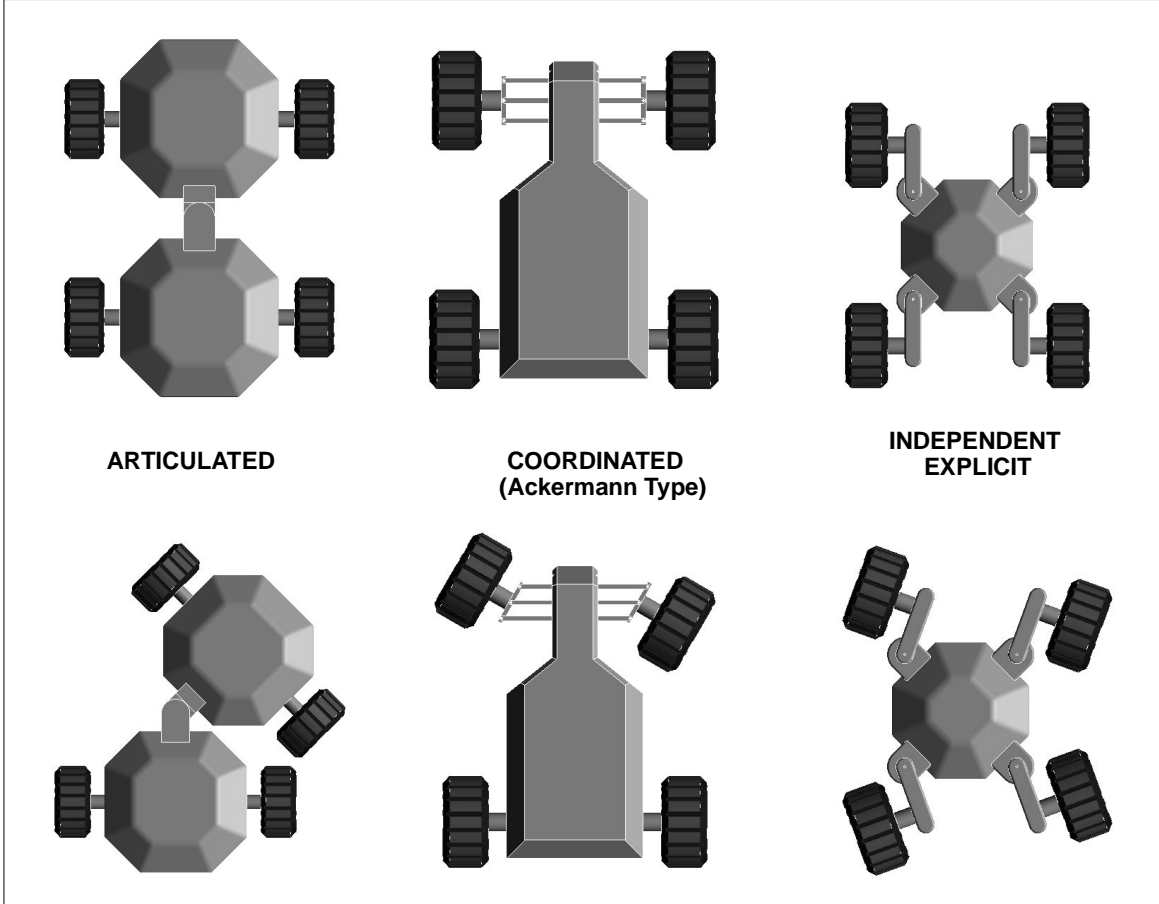

ARTICULATED   **COORDINATED (Ackermann Type)**   **INDEPENDENT EXPLICIT**

Figure 10: Steering geometries.

3.3.2 Motion Resistance and Traction for Steering

When a robot is skid steering, the lateral motion of the wheels causes a significant dissipation of energy due to the bulldozing and compaction of the terrain. The lower the wheel sinkage, the higher the efficiency of the steering motions and the lower the power draw to complete those motions.

Consider the case of a four-wheel skid steered robot. To achieve a specified heading change the wheels on the left and right sides of the chassis are servoed to different velocities. This particular steering is known as *differential steering*. Assuming that the robot is on level ground and that the contact pressure is uniformly distributed on each wheel, the wheels are subjected to longitudinal resistive forces R_i (primarily due to soil compaction) and lateral resistive forces $R_{l/i}$ (due to scrubbing on the ground or bulldozing of the soil). L_{ww} and B_{ww} denote the wheel base and wheel stance of the chassis, respectively. Due to the large inertia of the chassis and the interaction between the wheel and the ground, any heading change

involves a dynamic response of the locomotion system. When the skid steering maneuver is performed at low speeds one can describe the kinetics of the robot in steady-state terms.
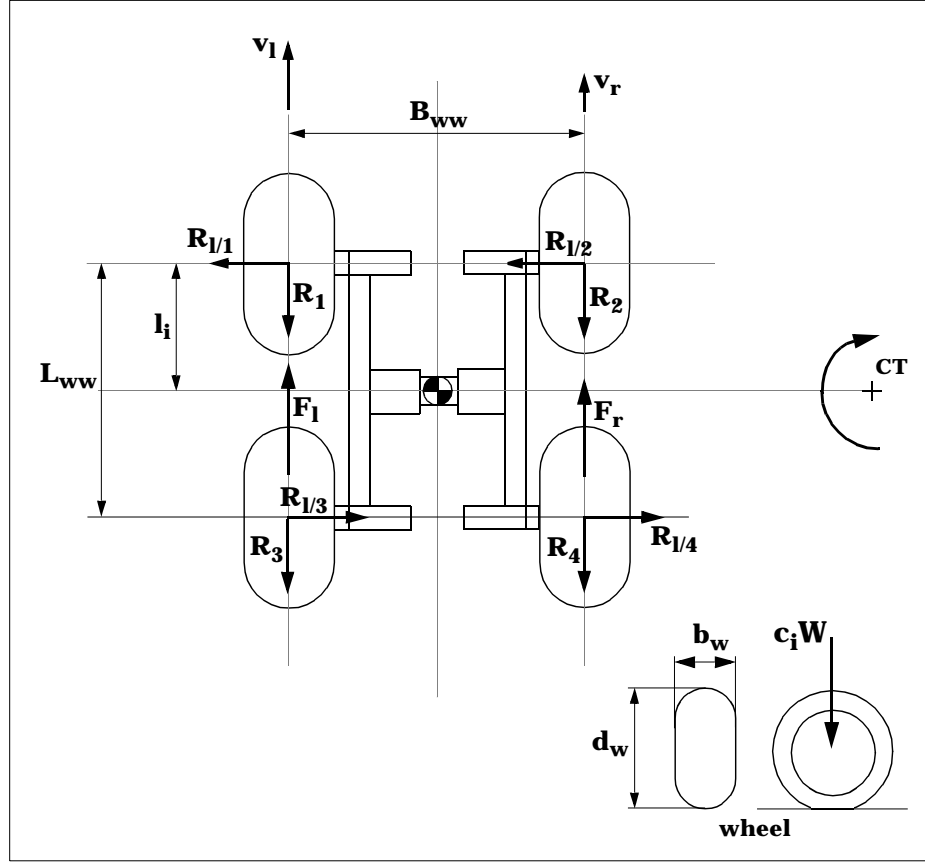
Figure 11: Differential skid steering of a four-wheel robot on flat terrain.

To sustain traction while turning, the sum of the tractive forces must be greater than the total motion resistance, and the moment of the steering resistance M_{sr} (the sum of the moments of the lateral resistance forces about the center of gravity of the robot) must equal the total moment of the tractive forces about the same point:

$$F_l + F_r \geq \sum_{i=1, N_w} R_i$$

$$\left(\frac{B_{ww}}{2}\right)(F_l - F_r) = \sum_{i=1, N_w} R_{s/i} l_i = M_{sr}$$

$$R_{s/i} = \mu_s(c_i W)$$

$$\sum_{i=1, N_w} c_i = 1$$

[39]

These equations apply to skid steering of a locomotion chassis with N_w wheels and wheel loading $c_i W$, where W is the weight of the robot and c_i are the coefficients of weight distribution. The lateral motion resistance $R_{s/i}$ is proportional to the wheel loading and a coefficient of sliding friction, μ_s.

In the case of a four-wheel chassis with equal weight distribution on the wheels, the equation of the steering moment becomes:

$$\left(\frac{B_{ww}}{2}\right)(F_l - F_r) = \frac{\mu_s W L_{ww}}{2} \qquad [40]$$

The tractive force developed by the left and right sides of the chassis can then be derived from the traction-resistance and the steering moment relationships:

$$F_r = F_l - \frac{\mu_s W L_{ww}}{B_{ww}}$$

$$F_l \geq \frac{\mu_s W L_{ww}}{2B_{ww}} + \frac{1}{2} \sum_{i=1,N_w} R_i \qquad [41]$$

Considering that the motion resistance to a steady-state skid steering maneuver consists primarily of compaction and bulldozing of the soil, as well as the rolling resistance of the tire, then:

$$(cA_l + W_l \tan\phi)\left(1 - e^{\frac{-j}{K}}\right) \geq \frac{\mu_s W L_{ww}}{2B_{ww}} + \frac{1}{2} \sum_{i=1,N_w} (R_{c/i} + R_{b/i} + R_{r/i}) \qquad [42]$$

or in terms of the robot locomotion parameters L_{ww} and B_{ww}:

$$\frac{L_{ww}}{B_{ww}} \leq \left(\frac{2}{\mu_s W}\right)\left((cA_l + W_l \tan\phi)\left(1 - e^{\frac{-j}{K}}\right) - \left(\frac{1}{2} \sum_{i=1,N_w} (R_{c/i} + R_{b/i} + R_{r/i})\right)\right) \qquad [43]$$

Configuration equation [43] can be used to estimate the configuration parameters L_{ww} and B_{ww} that allow a four-wheel robot to skid steer without loss of traction on specific terrain (c, ϕ, j, K) and vehicle-terrain interaction (A, μ_s). If this condition is not satisfied, the wheels on the chassis side away from the center of turning will experience excessive slipping, and the necessary traction to perform the turn will be lost. If the wheelbase and stance dimensions are specified from the stowability or other system-level geometric constraints, one can use the above equations to estimate the wheel dimensions d_w and b_w as they appear in the analytical expressions for motion resistance terms described in the previous sections. The selected wheel dimensions should satisfy both trafficability and steerability constraints.

3.4 Configuration for Terrainability

In addition to generating traction and changing the vehicle's heading, locomotion may carry the robot through rough terrain. Terrainability is the locomotion's ability to negotiate rough terrain features without compromising the vehicle's stability and forward progress. As a metric of robotic locomotion performance, terrainability is related to perception and autonomous navigation, whose safe and accurate execution depend on locomotion's capacity to overcome or adapt to terrain irregularities.

This chapter focuses on configuration issues of gradeability. Gradeability is the maximum slope a vehicle can climb without compromising its static stability or stalling the traction prime movers. Equally important limitation on gradeability is the ground's strength to provide the thrust required for locomotion, assuming there is enough continuous torque and power to propel the robot. The objective of configuration for gradeability is to formulate and analyze the constraints of static stability, applied drive torque, and soil thrust in terms of locomotion configuration parameters. In addition, the capability of a robot to climb a slope could be assessed by its *energy stability margin*, which, in the case of wheeled robots, is the minimum amount of energy required to tip the rover about pairs of wheels.

3.4.1 Static Stability

The stability of a wheeled robot which is stationary or moving at a constant speed is expressed in terms of the *gravitational stability margin*, which is the minimum distance from the center of gravity projected on the ground plane to the edge defined by the contact points of two wheels. If the robot is driving parallel to a downhill slope the gravitational stability margin is the margin of longitudinal stability, and if it drives along a cross-hill slope (or normal to a downhill) it is the lateral stability margin, respectively.

Without loss of generality, it is assumed that soil properties are homogenous over wide areas and that the terrain is undisturbed. This means that the detailed models of motion resistance and traction developed for trafficability on flat terrain are applicable here. If locomotion on compacted ground is assumed, the analysis is modified in that there are no motion resistance due to compaction or bulldozing, and that ground thrust is produced by the adhesion of the tire with the hard ground surface.

At maximum gradeability the gravitational stability margin is zero and can be estimated from the coordinates of the center of gravity with respect to the ground and the contact point of the wheels:

• Downhill gradeability

$$\theta_{dmax} = min\left\{ atan\left(\frac{(Y_{CG})_f}{Z_{CG}}\right), atan\left(\frac{(Y_{CG})_b}{Z_{CG}}\right)\right\} \qquad [44]$$
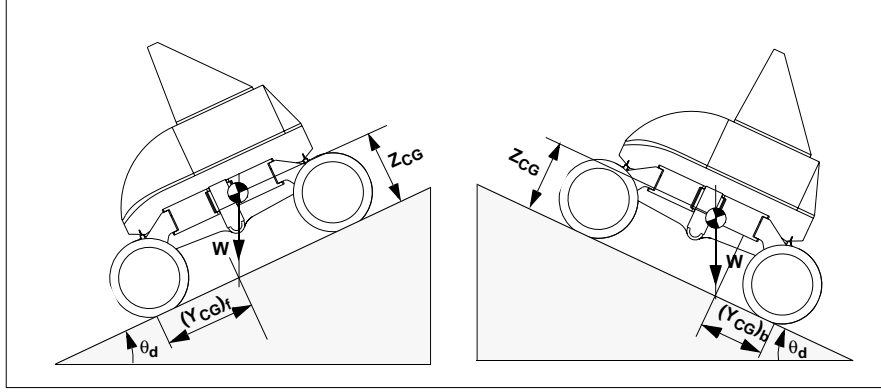
Figure 12: Maximum front $(Y_{CG})_f$ and rear $(Y_{CG})_b$ longitudinal stability margins.

• Cross-hill gradeability

$$\theta_{cmax} = min\left\{ atan\left(\frac{(X_{CG})_l}{Z_{CG}}\right),\ atan\left(\frac{(X_{CG})_r}{Z_{CG}}\right)\right\} \tag{45}$$
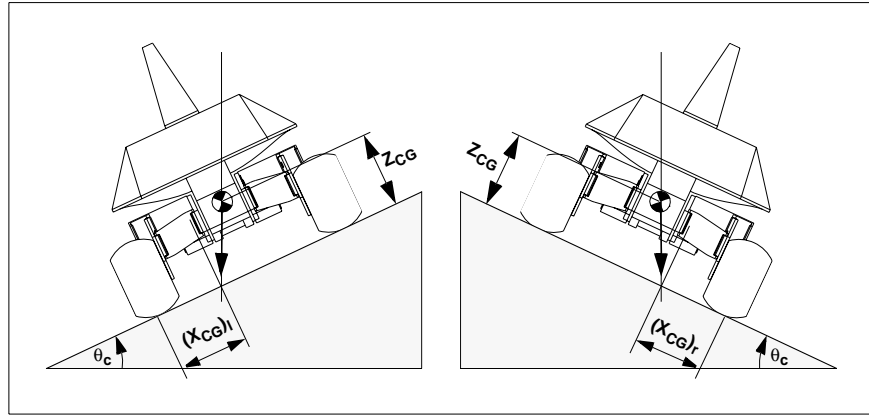
Figure 13: Maximum left $(X_{CG})_l$ and right $(X_{CG})_r$ lateral stability margins.

If the projection of the center of gravity on the ground coincides with the geometric center of the polygon whose edges are the contact points of the wheels (axisymmetric configuration), the maximum stability margins are half the wheelbase and wheel stance:

$$Y_{CG} = \frac{L_{ww}}{2}, X_{CG} = \frac{B_{ww}}{2} \Rightarrow$$
$$L_{ww} \geq 2Z_{CG} tan\theta_{dmax}(1 + SM) \tag{46}$$
$$B_{ww} \geq 2Z_{CG} tan\theta_{cmax}(1 + SM)$$

The configuration parameters L_{ww} and B_{ww} can be computed from the above equations by assuming the position of the center of gravity and estimating the desired gradeability based on information about the terrain of locomotion. SM is a configuration safety margin which

accounts for uncertainties such as the exact location of the wheel contact points and center of gravity.

3.4.2 Terrain Limitations on Gradeability

Even if a robot is stable on a slope it might not be able to climb it if the ground cannot sustain the shear forces developed at the tire-soil interface. As shown in the trafficability section, the criterion for forward motion is that the traction must exceed the summary of resistive forces. The primary component of motion resistance on steep slopes is due to the gravity component parallel to the slope and is normally greater than compaction or bulldozing resistance.

The basic model for locomotion on a slope is illustrated below:
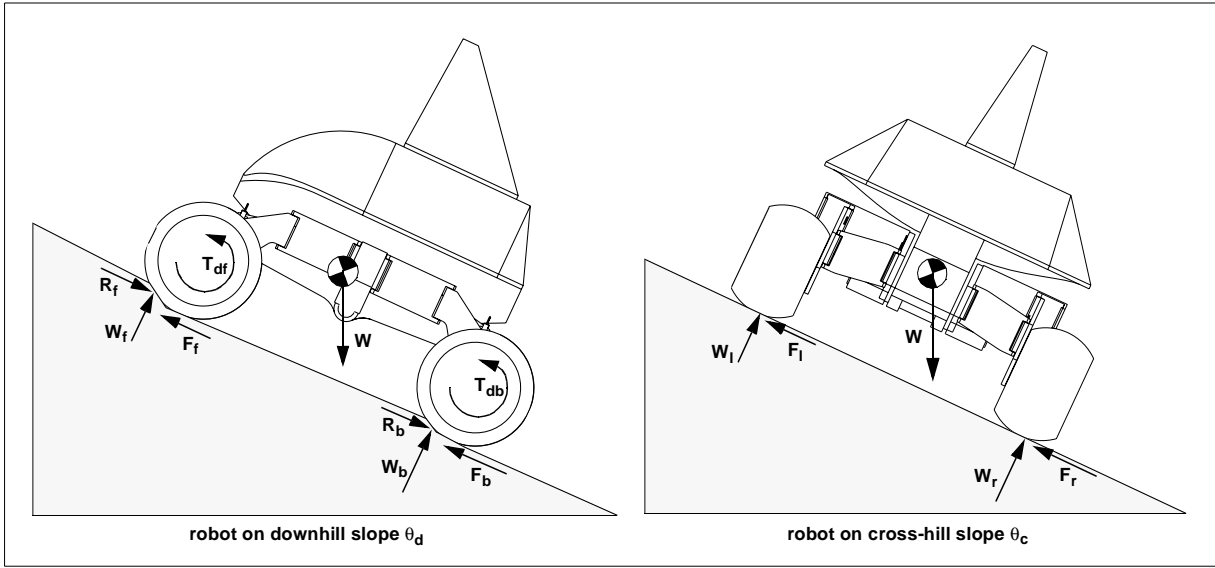
Figure 14: Forces exerted on an all-wheel drive robot on a slope.

Due to the dynamic weight transfer during slope climbing, the wheels on the downhill side are subject to higher sinkage and motion resistance than the wheels on the uphill side. However, due to greater wheel loading and increased contact patch the downhill wheels will produce more traction.

Traction can be sustained if:

$$F_{wheel} \geq \sum R_{wheel} \Rightarrow$$

$$(cA_w + W_w cos\theta_d tan\phi)\left(1 - e^{-\frac{J}{K}}\right) \geq R_{cw} + R_{bw} + R_{rw} + R_{gw}$$

[47]

Configuration equation [47] is non-linear with respect to slope angle, wheel loading and wheel dimensions. To facilitate configuration wheel slip is assumed zero and compaction and bulldozing can be neglected providing a very low sinkage value. By substituting rolling

and gravitational resistance the condition for sustaining traction on a slope becomes:

$$cA_w + W_w\cos\theta_d\tan\phi \geq f_r W_w\cos\theta_d + W_w\sin\theta_d \Rightarrow$$

$$(-1)\sin\theta_d + (\tan\phi - f_r)\cos\theta_d + \frac{cA_w}{W_w} \geq 0 \tag{48}$$

The gradeability of the wheel is:

$$\theta_{dmax} = 2\,atan\left(\frac{1 + \sqrt{1 - (f_r - \tan\phi)^2 - \left(\frac{cA_w}{W_w}\right)^2}}{\left(f_r - \tan\phi + \frac{cA_w}{W_w}\right)}\right) \tag{49}$$

Acceptable solutions to [49] are those for which both the numerator and denominator are positive real numbers. Assuming a weight distribution on the wheels as discussed in [3.2.3.4], these constraints provide a basis for selecting tire material and geometry based on the calculation of the coefficient of rolling resistance and the contact area between the tire and the ground. Alternatively, for a given tire material an optimal wheel loading can be computed and estimates of the location of the center of gravity can be made.

As a special case, the gradeability of a robot with pneumatic tires can be estimated from the simplified traction constraint, by substituting the contact area with the average ground pressure and the wheel loading (the sum of the inflation pressure of the tire and the stiffness of the carcass):

$$A_w = \frac{W_w\cos\theta_d}{p_{gr}}$$

$$c\frac{W_w\cos\theta_d}{p_{gr}} + W_w\cos\theta_d\tan\phi \geq f_r W_w\cos\theta_d + W_w\sin\theta_d \Rightarrow \tag{50}$$

$$\theta_{dmax} = atan\left(\frac{c}{p_{gr}} + \tan\phi - f_r\right)$$

The profound effect of soil composition on gradeability is captured by a parametric study using [50] (summarized in Table 3). Gradeability as determined by the strength of the soil varies significantly from cohesive to frictional soils, tire inflation, and the coefficient of rolling resistance between the tire and the ground. For weak soils such as lean clay, soil strength appears to be the determining factor of gradeability. At the other end of the spectrum, cohesive soils could sustain locomotion on slopes greater than 45 degrees, which implies that considerations of static stability or maximum available traction power become the determining factors of gradeability.

Soil type	f_r	c (psi)	ϕ (deg)	Gradeability (deg) p_{gr}= 15 psi	Gradeability (deg) p_{gr}= 30 psi
Dry sand	0.20-0.30	0.15	28	18.9	13.3
Lean clay	0.15	2.90	12	14.4	9.1
Heavy clay	0.08	9.87	33	50.8	41.2
Sandy loam	0.25	1.18	32	24.4	22.5

Table 3: **Effect of soil geophysical properties on the gradeability of a robot with pneumatic tires.**

3.4.3 Power Limitations on Gradeability

In addition to stability and soil trafficability limitations, a robot's gradeability could be constrained by the amount of power and torque transmitted to the powered wheels. Assuming no wheel slippage, minimal sinkage, and no dynamic effects, the robot's gradeability subject to power limitations can be determined from the expression:

$$P_{wheel} \geq (f_r W_w \cos\theta_d + W_w \sin\theta_d) V \Rightarrow$$

$$\theta_{dmax} = 2\,atan\left(\frac{1 + \sqrt{1 - f_r^2 - \left(\frac{P_w}{VW_w}\right)}}{f_r + \frac{P_w}{VW_w}}\right),\ 1 - f_r^2 - \left(\frac{P_w}{VW_w}\right) \geq 0 \qquad [51]$$

If a maximum output torque is specified, gradeability can be calculated as:

$$\theta_{dmax} = 2\,atan\left(\frac{1 + \sqrt{1 - f_r^2 - \left(\frac{2T_{drw}}{d_w W_w}\right)}}{f_r + \frac{T_{drw}}{d_w W_w}}\right),\ 1 - f_r^2 - \left(\frac{T_{drw}}{d_w W_w}\right) \geq 0 \qquad [52]$$

3.4.4 Drawbar Pull Limitations on Gradeability

The capability of a wheeled robot to climb over sloped terrain is limited by the shear strength of the soil and the static stability margins. The ratio of drawbar pull to wheel loading of a robot climbing a slope at a steady-state fashion and at a 20% slip, is approximately equal to its gradeability [Turnage89]. Assuming that the robot's prime mover and drivetrain can deliver the necessary power, the configuration equation that captures drawbar pull's limitation on gradeability is as follows:

$$\theta_{max} = atan\left(\frac{DP}{W_w}\right) \qquad [53]$$

For any given type of terrain there exists a wheel loading distribution that maximizes gradeability. To maximize drawbar pull when climbing slopes of varying terrain composition, the position of the center of gravity needs to vary by actively changing the posture of the robot's body or by shifting mass towards the downhill wheels.

Chapter 4

CONFIGURATION OF NOMAD'S ROBOTIC LOCOMOTION

Configuration parameters derived through LocSyn established the constraints upon which the design of the robot Nomad was synthesized and built. Three experimental programs allowed for the characterization of Nomad's locomotion performance and comparisons with LocSyn's results. The first program evaluated the performance of single wheel in sand. The wheel was equipped with the actuation and control units of Nomad's wheels. The second program studied Nomad's gradeability and drawbar pull performance on hard ground. Finally, an elaborate experimental program quantified Nomad's maneuverability using two distinct types of tires and two modes of steering achievable with Nomad's transforming chassis. The ultimate proving ground for Nomad's robotic locomotion was the Atacama desert in Chile where it successfully traversed 223.5 kilometers of rugged desert terrain in 45 days. Nomad's locomotion performance is probably unmatched by any robot of the similar mass and geometry scale.
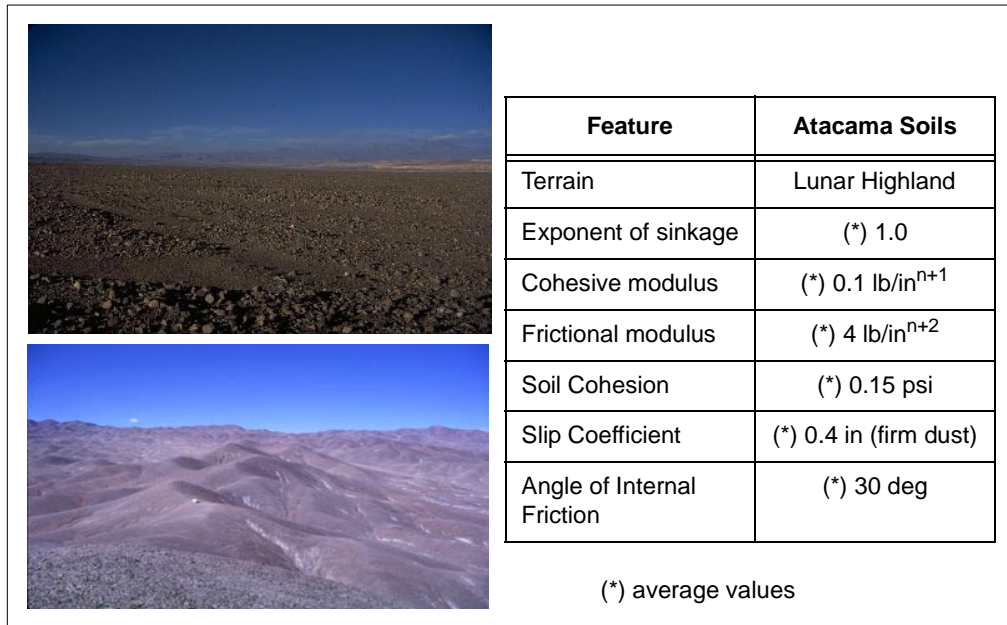
4.1   Exploration of a Terrestrial Planetary Analog

Planetary exploration is one of the most intriguing application domains for robotics. The unique requirements of space transportation and operations in environments radically different than those on Earth has prompted great innovation in robot mechanism design. Some the most unique locomotion systems such as that of the Lunar Roving Vehicle [Heiken91], the Russian Lunokhods [Kemurdjian92] and Sojourner Pathfinder [Bickler92] have showcased the significance of unique locomotion concepts carefully engineered for missions that involve mobility over unknown terrains.

Some of Earth's most challenging environments such as deserts and polar regions are ideal proving grounds for robot designs with potential for future space missions. The diurnal cycle, solar insolation, terrain morphology, and remoteness are some of the features that make these environments planetary analogs. However, due to major differences in atmospheric composition and the weathering processes areas in which the geophysical properties of soils can approximate those of lunar or Martian regolith are rare. In the Atacama desert in Chile, no measurable rainfall in centuries has made it one of the driest and most arid places on Earth. High weathering due to wind has resulted in similarities to the lunar and Martian highlands. The Atacama desert was selected as the site for a long-distance, month-long robotic traverse by Nomad.

| Feature	Atacama Soils
Terrain	Lunar Highland
Exponent of sinkage	(*) 1.0
Cohesive modulus	(*) 0.1 lb/in^{n+1}
Frictional modulus	(*) 4 lb/in^{n+2}
Soil Cohesion	(*) 0.15 psi
Slip Coefficient	(*) 0.4 in (firm dust)
Angle of Internal Friction	(*) 30 deg

(*) average values

Figure 15: Characteristic terrain geomorphology and expected soil geophysical properties of the Atacama desert.

An accurate *a priori* characterization of the Atacama terrain was not possible because there had been no data on the statistical distribution of major terrain features, detailed geomorphological maps or soil classifications. Even if some data had existed, elaborate stochastic models would have to devised to capture the wide variations in local terrain composition.

Due to the similarities between Atacama and lunar landscapes, a terrain model for obstacle and slope distribution for lunar highlands was adapted [Heiken91]. The lunar highlands model proved to be a conservative estimate of the actual distribution of positive and negative obstacles and slopes in the Atacama desert. Other environmental considerations such as average daily temperature variations and wind speed were taken into account in the detailed design of the rover once the optimal locomotion configuration was selected.

A scouting expedition to the Atacama desert provided additional information on the type of hard obstacles and composition of weak soils. Returned soil samples offered an important input to the selection of a fine-grain sand that was used to test the rover's locomotion elements.
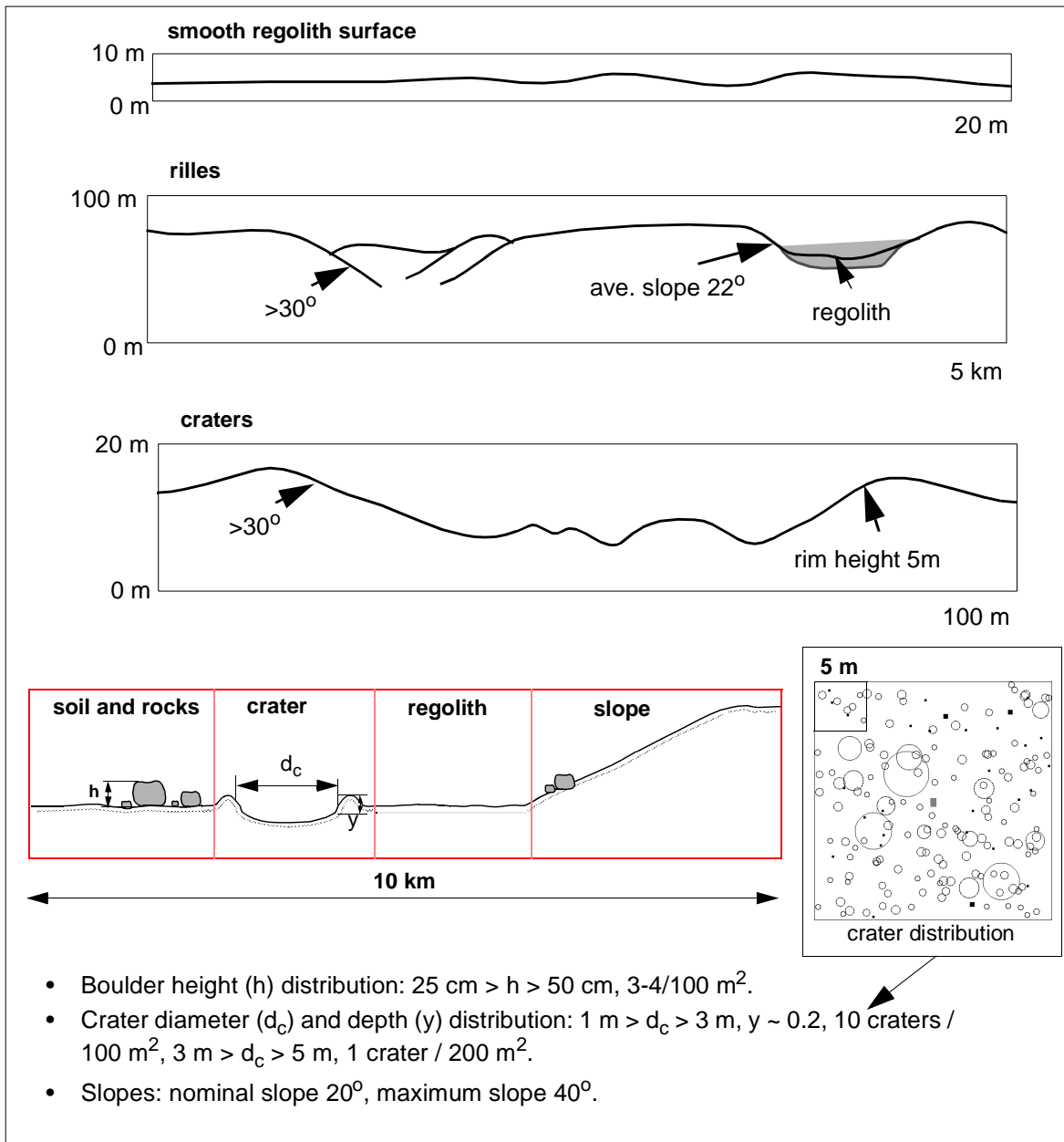
Figure 16: Distribution of positive (boulder) and negative (crater) obstacles and slopes in lunar highlands. A scouting trip to the Atacama desert revealed that the illustrated lunar model is conservative compared to the actual obstacle and slope distributions in the Atacama.

The following text appears within the figure:

smooth regolith surface
10 m
0 m
20 m

rilles
100 m
>30°
ave. slope 22°
regolith
0 m
5 km

craters
20 m
>30°
rim height 5m
0 m
100 m

5 m
crater distribution

soil and rocks | crater | regolith | slope
d_c
h
y
10 km

- Boulder height (h) distribution: 25 cm > h > 50 cm, 3-4/100 m^2.
- Crater diameter (d_c) and depth (y) distribution: 1 m > d_c > 3 m, y ~ 0.2, 10 craters / 100 m^2, 3 m > d_c > 5 m, 1 crater / 200 m^2.
- Slopes: nominal slope 20°, maximum slope 40°.

4.2 LocSyn's Implementation on Nomad's Configuration

Nomad's locomotion configuration was synthesized using LocSyn's trafficability, maneuverability and terrainability configuration equations. Environmental/task parameters were derived from the specification of the environment using the terrain model of lunar highlands and geophysical properties of low-cohesion soils (characteristic of desert sands and lunar regolith) as summarized in Section 4.1.

Additional design and performance constraints were established in response to a programmatic requirement that the Nomad robot should exhibit the mass and geometric scale of one of a pair of lunar rovers that could be carried onboard a Phobos-class Lander, and that the combined system of rovers and lander would fit into the payload fairing of the Russian Proton launch vehicle [Whittaker95]. The most critical requirements were that the weight of the flight rover should be less than 600 pounds and that it should fit in a rectangular volume whose maximum length should be less than 8 feet and the maximum width and height should be less than 6 feet [Apostolopoulos96]. Considerations of state-of-the-art in autonomous navigation and safeguarded teleoperation yielded important requirements of speed and chassis geometry. Research at the time of Nomad's configuration had demonstrated reliable autonomous speeds of 0.5 ft/s (0.15 m/s) on rugged terrain and 1.5 ft/s (0.45 m/s) in benign terrain. These constraints were taken into account not only in the locomotion configuration but also in the detailed design of Nomad's actuation and drivetrain subsystems.
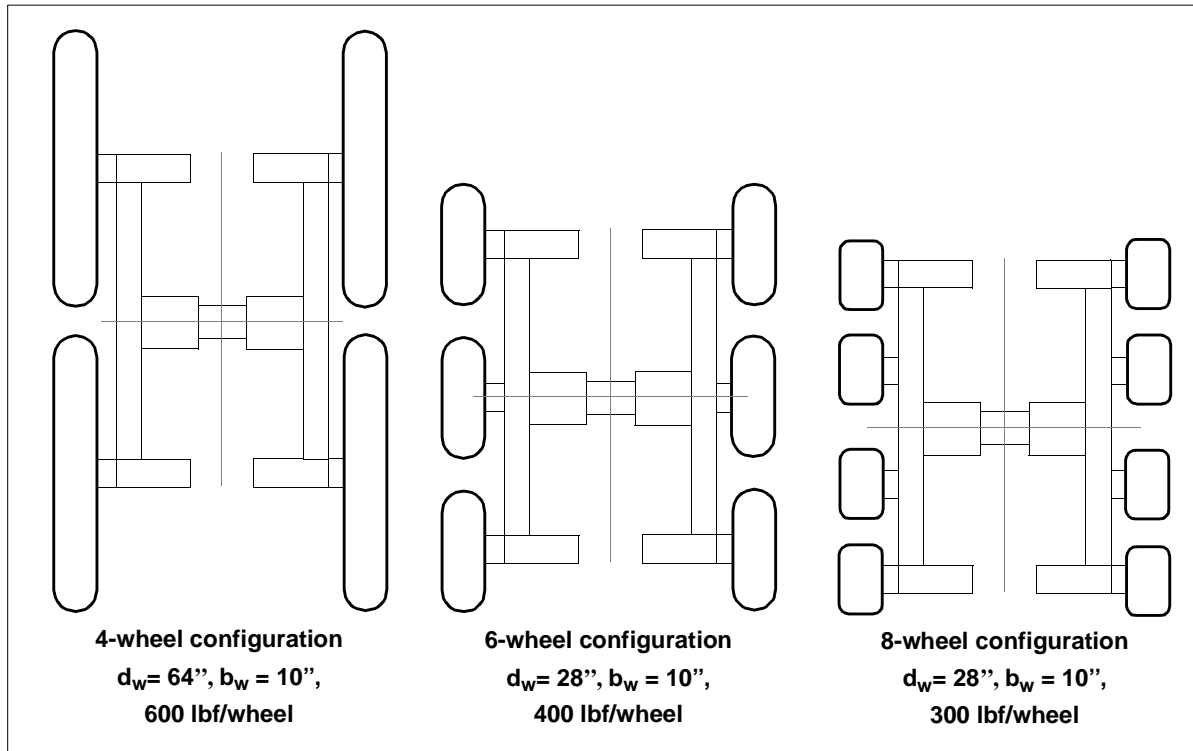
4.2.1 Wheel Dimensions

LocSyn's configuration equations of sinkage, motion resistance and drawbar pull were exhaustively utilized to define the trade-offs among various wheel types. To demonstrate how configurations can be synthesized from configuration equations, consider the study of static sinkage of a solid wheel in fine-grained sand. The configuration issue is to estimate the wheel dimensions that limit sinkage to within a performance specification. The following table summarizes LocSyn's output of a study in which the configuration parameter of interest is wheel diameter and is computed for a variety of wheel loads, sinkage values, and two different types of terrains.

SINKAGE / WHEEL WIDTH	LOADING		
	300 lbf	400 lbf	600 lbf
$z= 2$", $b_w= 10$"	$d_w= 28.5$"	50.5"	114"
$z= 3$", $b_w= 20$"	16"	29"	65"
$z= 2$", $b_w= 10$"	9"	15.5"	35"
$z= 3$", $b_w= 20$"	5"	9"	20"

Table 4:   **Minimum wheel diameter required to maintain sinkage below a desired value, given a nominal wheel width and wheel loading.**

For a given vehicle configuration there is a substantial increase in the wheel diameter if sinkage is to be kept the same for radically different types of terrain. This effect is more pronounced as wheel loading increases. Also, if the wheel width is kept constant, a 50% decrease in expected sinkage requires an average increase of 300-400% in wheel diameter, depending on the geophysical properties of the terrain.

4-wheel configuration
d_w= 64", b_w = 10",
600 lbf/wheel

6-wheel configuration
d_w= 28", b_w = 10",
400 lbf/wheel

8-wheel configuration
d_w= 28", b_w = 10",
300 lbf/wheel

Figure 17: The impact of wheel sinkage on the geometric configuration of four-wheel, six-wheel, and eight-wheel locomotion configurations that use the same shape tires. In this case the assumed medium of locomotion is fine sand and the maximum allowable sinkage is 2.5" and nominal wheel width is 10". This analysis assumes a safety factor of 4 in all cases which means that each wheel is expected to sustain four times the nominal load of 600 lbf divided over the number of wheels. The chassis dimensions are the same for all three configurations.

This case illustrates the power of parametric analysis in configuration. An eight-wheel configuration offers the most compact solution when the optimization criterion is to minimize wheel sinkage. However, the eight wheel configuration may be disadvantageous because of increased actuation mass and wiring complexity.

At this point, it is important to make note of two significant points. The first is that the configuration of Nomad considered only all-wheel drive concepts. This is because, independent of configuration, an all-wheel drive robot, like any all-wheel drive traditional ground vehicle, produces greater traction and drawbar pull and can climb greater obstacles than any equivalent configuration that does not feature all-wheel drive. The second point is that the type of optimization required for some performance parameters is independent of the specific mission and requirements of the robot under configuration. For instance, locomotion configuration should always maximize traction. A counter example is that of

sinkage for which the optimal configurations may not necessarily be the ones that minimize sinkage. In special cases such as those involving locomotion in weak soils, an increase in sinkage leads to measurable increase in traction which may overweigh any negative effects due to additional compaction and bulldozing of the soil.

4.2.2 Wheel Shape

LocSyn's study of the wheel shape that maximizes soil thrust considered equations [14], [15] and [16]. LocSyn estimated the maximum available traction that could be sustained between a cylindrical, spherical or road-tire shaped wheel in sand. The results are summarized in the following tables. In addition to evaluating the effects of wheel shape on traction, a comparison between rigid and flexible tires was made for each one of the wheel-shape classes. In all cases it was assumed that the tire inflation pressure was 4 psi and the maximum allowable sinkage was 0.8".

|	with sinkage		zero sinkage	
Cylindrical	**300 lbf**	**600 lbf**	**300 lbf**	**600 lbf**
d_w= 30", b_w= 15"	F= 126	253	139	268
d_w= 20", b_w= 20"	126	253	139	268
d_w= 25", b_w= 20"	126	253	140	270
d_w= 30", b_w= 20"	126	253	141	271

Table 5: Maximum traction (lbf) developed by a solid (non-zero sinkage) and flexible (zero sinkage) cylindrical wheel in sand.

	with sinkage		zero sinkage	
Tire shaped	**300 lbf**	**600 lbf**	**300 lbf**	**600 lbf**
d_w= 15", b_w= 10"	F= 130	259	144	284
d_w= 20", b_w= 10"	129	254	142	271
d_w= 15", b_w= 15"	128	261	138	287
d_w= 20", b_w= 15"	134	261	155	287

Table 6: Maximum traction (lbf) developed by a solid (non-zero sinkage) and flexible (zero sinkage) road-tire shaped and spherical wheel in sand.

The range of values for the configuration parameters of wheel diameter and nominal wheel width were such that a configuration with three to eight wheels could meet the stowability requirements of the combined Phobos payload in a Proton fairing. In all cases, the road-tire shaped and spherical wheels produce more traction than the cylindrical wheels in fine sand.

If the configuration optimization is based on a maximum expected available traction on the drive shafts (this is a design limitation that may be imposed if, for example, there is only one type of available actuator), then in all cases road-tire shaped wheels offer the most compact solution.
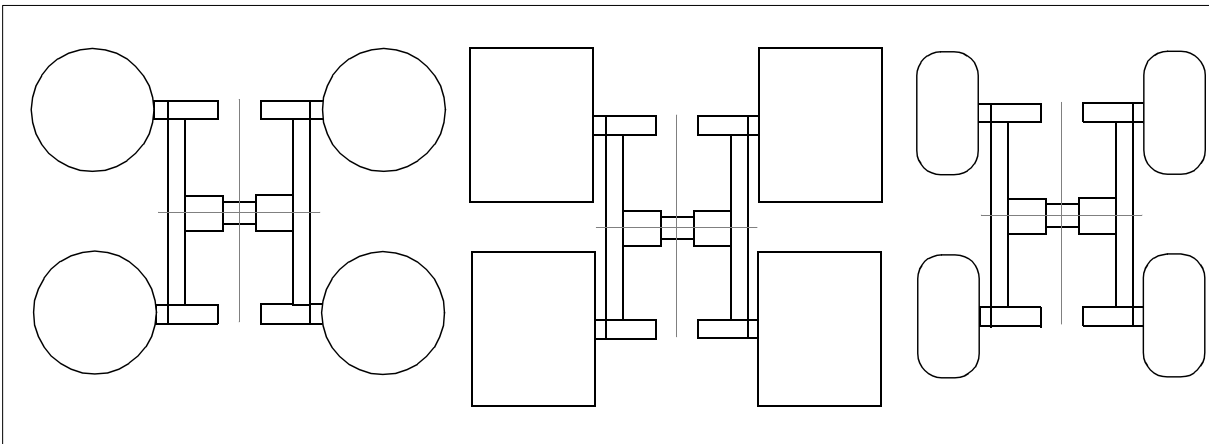
Figure 18: **Comparison of locomotion configurations that could develop the same amount of traction in sand. The road-tire shaped wheels (right) offer the most compact solution in terms of maximum locomotion volume. Spherical (left) and cylindrical wheels (middle) are advantageous in terms of the available enclosed volume for actuation and drivetrain components.**

The combined results of the wheel sinkage and traction studies had a direct impact on Nomad's robotic locomotion. A decision was made to use a tire that exploits the benefits of both spherical and road-tire shapes because of their high traction potential for locomotion in sand. The observed lower bounds for the wheel diameter and nominal wheel width were 20" and 15", respectively. The upper bounds of these configuration parameters were to be determined by detailed study of the optimal number of wheels for the specified terrain and soil properties, and requirements of mass, volume and speed.

Analytical results of single-wheel performance were used to make predictions of the overall locomotion performance. This is an acceptable practice in the design of all-wheel drive locomotion, even if the design of the suspension is not known. [Turnage89] demonstrated through experimentation with various wheel types and scale models, that the difference between the in-soil drawbar pull performance of a wheeled rover and the predicted vehicle performance from single powered wheel tests in sand is insignificant.

Nomad was first fitted with all-metal tires in an effort to improve its space relevance. Metal tires have been used on lunar and Martian rovers and behave admirably in weak soils similar to planetary regolith, but suffer from loss of traction and wear in saturated soils and rocky terrain. Other efforts to enhance Nomad's space relevance included the use of in-wheel electric actuators and brushless direct current motors [Whittaker95].

4.2.3 Number of Wheels

One of the most critical configuration decisions is that of the optimal number of wheels and

their placement on the chassis. LocSyn was used to examine multiple trafficability trade-offs. It considered the results of the sinkage and traction studies as input to constrain the range of acceptable wheel configuration and performance parameters. It also used the results of single wheel performance to extrapolate the performance of four, six and eight wheel configurations with rigid suspensions. The following parametric graphs capture the primary trade-off studies pursued to make a decision on the optimal number of wheels.
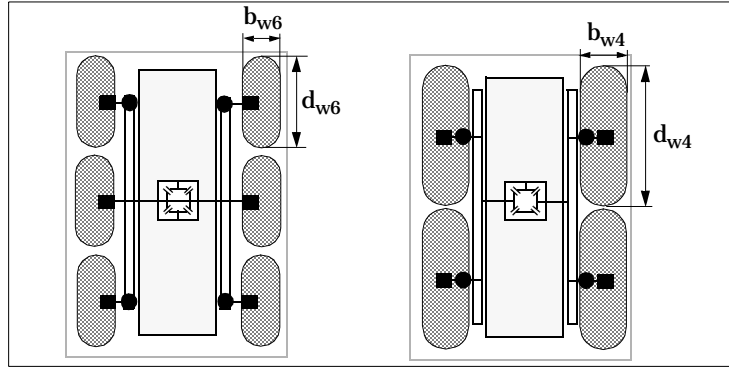

Figure 19: Locomotion configurations considered for the study of optimal number of wheels.
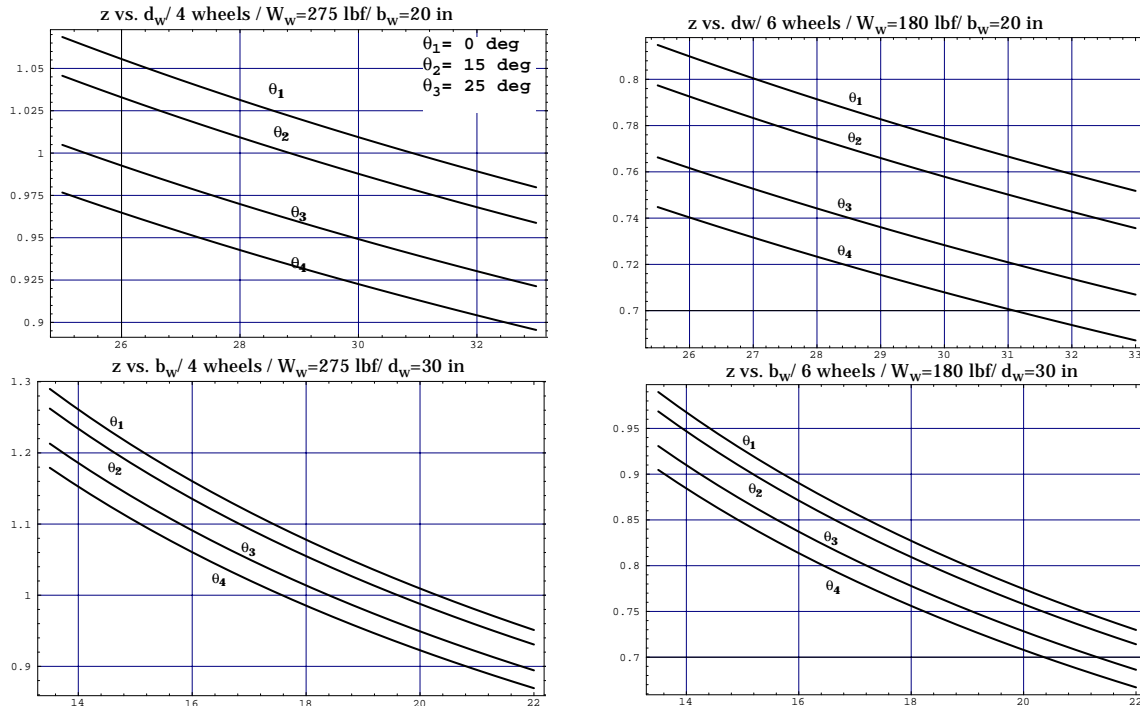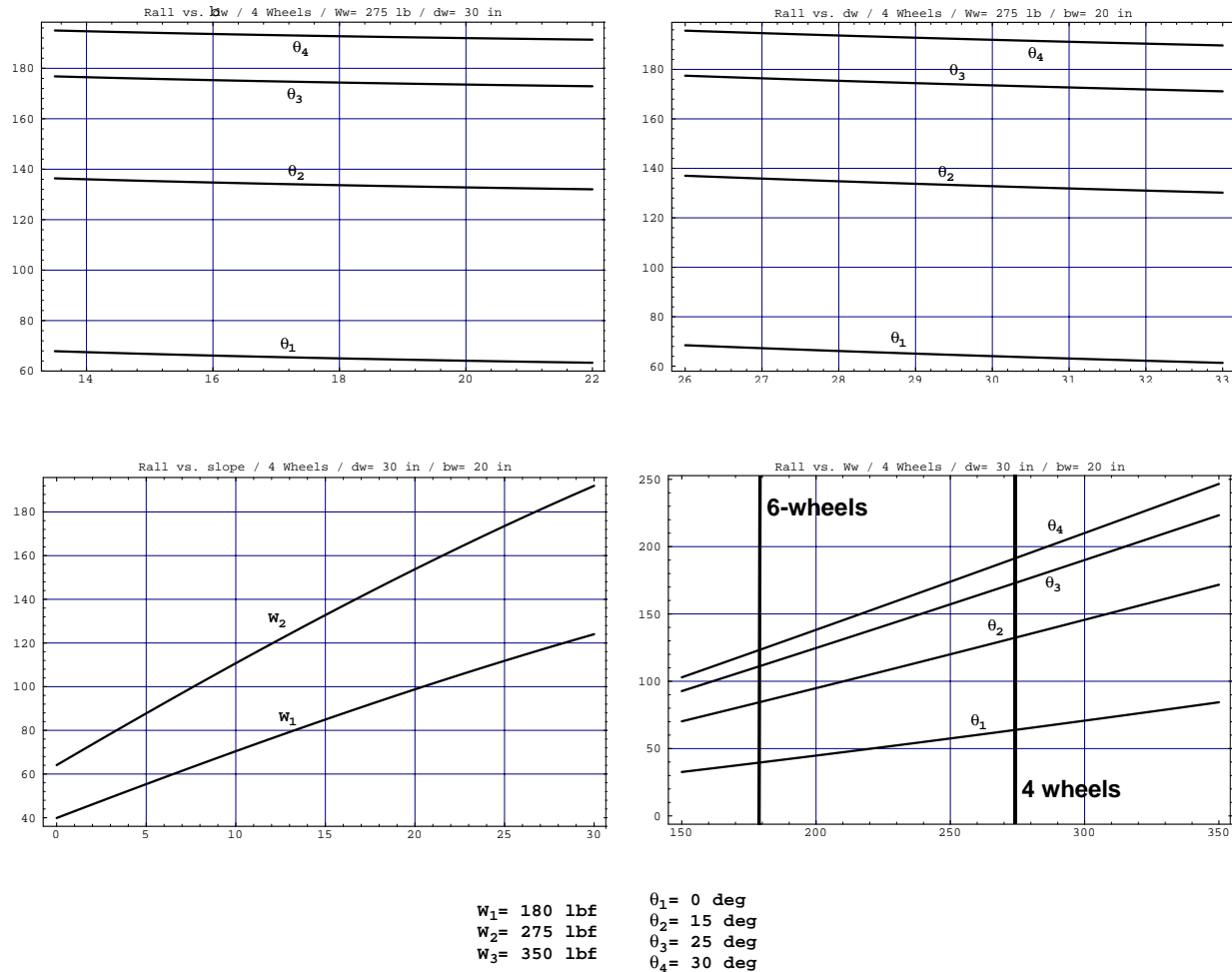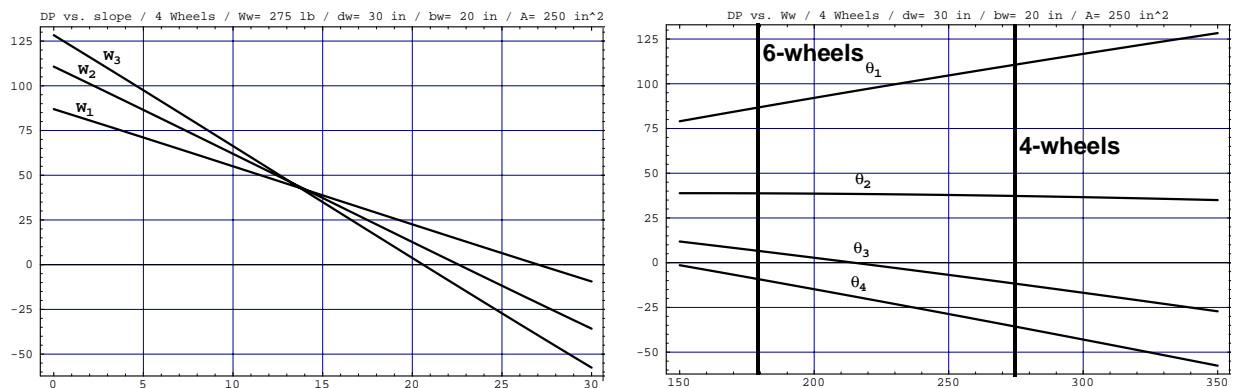

Figure 20: Wheel sinkage (in) as a function of wheel diameter (in), nominal width (in), weight distribution per wheel (lbf), slope angle (deg) and contact area (in^2). LocSyn results for four and six wheel configurations.

TOTAL MOTION RESISTANCE

DRAWBAR PULL

Figure 21: Total wheel motion resistance (lbf) and drawbar pull (lbf) as functions of wheel diameter (in), nominal wheel width (in), weight distribution (lbf) and contact area (in^2). Results obtained by LocSyn assuming circular contact patch. The graphs in which weight distribution is used are notable because they encapsulate the expected performance of the four and six wheel configurations. The weight distribution over individual wheels is 180 lbf for the six wheel configuration and 275 lbf for the four wheel configuration.

DRIVE TORQUE

Figure 22: Drive torque (in-lb) as a function of wheel loading (lbf) and slope angle (deg) for a four-wheel configuration (30" wheel diameter and 20" nominal wheel width). Similar results are presented for a six wheel configuration in Appendix A.

DRIVE POWER
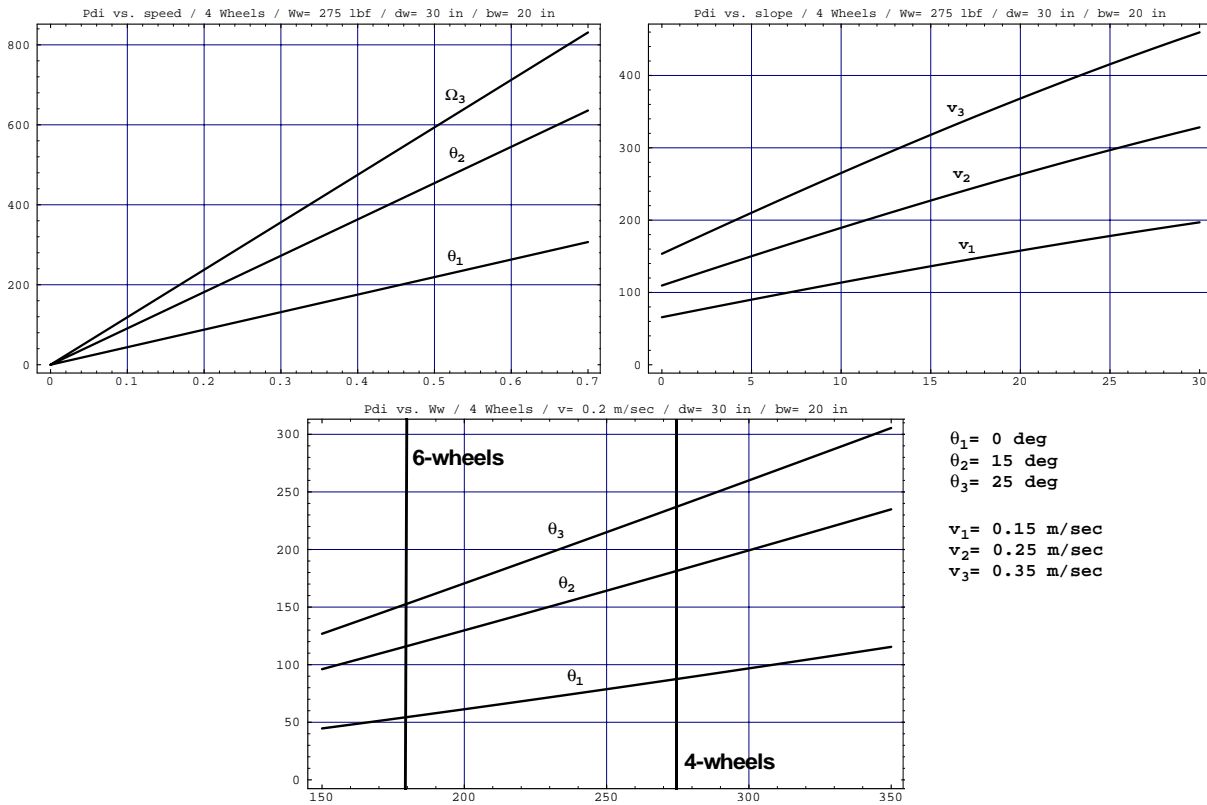
Figure 23: Drive power (W) as a function of speed (ft/s) (top-left), slope angle (deg) (top-right) and wheel loading (lbf) (bottom). The weight distribution over individual wheels is 180 lbf for the six wheel configuration and 275 lbf for the four wheel configuration. These graphs actu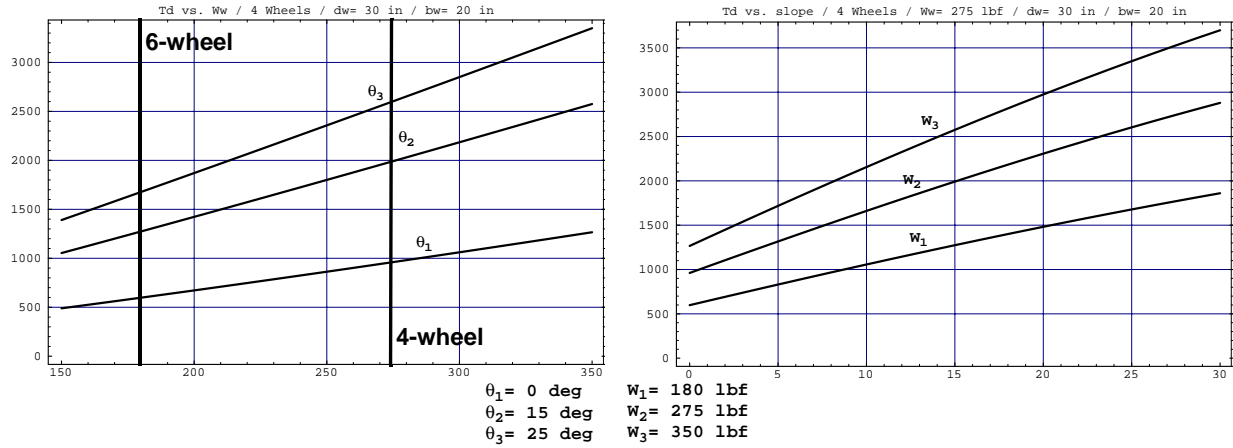ally illustrate the total input drive power which takes into consideration the following efficiencies: $\eta_{(drivetrain)}$= 0.85, $\eta_{(motor)}$= 0.85, $\eta_{(amplifier)}$= 0.90.

PERFORMANCE METRIC	6-WHEEL CONFG (d_w= 20 in, b_w= 15.75 in)	4-WHEEL CONFG (d_w= 30 in, b_w= 20 in)	% change from 6 to 4
sinkage [in]	1.34	1.01	↓ 24.6%
soil thrust [lbf]	175	175	-
total resistance [lbf]	82	62	↓ 24.4%
drawbar pull [lbf]	93	113	↑ 21.5%
max. negotiable slope [deg]	18.7	22.3	↑ 21.2%
drive torque/wheel [in-lb]	860	930	↑ 8.1%
travelling speed [ft/s]	*1.15*	*1.15*	-
drive power/wheel (output) [W]	128	96.5	↓ 24.6%
drive power/wheel (input) [W]	222	167.5	↓ 24.6%
total drive power [W]	444	335	↓ 24.6%

Table 7: Summary of the expected trafficability of six-wheel and four-wheel configurations with rigid suspension on flat terrain (LocSyn data).

PERFORMANCE METRIC	6-WHEEL CONFG (d_w= 20 in, b_w= 15.75 in)	4-WHEEL CONFG (d_w= 30 in, b_w= 20 in)	% change from 6 to 4
sinkage [in]	18.7	18.7	-
soil thrust [lbf]	1.29	0.98	↓24%
total resistance [lbf]	163	148.3	↓ 9%
drawbar pull [lbf]	~ 3	~ 16	~0%
drive torque/wheel [in-lb]	1,604	2,224.5 @18.7 deg	↑ 38.7%
travelling speed [ft/s]	*1.15*	*1.15*	-
drive power/wheel (output) [W]	108.8	99 @18.7 deg	↓7.5%
drive power/wheel (input) [W]	189	172 @18.7 deg	↓7.5%
total drive power [W]	378	344 @18.7 deg	↓7.5%

Table 8: Summary of the expected trafficability of six-wheel and four-wheel configurations with rigid suspension on inclined terrain (LocSyn data). These results were obtained for a slope of 18.7 deg which according to the study of flat terrain trafficability (Table 7) is the maximum slope that the six wheel configuration could negotiate based on limitations of drawbar pull.

The results showcased in Tables 7 and 8 give an advantage to the four-wheel configuration primary because of the expected benefits in drawbar pull and slope climbing. Based on LocSyn's results the four-wheel configuration would produce 20% more drawbar pull and could climb a 5-degree steeper slope than the six-wheel configuration Moreover, due to reduced motion resistance, the drive torque and power requirements for the four-wheel configuration are 25% lower than the six-wheel.

The results of analyses in [4.2.3] led to the selection of a four-wheel configuration and optimized wheel dimensions for sinkage, traction and drawbar pull. Configuration studies pertaining to maneuverability and obstacle negotiation were also pursued and will be summarized in a future technical report. The main result was that the six-wheel configuration had an advantage over the four-wheel configuration regarding obstacle negotiation and smoothing of body roll and pitch motions, but the difference was insignificant. All configuration studies considered a rigid suspension which is a worst-case choice. The four-wheel, all-wheel drive configuration also offers greater design simplicity and lower control complexity than the six-wheel configuration.

4.3 Nomad's Electromechanism

Nomad features four-wheel drive locomotion with the propulsion actuators enclosed in the wheel hubs. The chassis can expand or compact by driving two pairs of four-bar mechanisms with an electric actuator on each side of the chassis. Nomad's suspension consists of loading arms pivoted on a central axle (Figure 25). Body posture averaging is achieved by the combined motion of the pivoted suspension arms and an internal averaging linkage. As a result of this type of suspension, body elevation is the average of all wheel elevations, and body pitch and roll are first differences of wheel elevations about the longitudinal and transverse axes, respectively. There are six identical actuators, four for propulsion and two for deployment/steering. The body fuselage is mounted on the central axle and the linkages of the internal averaging mechanism.

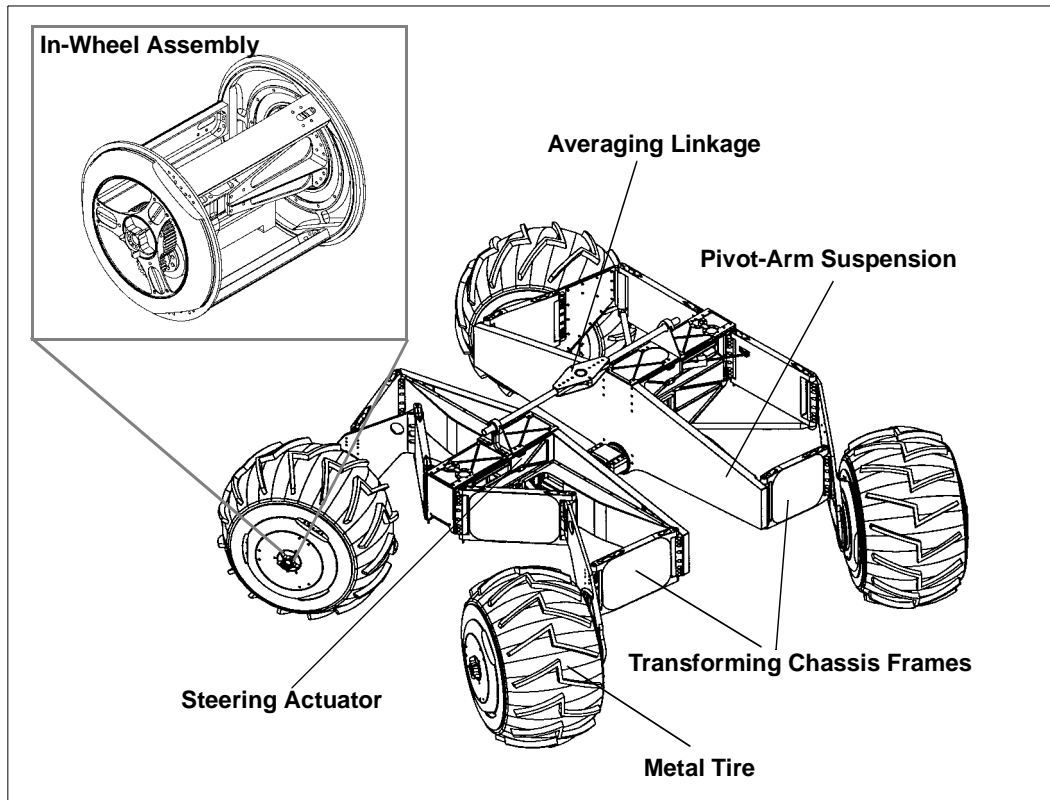**Figure 24: Nomad during the 1997 Atacama desert trek.**

Figure 25: Nomad's primary locomotion subsystems.

4.3.1 In-Wheel Propulsion

Nomad's propulsion system consists of four identical actuators placed inside the wheels. The motor and drivetrain assembly is at an offset distance below the wheel axle. In the drive unit a brushless DC motor transmits torque and power to the wheel hub through a harmonic drive and a single stage gearing reduction. The output gear is mounted on the inside face of the outward facing wheel hub. Only two bearings are needed to decouple the moving from stationary wheel parts. Wheel motion coordination is achieved electronically. Independent velocity-torque control allows for closed-loop response to traction demands on each wheel.

No electromechanical components are needed for propulsion beyond those enclosed in the wheel, with the exception of the motor wires which are routed to the body fuselage through the deployment/steering linkages. The selection of independent propulsion for all wheels has had a profound impact on Nomad's design in that it eliminated the need for mechanical transmissions and coupling.

4.3.2 Transforming Chassis

A unique feature of Nomad locomotion is a transforming chassis. Two pairs of four-bar mechanisms, each driven by an actuator are mounted on each side of the chassis. When both pairs are driven from the nominal compacted to the fully deployed configuration, the

footprint of the locomotion increases by 35% (Figure 26). The ability to change footprint has had a major impact on Nomad's overall trafficability and its amenability to autonomous control. The deployed chassis has a 20% greater static stability over its stowed configuration. Furthermore, because of reduced load transfer from the front to the rear wheels when driving on slopes, the deployed chassis can develop 10% more tractive effort than its stowed configuration and can therefore improve its gradeability by 10% based on vehicle-terrain limitations. The gradeability of the stowed rover on sandy hills has been estimated at 23 degrees, whereas the deployed chassis can climb slopes up to 28 degrees.
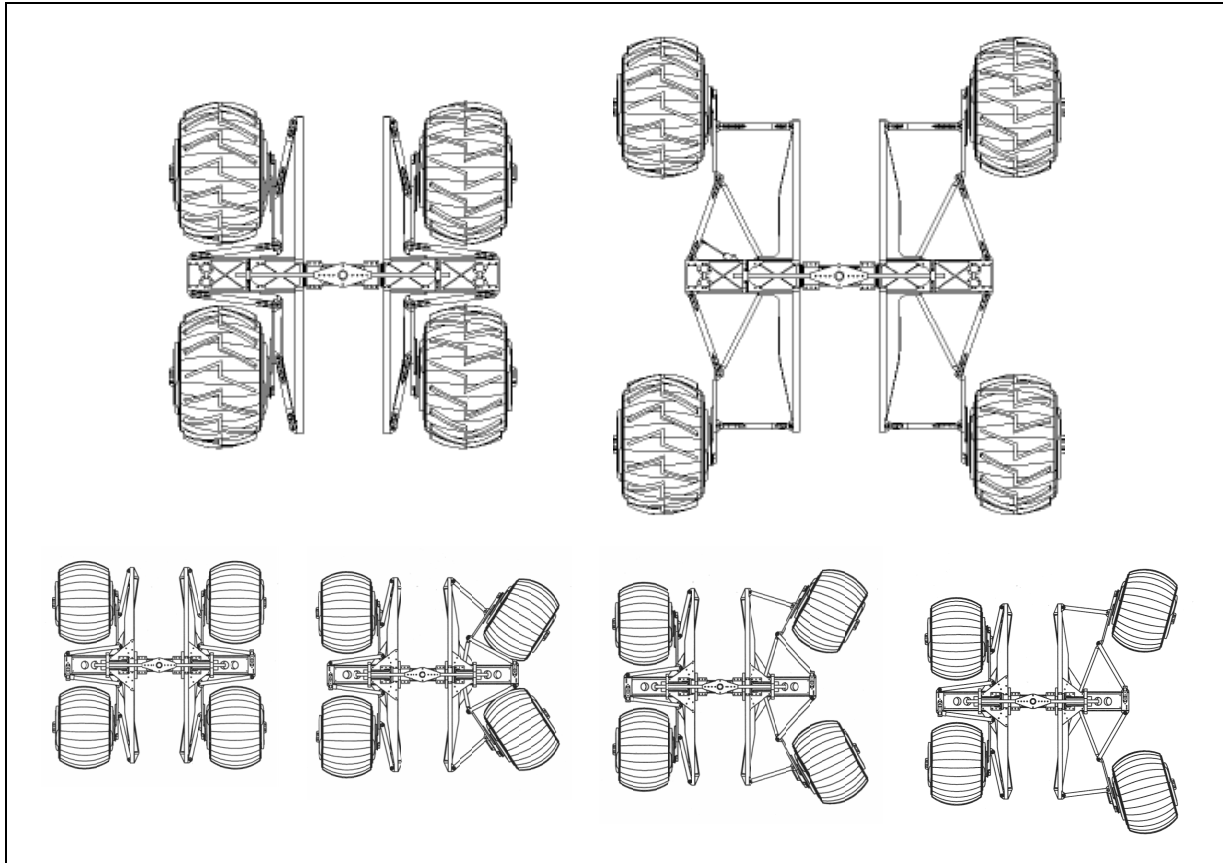
Figure 26: Nomad's transforming chassis in a compacted and deployed configuration (top). Four steps in the deployment of the right chassis frame (bottom).

4.3.3 Coordinated Steering

The kinematics and actuation of the transforming chassis accommodate the execution of various steering geometries such as a dual Ackermann and differential skid steering (Figure 27). In addition, Nomad can point-turn without any lateral resistance when the two sides of the transforming chassis are deployed to the maximum kinematic limit of the four-bar mechanisms. In this case Nomad's wheels roll smoothly on the desired steering arc without slipping.

Any steering scheme is achieved through kinematic coordination of the two chassis frames. The velocities of the "inner" and "outer" pairs of wheels are electronically servoed based

on the kinematics of a turn and possible limitations of power draw. For example, with the chassis at its deployed configuration, if the left-side and right-side actuators both rotate clockwise by 20 degrees, the rover makes a right turn on a 6-foot inner turning radius which equals the total length of the stowed chassis. The minimum inner turning radius is estimated to be 20 in [Shamah98].
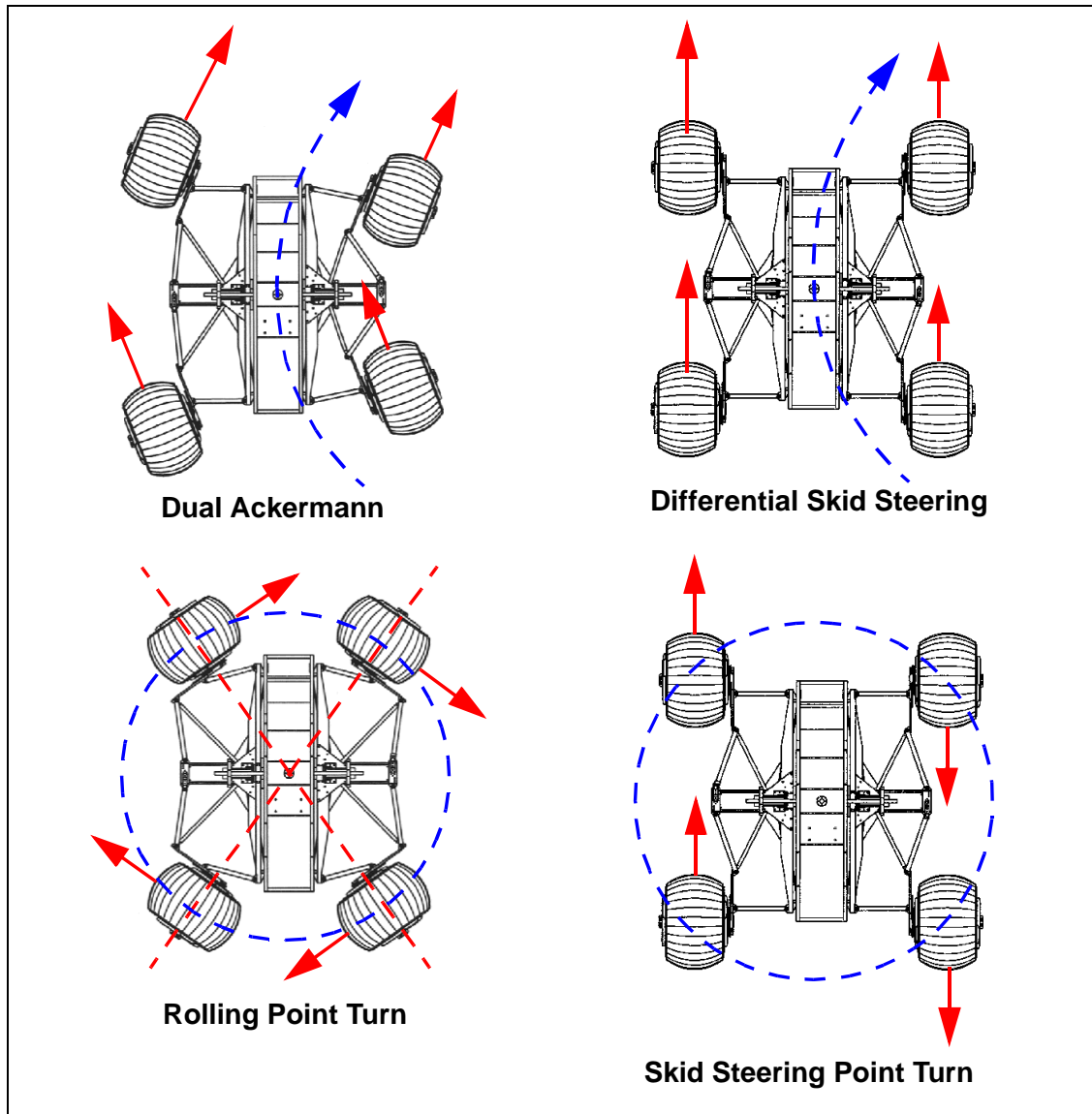
Figure 27: Steering schemes accommodated by Nomad's transforming chassis [Shamah98].

4.3.4 Tire Design

Nomad's metal tires are constructed of a thin aluminum shell manufactured to the shape of a wide-profile pneumatic tire. The compound spherical shell provides maximum strength and resilience for minimum mass. Despite the negative impact of a wider tire on steering resistance, the selected diameter to width ratio improves vehicle flotation and reduces ground contact pressure with positive effects on trafficability in loose sand. The tire contact

profile allows for uniform load distribution over the contact patch and for gradual soil compaction. Grousers were added to the metal tire to improve traction. A pattern similar to that used on tractors and other earth moving equipment was used. The shape and orientation of the grousers limits steering resistance on the tires as the chassis expands or contracts but increases traction for normal driving. Pneumatic tires were also fitted on Nomad. Snow tires with the desired dimensions were modified to fit custom rims. The tires have an aggressive rubber tread pattern as well as metal studs imbedded in the rubber treads. An inner tube maintains a tire pressure of 3 to 5 psi. Maneuverability experiments were carried out using both types.

Figure 28: Form comparison of the metal tire with grousers (left) and the pneumatic tire (right).

Nomad's locomotion dimensions of significance to the experimental program are summarized in the following Table:

Dimension	Value
Total Length (L_v)	72 in (1.83 m) stowed 96 in (2.44 m) deployed
Total Width (B_v)	72 in (1.83 m) stowed 96 in (2.44 m) deployed
Wheelbase (L_{ww})	42 in (1.07 m) stowed 66 in (1.68 m) deployed
Wheel stance (B_{ww})	52 in (1.32 m) stowed 76 in (1.93 m) deployed
Ground clearance	16 in (40.5 cm)
Nominal tire diameter (d_w)	metal 28 in (71 cm) pneumatic 32 in (81 cm)
Nominal tire width (b_w)	metal 17.5 in (44.5 cm) pneumatic 14.5 in (37 cm)

Table 9:   Nomad's geometric specification.

4.4 Performance Characterization of Nomad's Locomotion

LocSyn' results were compared against actual data obtained through experimentation with a single wheel and Nomad. Single-wheel experiments measured the in-soil and discrete obstacle performance of various metal tires fitted on the same wheel assembly. The results were used to extrapolate Nomad's gross locomotion performance in low cohesion soils. The second sets of experiments studied Nomad's performance on hard compacted soils. This phase produced results of drawbar pull and gradeability using all-metal tires. Finally, an elaborate experimental program allowed for the quantitative characterization of Nomad's maneuverability using two distinct types of tires and two modes of steering both achievable with Nomad's transforming chassis.

4.4.1 Single Wheel Testing

The purpose of this experimental work was to quantify the in soil performance of a single robotic wheel. Fine grained industrial sand was selected as the medium. Three different tire designs were tested, but the bulk of the work was carried out using a spherical tire with opposing sections removed to create sidewalls and emulate the toroidal shape of a standard tire. Experiments measured drive power for continuous driving and negotiation of hard obstacles submerged in the sand. The drive and control unit of the wheel were the same as those used on Nomad. Another goal of the experiment was to measure the endurance and behavior of the wheel's drive unit. The performance of the wheel was measured against a variety of loads similar to those experienced by Nomad's wheel.

Figure 29: The single wheel testbed was a polygonal sandbox filled with fine grained sand 20 inches deep. The wheel traveled in a 27 foot diameter circle. At the center of the testbed was a slip ring, which provided power and control signals to the wheel. The wheel was supported from the slip ring by two parallel linkages.

The smooth aluminum tire was run in the fine sand varying both speed and wheel loading in order to compare experimental and LocSyn power values.

WHEEL LOAD [lbf]	165			235		
SPEED [ft/s]	0.89	1.18	1.48	0.89	1.18	1.48
LocSyn power [watts]	78	104	130	120	160	200
Measured power [watts]	74	95	113	105	130	150

Table 10:   Comparison between LocSyn and experimental results obtained using the metal tire.

LocSyn's results closely match the experimental results obtained for loading of 165 lbf. For the higher wheel loading of 235 lbf the LocSyn values are higher than the measured values by 12-25%. As the wheel loading increases the fine sand becomes more compacted acting like a hard soil such that resistance components of sinkage and bulldozing no longer apply. LocSyn's predictions were more conservative than the measured values. This is the only case where a reliable comparison between the predicted and actual results could be made because there was a good understanding about the testing medium and the physical design.

Additionally, tests were carried out to determine the effect of the grousers on mobility. The wheel was run at 4 velocities and the power draw was monitored. The results in Table 11 show how the tread pattern had an increasingly significant affect on the power draw as the velocity increased.
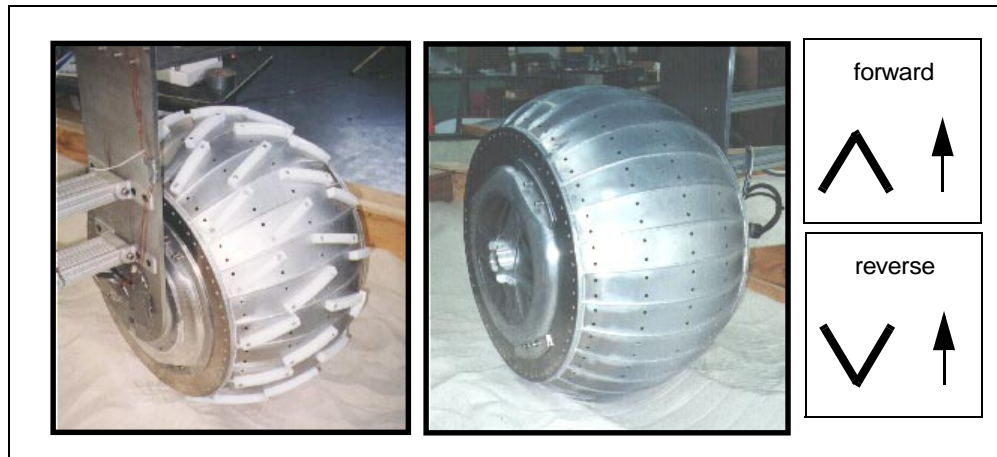
Figure 30: Rigid wheel with (left) and without grousers (right).

The grousers attached to the aluminum tire increase the thrust provided but at a price to the required drive power due to increased compaction and bulldozing of the soil. The effects of increased motion resistance can be predicted through a comparison of the results for forward and reverse grouser orientation (Figure 30). The forward grouser design facilitates the displacement of soil to the sides. Modeling the effect of soil motion is a non-trivial task and has been omitted from LocSyn's trafficability equations.

	No Treads	Treads Forward	Treads Reverse
Velocity [ft/s]	Mean Power [Watts]	Mean Power [Watts]	Mean Power [Watts]
0.89	74	84	112
1.18	95	120	153
1.48	113	157	193

Table 11: Experimental results illustrating the effect of grousers and grouser orientation on drive power.

Finally experiments were carried out to measure the effect of repeated traffic. This experiment allowed an understanding of how much power is lost while negotiating weak soils rather than compacted terrain. The wheel without grousers was run at a constant velocity of 1.2 ft/s for 600 laps. The wheel loading was 165 lbf. Mean power readings were recorded at 10, 200, 400 and 600 laps. The results are shown in Table 12 with the average power decreasing 37% from lap 10 to lap 600.

	Average Power Draw [Watts]
After 10 Laps	93
After 200 Laps	65
After 400 Laps	61
After 600 Laps	59

Table 12: Experimental results illustrating the effects of repeated traffic on drive power.

4.4.2 Drawbar Pull and Slope Negotiation Experiments with Nomad

These tests were carried out with Nomad in an outdoor location in Pittsburgh. The terrain was compacted dirt covered with gravel. While these tests do not match the terrain parameters used for the LocSyn analysis they provide a means to qualitatively evaluate the predicted results. For the straight driving and slope tests encoder ticks were monitored to provide wheel velocities for each wheel. Current monitors were also used to evaluate motor torque for each wheel. The combination of voltage and current was used to provide the locomotive power required for each experiment. The drawbar pull experiment was performed by attaching a dynamometer to Nomad's frame and then recording the maximum force before the wheels slip for a commanded velocity (Figure 31).
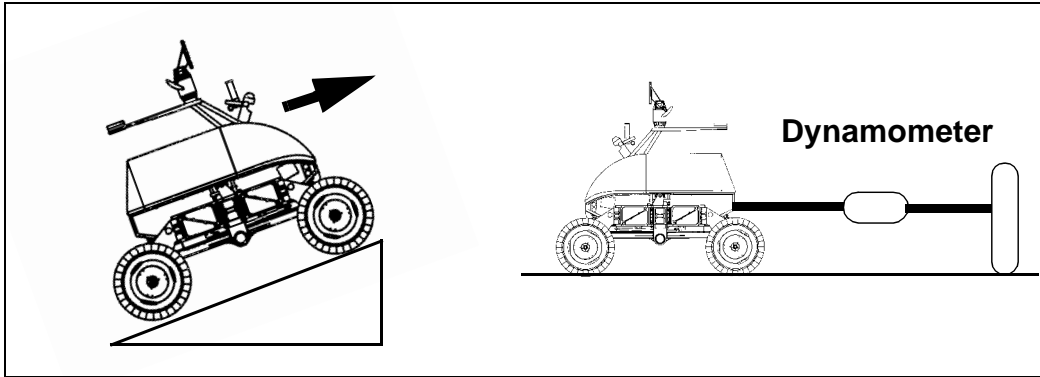
Figure 31: Slope climbing and drawbar pull experimental set-ups.

Terrain	slope 0 deg	slope 10 deg	slope 17 deg	slope 0 deg
Test	Driving	Driving	Driving	Drawbar Pull
LocSyn Value	975 lbf	1290 W	1665 W	740
Measured Value	650 lbf	1000 W	1250 W	670 W

Table 13:   Comparison between LocSyn's output and experimental results obtained with Nomad.

These results show significant discrepancies between LocSyn and the actual measurements, even though LocSyn estimates are conservative. This is because LocSyn estimated the drive power and drawbar pull using the configuration equation for trafficability in unprepared terrains. As expected, locomotion over gravel covered hard soil did not yield any significant sinkage, compaction, or bulldozing resistance. As discussed in the trafficability section the case of negligible sinkage the primary component to motion resistance is the rolling resistance. Inevitably, because of the use of all metal tires with grousers theoretical values of the coefficient of rolling resistance must be corrected and that is possible only through experimentation.

4.4.3 Explicit and Skid Steering Experiments with Nomad

Experiments were performed to characterize the steering modes accommodated by Nomad. To compare explicit and skid steering as well as rigid and pneumatic tires, empirical performance was derived from experimental data. The data were gathered exploiting Nomad's ability to accommodate both skid and explicit steering. GPS was used as a measure of independent absolute position. The GPS data from steady state turning were post processed to determine the radius of each turn. Using measurements of wheel velocity as well as current and voltage values, torque and power were computed for each in wheel drive unit.

These experiments consider steady state turning which does not include the transition from driving straight into a turning condition. All experiments were performed on flat gravel terrain in an outdoor environment. The terrain is naturally flat and without obstacles. However, locally varying slopes up to +/-2 degrees and terrain inconsistencies were encountered.

The experiments covered explicit and skid turning over a range of turning radii with rigid and pneumatic tires. For each case an infinite radius (equivalent to straight driving), 39, 26, 13, and a 0 feet or point turn was studied at a vehicle velocity of 0.5 ft/s (0.15 m/s). The velocity studied is representative of the state-of-art speed for autonomous driving of planetary robots.

For each test data signals were recorded including vehicle position, wheel motor current, voltage and velocity at 60 Hz. The PID controller used on the velocity loop for the drive motors did not change during any of the experiments. The nominal direction of turn studied was clockwise. However, the 13 foot-radius turn was studied in both the clockwise and counterclockwise direction to examine inconsistencies with respect to turn direction.

During the skid steer experiments the steering motors hold the linkages in the position for straight driving. Individual wheel velocities for skid steering were based on the kinematic model of the vehicle. Due to the inaccuracies of the kinematic model the wheel velocities were modified experimentally until Nomad traversed the desired radius while holding a vehicle velocity of 0.5 ft/s (1.5 m/s).

4.4.3.1 Power for Explicit Steering

Power for explicit steering degenerates to a minimum value at infinite radius, i.e. straight driving, for both rigid and pneumatic tires. Figure 32 shows that greater power is required as the turn radius decreases from straight driving to a point turn. This can be attributed to an increase in the wheel slip angle. The slip angle is the difference between the thrust vector provided by the wheel and the actual direction of travel of the wheel.

The rigid tires show a smooth reduction of power as the radius increases with the max power differential of 100 Watts occurring between the point turn and straight driving. However, the pneumatic tires show a notably high power draw for a point turn then a flat profile for the 13, 26, and 39 foot radii and a minimum value for straight driving. This suggests that for very tight turn radii (less than 13 feet), power is consumed in the lateral deformation of the pneumatic tire.

The reduced power draw of the pneumatic tire versus the rigid tire is due to several factors. The larger diameter of the pneumatic tire as well as the elastic nature of the tire result in an increased contact patch area between the tire and the ground. The larger contact patch reduces the ground pressure which lowers motion resistance and thus reduces power draw for each wheel.
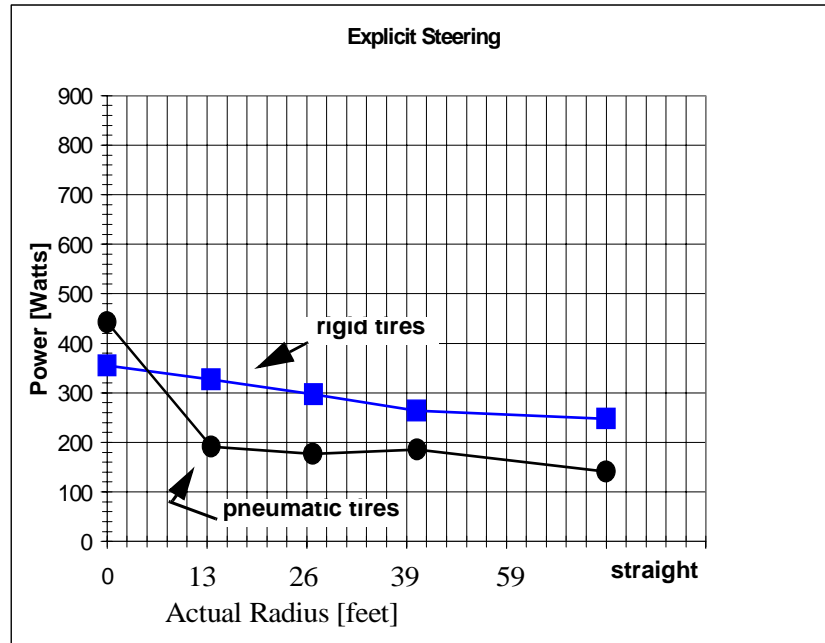
Figure 32: Power for explicit steering with rigid and pneumatic tires.

The fact that the pneumatic tire shows a flat profile between 13 and 40 foot radii suggests that there is twisting of the tire carcass to cause increased power at smaller radii. The flat profile also suggests that the slip angle is constant between 13 and 40 foot radii, unlike the rigid tire profile where the slip angle, and thus the power draw, increases at the same rate as the radius decreases.

4.4.3.2 Torque for Explicit Steering

By monitoring the current of the drive motor amplifiers the torque used to propel each wheel was estimated. The torque constant for the drive motors was given as 0.56 Nm/Amp from the motor manufacturer. Using the gear reduction of 218, wheel torque was determined.

Figures 33 and 34 show the torque values for explicit steering with rigid and pneumatic tires. The markers show the actual data points of 0, 13, 26, 39 and infinite (straight driving) foot radii. For both rigid and pneumatic tires the values from 13 to 39 meter radii are grouped well showing that by explicitly changing the heading of the wheels the torque is evenly distributed for each wheel. The point turn exhibits an interesting phenomenon where the front inner and rear outer wheels are carrying approximately 55 ft-lb more torque for the rigid tires and approximately 740 ft-lb more for the pneumatic tires than the front outer and rear inner wheels.
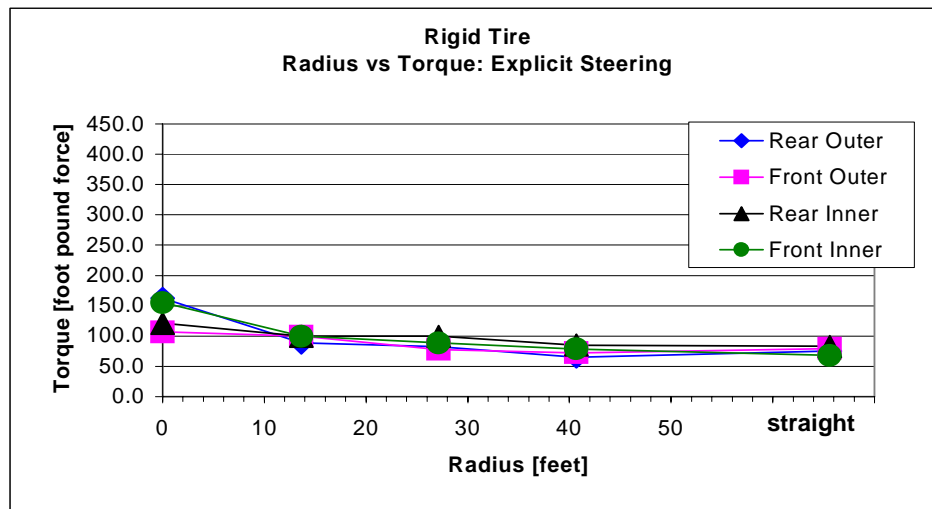
Figure 33: Torque for explicit steering with rigid tires.
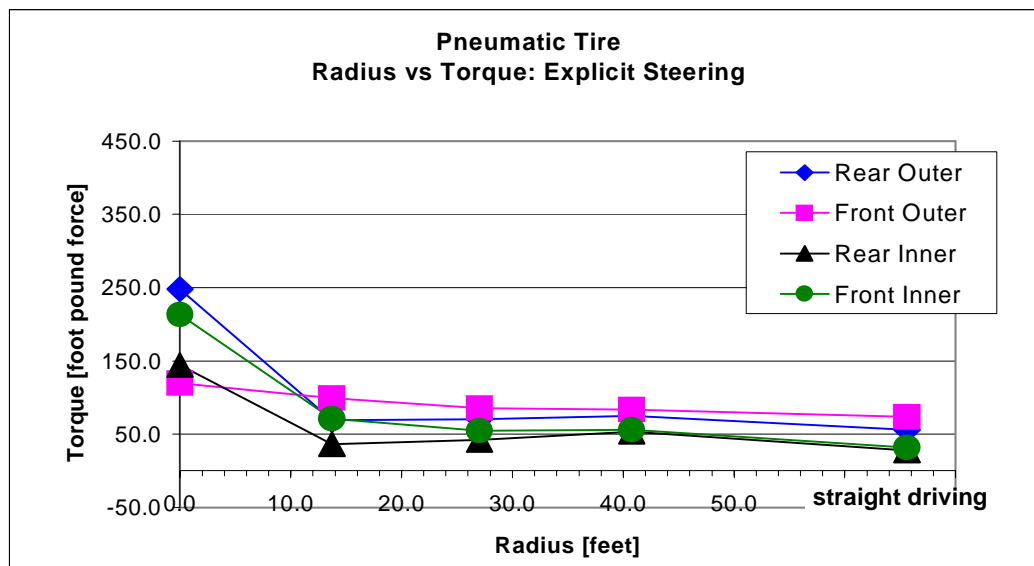
Figure 34: Torque for explicit steering with pneumatic tires.

4.4.3.3 Power for Skid Steering

Due to the significant lateral forces that occur during skid steering the power draw is expected to be higher than that observed for explicit steering regardless of tire design. Figure 35 shows that skid steering with pneumatic tires requires more power than with the rigid tires. For pneumatic tires the lateral forces act to deform the tire carcass, thus requiring increased power for forward propulsion.

The dramatic increase in power draw (350 Watts) from straight driving to a 39 foot radii for the pneumatic tires shows the effect of small lateral forces on elastic material. While the

rigid tires require an higher power draw than the pneumatic tires for straight driving, the further increase of power draw as the radius decreases is much smoother than that for pneumatic tires. It can also be noted that the effect of grousers was not significant during tight radius turning.

Figure 35: Power for skid steering with rigid and pneumatic tires.

4.4.3.4 Torque for Skid Steering

Figure 36 summarizes torque measurements for skid steering. It is interesting to note the difference between the inner wheel torque of the rigid and pneumatic tires. With rigid tires at radii of 13, 26, and 39 feet the inner wheels require almost half the torque required during straight driving. However, in all of the trials using pneumatic tires the minimum torque for any individual wheel occurs in the straight driving condition

Regarding wheel torque, the skid steer point turn showed the same trend as the explicit point turn for both types of tires. The torques were split in the same diagonal fashion with the rear outer and front inner carrying 90 ft-lb more than the front outer and rear inner wheels for both rigid and pneumatic tires. As the radius increased the rear outer wheel consistently carried between 55 and 100 ft-lb more than the front outer wheel.

.
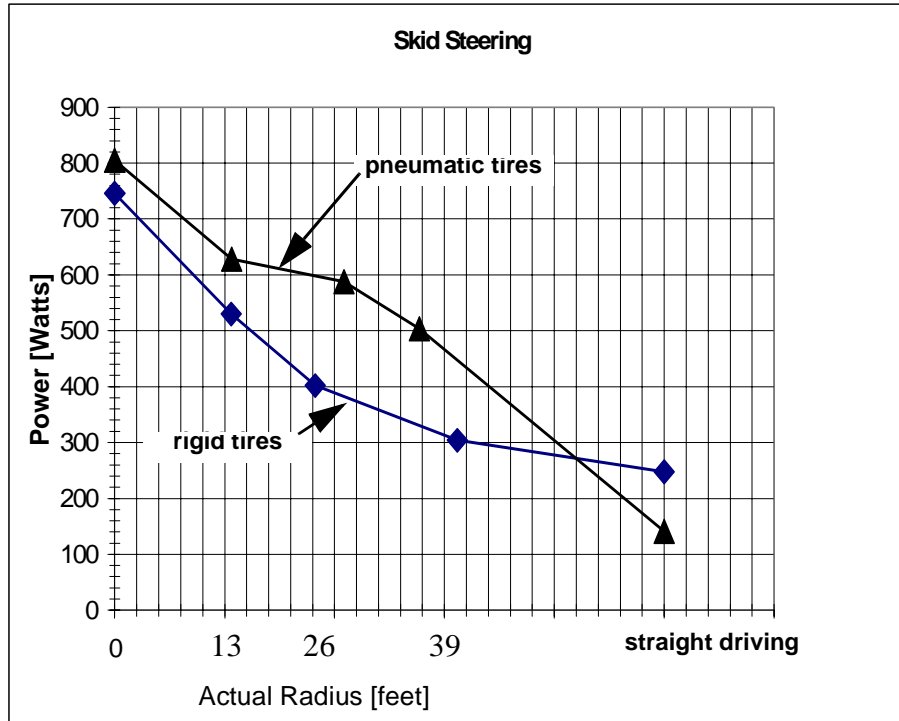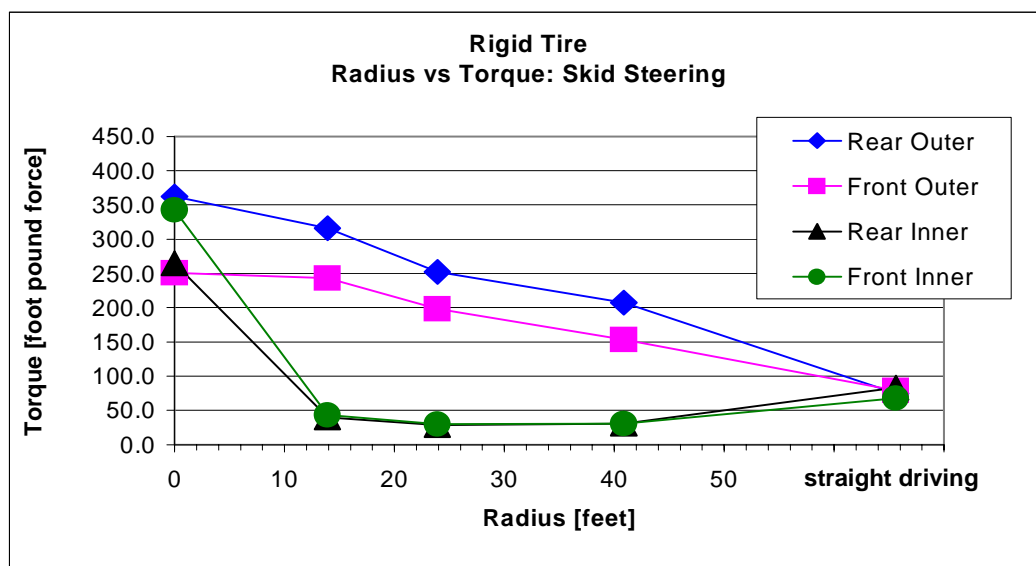

Figure 36: Torque for skid steering with rigid tires.

4.4.3.5 Discussion

In this comparison of rigid and pneumatic tires for skid and explicit steering several assumptions need to be highlighted. First, no correction or normalization was made to the data even though the tires are of different diameters and width, which does affect power draw and torque measurements. Second, Nomad's weight changed slightly between the time that the tests were performed with rigid and pneumatic tires (less than 100 lbf). The torque of individual wheels for straight driving is evenly distributed for the rigid tires while there is a discrepancy of wheel torque for the pneumatic tires. The testing for the pneumatic tires occurred almost one year after testing was completed with the rigid tires at the same testing site. Variations of mechanical wear in wheel drive units could be the source of small discrepancies.

Skid steering with pneumatic tires required more power and torque than skid steering with rigid tires. Even at a 39 foot radius the power draw for pneumatic tires was 1.5 times that of the same turn with rigid tires. Notably higher power and torque was observed for the explicit point turn (75 Watts more than with rigid tires). This could be attributed to significant tire distortion or slip angle for tight turning. However, explicit steering with pneumatic tires at a radius greater than 13 feet required the minimum power and torque. Straight driving with pneumatic tires required 100 Watts less than that required for straight driving with rigid tires.

The significance of this comparative analysis from field data is multifold. First, it provides a quantitative assessment of the terrain performance of two generic tire classes and two steering modalities used by the vast majority of off-road and planetary robots. The results of this work complement LocSyn's configuration equations for maneuverability and reveal

key trades not possible through analytical formulations especially in the case of the rigid tire with grousers.

Second, the summarization of torque and power profiles for a wide range of steering angles, enables a first order appreciation of the complexity of power management and control for such a robot. A smoother steering response to heading changes has a positive effect to power management and control, especially for rough terrain robotic mobility.

Third, this work lays the foundation for more advanced concepts of traction control in which a priori knowledge of steering performance could be used to tune the parameters of an adaptive scheme to optimize smoothness of motion, power utilization, and dynamic performance. For instance, the observation of consistent discrepancies in power draw by individual wheels during skid steering could be taken into account by a centralized planner, allowing effective tuning of control gains when executing a specific maneuver.

Chapter 5

SUMMARY

This research has developed a new framework for synthesizing configurations of wheeled robotic locomotion and for evaluating alternative configurations through analytical predictions of performance. The framework, LocSyn, balances traditional models of vehicle-terrain interaction with novel metrics and functions of performance, some of which are unique to robotic locomotion. Engineering analysis is used to derive configuration equations, which relate locomotion system dimensions to terrain properties and robot performance.

Locomotion configurations can now be synthesized in a rationalized and systematic fashion using configuration equations of trafficability, maneuverability and terrainability. Trafficability primarily impacts the selection of dimensions and shape of the wheels, as well as the drive scheme and mechanism. Maneuverability configuration equations are for estimating the overall locomotion dimensions, steering scheme and chassis geometry. Finally, analysis of terrainability aids the selection of the optimal number of wheels and the configuration of the robot's suspension.

5.1 Observations

This work promotes in-depth examination of vehicle-terrain relationships at the outset of robotic configuration. Through LocSyn's parametric simulations, and the analytical configuration and experimental validation of Nomad's robotic locomotion this thesis has shown the value in examining conventional vehicle-terrain equations to rationalize configuration. The underlying idea is that robotic locomotion should be optimized for maximum mechanical capability before real-time control and autonomous safeguarding functions are implemented. The terramechanical models of robotic locomotion are refined to a level of detail that allows implementation of in the traction control scheme or even in the navigational planner so that it can take into consideration real-time observations of the soil behavior or overall terrain features.

The search for techniques that involve terrain, locomotion and performance quantities naturally have led to the consideration of empirical wheel/soil interaction models. It is important to note that the majority of parametric equations for trafficability have been derived from semi-empirical equations and are therefore subject to the limitations of the work that originally developed them. Nevertheless, a concerted effort has been made to implement analytical models that utilize theories of broad applicability.

The effects of trafficability parameters on the physical configuration of a robot are significant. A recommendation of this thesis is that unless terrain properties have been accurately measured, one must consider worst-case conditions not only in relation to slope

or obstacle distributions, but also soil cohesion and internal friction. If little is known about the terrain in which the robot will navigate, it is necessary to utilize stochastic models to approximate the soil trafficability parameters.

The experimental validation of Nomad's locomotion and comparisons with LocSyn's results illustrate the difficulty in devising analytical models to accurately predict the performance of the physical locomotion design. Nevertheless, this work has produced locomotion configurations through the implementation of quantitative models of locomotion performance. As evident from Nomad's locomotion configuration, LocSyn's analysis manages configuration issues to sufficient detail and quantitative rationalization to enable critical configuration decisions to be made.

5.2 Contributions

The main contributions of this work are that it:

- Addresses the configuration of wheeled robotic locomotion and implements a new framework for the synthesis and evaluation of innovative configurations. The devised configuration framework is the first of its kind in the robotics literature.

- Introduces the concept of configuration equations which are analytical expressions for the synthesis of configuration geometries. They are also a powerful aid to a robot designer in that they capture the relationships between form and performance of robotic locomotion.

- Devises analysis and performance metrics of value to any wheeled robot design. Metrics known for their utility to conventional vehicles, are also reformulated in the context of robotic mobility.

- Makes explicit the role of terramechanics in robotic locomotion configuration through in-depth analytical formulations and discussion using practical examples. Configuration equations derived from classical terramechanics are the foundation for the characterization of the mechanics of robotic locomotion at a level of detail and fidelity not achieved with the current state-of-practice.

- Presents new quasi-static analyses of trafficability, maneuverability and terrainability. As with configuration equations, all studies are pursued in a manner that makes them applicable to any type of wheeled robotic locomotion.

- Demonstrates the importance of analytical approaches to configuration through practical examples and trade studies. In addition, this thesis illustrates the benefit of parametric analysis in the capturing the space of feasible configurations rather than seeking a single optimal configuration solution.

- Produced LocSyn, the computational manifestation of the configuration framework. LocSyn allows for an in-depth evaluation of candidates and selection of optimal configurations through parametric simulations.

- Quantified the applicability and limitations of LocSyn in the locomotion configuration of Nomad, a robotic prototype for planetary exploration.

• Configured, designed and validated Nomad's robotic locomotion using the principles and methods of this thesis. This work also produced a comprehensive characterization of the in-soil performance of Nomad's wheels including the performance quantification of metal tires. It also addressed the relative merits of various wheel designs and steering schemes in the locomotion performance of Nomad.

5.3 Future Directions

An important extension to this thesis would be the inclusion of the issue of *automobility*. Automobility is the ability of robotic locomotion to accommodate autonomous navigation, closed-loop control, sensor utilization, and other robotic functions such as deployment of robotic manipulation tools. Currently, these issues are deferred until after a robot's electromechanism is designed and are treated as issues of engineering along with the development of control software and integration of sensors. Because of the significance of automobility to the performance of a robot there is a need to develop the configuration equations that capture the relationships among robotic locomotion, perception and control.

Configuration for automobility should consider the geometric and physics-based models of robot kinematics, sensor placement, safeguarding mechanics and others. For example, design for safe obstacle avoidance calls for locomotion configurations that minimize interferences to the field-of-view of the sensors and possess great maneuverability. Another example is that of maximizing the performance of terrain viewing sensors by minimizing the terrain excursions transferred to them. In this case the locomotion configuration and in particular the configuration of the wheel and suspension are key to optimize sensor motion smoothing. Optimal configurations should reduce the need for active body posturing.

Configuration for automobility should also address the trade-offs between mechanical capability and computational demand as it relates to CPU loading, sensor utilization, health monitoring and autonomous safeguarding. The idea is that configuration should always aim at generating locomotion concepts with high intrinsic mechanical capability and thus reduce the performance burden on planning and control. However, because of limitations on how much physical capability can be designed into a robot due to mass, volume and other engineering constraints, it is necessary to quantify the expected increase in computational demand in relation to reduced mechanical capability.

Configuration optimization against task and performance requirements of automobility could be quite convoluted. Consider the example of locomotion configuration for optimal placement and orientation of perception sensors. The sensors must be placed high enough above the robot and oriented properly to perceive obstacles ahead so a braking or steering maneuver could safeguard the vehicle. Conservatively, the field of view should include objects at or beyond the vehicle's stopping distance, measured from the forward-most point of the robot. While perceiving obstacles at larger distances requires less maneuverability, sensors are less capable of detecting obstacles further away. Simultaneously, terrain perception sensors should be placed wide enough to see at least the width of the vehicle and ideally wide enough to utilize multi-baseline stereo. As can be inferred from this

discussion, configuration for "optimal sensor placement" impacts the configuration of various locomotion subsystems and requires numerical optimization.

The development and incorporation of configuration equations for automobility to those of trafficability, maneuverability and terrainability would carry the rationalized design of robotic locomotion configurations to the next level of sophistication. Beyond automobility, configuration should also take on studies that consider traditional design issues such as manufacturability, assembly and maintenance. Finally, as the discipline of robotic configuration grows and more knowledge is gained through practical experience, it should address the methods and metrics for configuration for reliability.

The long term aspiration should be the automation of the robotic configuration process. This and other recent theses have built the foundation to pursue such a goal. It is hoped that this dissertation will motivate new advances in robotics and prove to be a useful reference to researchers and designers alike.

Bibliography

[Amai93]   Amai, W. A., et al.
                "Robotic All-Terrain Lunar Exploration Rover (RATLER): FY93 Program Status Report."
                Sandia National Laboratories, SAND94-1706, October 1994.

[Apostol95a]   Apostolopoulos, D., Bares, J.
                "Configuration of a Robust Rappelling Robot."
                Proceedings of the 1995 IEEE International conference on Intelligent Robots and Systems
                (IROS), Pittsburgh, PA, August 1995.

[Apostol95b]   Apostolopoulos, D., Whittaker, W. L.
                "Robotic Locomotion for Lunar Exploration."
                Proceedings of the 2nd International Lunar Exploration Conference, San Diego, CA, 1995.

[Apostol96]   Apostolopoulos, D.
                "Systematic Configuration of Robotic Locomotion."
                Technical Report CMU-RI-TR-96-30, The Robotics Institute, Carnegie Mellon University,
                Pittsburgh, PA, July 1996.

[Bares87]   Bares, J.
                Responsive Prototyping of Mobile Unmanned Work Systems.
                M.E. Thesis in Civil Engineering, Carnegie mellon University, May 1987.

[Bares89]   Bares, J., Whittaker, W.
                "Configuration of an Autonomous Robot for Mars Exploration."
                Proceedings of the World Robotics Conference on Robotics Research: The Next Five Years
                and Beyond, pp. 37-52, Gaithersburg, MD, May 1989.

[Bares91]   Bares, J.
                Configuration of Autonomous Walkers for Extreme Terrain.
                Ph.D. Dissertation in Civil Engineering, Carnegie Mellon University, 1991.

[Beitz87]   Beitz, W.
                "General Approach of Systematic Design."
                Proceedings of the ASME International Conference on Engineering Design, pp. 15-20,
                New York, NY, 1987.

[Bekker56]   Bekker, M. G.
                Theory of Land Locomotion: The Mechanics of Vehicle Mobility.
                University of Michigan Press, Ann Arbor, MI, 1956.

[Bekker60]   Bekker, M. G.
                Off-The-Road Locomotion.
                University of Michigan Press, Ann Arbor, MI, 1960.

[Bekker62]   Bekker, M. G.
                "Evaluation and Selection of Optimum Vehicle Types Under Random Terrain Conditions."
                Proceedings of the 1st International Conference on the Mechanics of Soil-Vehicle Systems,
                pp. 772-790, Edizoni, Minerva Tecnica, Italy, June 1962.

[Bekker64]   Bekker, M. G.
                "Mechanics of Locomotion and Lunar Surface Vehicle Concepts."
                Transactions of the Society of Automotive Engineers, Vol. 72, pp. 549-569, 1964.

[Bekker69]   Bekker, M. G.
                Introduction to Terrain-Vehicle Systems.
                University of Michigan Press, Ann Arbor, MI, 1969.

[Befforte90]   Belforte, G.
                "Locomotion Solutions for Mobile Robots."
                The Industrial Robot, pp. 217-221, December 1990.

[Bickler92]   Bickler, D. B.
"The New Family of JPL Planetary Surface Vehicles."
Proceedings of the Conference on Missions, Technologies and Design of Planetary Mobile Vehicles, pp. 301-306, Toulouse, France, September 1992.

[Boeing92]   The Boeing Company, Advanced Civil Space Systems Division.
"Piloted Rover Technology Task 9.4 Final Report."
NASA Contract NAS8-37857, 1992.

[Buchele62]   Buchele, W. F.
"Application of the Soil Parameters to Vehicular Mechanics."
Proceedings of the 1st International Conference on the Mechanics of Soil-Vehicle Systems, pp. 323-327, Edizoni, Minerva Tecnica, Italy, June 1962.

[Burke92]   Burke, J. D.
"Past US Studies and Developments for Planetary Rovers."
Proceedings of the Conference on Missions, Technologies and Design of Planetary Mobile Vehicles, pp. 45-60, Toulouse, France, September 1992.

[Chun87]   Chun, W.
"Ground Vehicle Options."
SPIE The International Society of Optical Engineering, Vol. 852, Mobile Robots, pp. 188-194, 1987.

[Cohen92]   Cohen, R., et al.
"Conceptual Design of a Modular Robot."
Transactions of ASME, Journal of Mechanical Design, Vol. 114, pp. 117-125, March 1992.

[Coulter94-1]   Coulter, R. C.
"A Partial Analysis of the Mechanics of the Cross Country Navigation Problem."
Technical Report CMU-RI-TR-94-02, The Robotics Institute, Carnegie Mellon University, Pittsburgh, PA, January 1994.

[Coulter94-2]   Coulter, R. C.
"A Systems Engineering Approach to Electro-Mechanical Reconfiguration for High Mobility Autonomy."
Technical Report CMU-RI-TR-94-27, The Robotics Institute, Carnegie Mellon University, Pittsburgh, PA, April 1994.

[Cross89]   Cross, N.
Engineering Design Methods.
John Wiley & Sons Ltd., Chichester, UK, 1989.

[Dowling95]   Dowling, K.
"Tessellator Robot Design Document."
Technical Report CMU-RI-TR-95-43, The Robotics Institute, Carnegie Mellon University, Pittsburgh, PA, January 1996.

[Dudzinski89]   Dudzinski, P. A.
"Design Characteristics of Steering Systems for Mobile Wheeled Earthmoving Equipment."
Journal of Terramechanics, Vol. 26, No. 1, pp. 25-82, 1989.

[Eder76]   Eder, W. E., Goslig, W.
Mechanical System Design.
Pergamon Press, Oxford, UK, 1976.

[Everett95]   Everett, H. R.
Sensors for Mobile Robots: Theory and Applications.
A K Peters, Ltd., Wellesley, MA, 1995.

[Farritor96]   Farritor, S., Dubowsky, S., Rutman, N., and Cole, J.
                 "A Systems-Level Modular Design Approach to Field Robots."
                 Proceedings of the 1996 International Conference on Robotics and Automation (ICRA),
                 Minneapolis, MN, April 1996.

[Freitag65]   Freitag, D. R.
                 "A Dimensional Analysis of the Performance of Pneumatic Tires on Soft Soils."
                 Technical Report 3-688, U. S. Army Engineer Waterways Experiment Station, Corps of
                 Engineers, Vicksburg, Mississippi, August 1965.

[Freitag70]   Freitag, D. R., Green, A. J., Melzer, K.-J.
                 "Performance Evaluation of Wheels for Lunar Vehicles (Summary Report)."
                 Miscellaneous Paper M-70-4, Mobility and Environmental Division, U. S. Army Engineer
                 Waterways Experiment Station, Vicksburg, Mississippi, May 1970.

[Gee79]   Gee-Clough, D.
                 "The Effect of Wheel Width on the Rolling Resistance of Rigid Wheels in Sand."
                 Journal of Terramechanics, Vol. 15, No. 4, pp. 161-184, 1979.

[Gillespie92]   Gillespie, T. D.
                 Fundamentals of Vehicle Dynamics.
                 Society of Automotive Engineers, Inc., Warrendale, PA, 1992.

[Harrison62]   Harrison, W. L.
                 "Analytical Prediction of Performance for Full Size and Small Scale Model Vehicles."
                 Proceedings of the 1st International Conference on the Mechanics of Soil-Vehicle Systems,
                 pp. 678-702, Edizoni, Minerva Tecnica, Italy, June 1962.

[Heiken91]   Heiken, G., et al, *Lunar Sourcebook: A User's Guide to the Moon*,
                 Cambridge University Press, Cambridge, UK, 1991.

[Hirose91]   Hirose, S.
                 "Three Basic Types of Locomotion in Mobile Robots."
                 Proceedings of the 5th IEEE International Conference on Advanced Robots, pp. 12-17,
                 Pisa, Italy, 1991.

[Hirose95]   Hirose, S., et al.
                 "Fundamental Considerations for the Design of a Planetary Rover."
                 Proceedings of the 1995 IEEE International Conference on Robotics and Automation, pp.
                 1939-1944, Minneapolis, MN, September 1995.

[Hoffman92]   Hoffman, S., J., Weaver, D., B.
                 "Results and Proceedings of the Lunar Rover/Mobility Systems Workshop."
                 EXPO-T2-920003-EXPO, NASA, 1992.

[Holm70]   Holm, I. C.
                 "Articulated, Wheeled Off-the-road Vehicles."
                 Journal of Terramechanics, Vol. 7, No. 1, pp. 19-54, 1970.

[Hubka88]   Hubka, V., and Eder, W. E.
                 Theory of Technical Systems.
                 Springer-Verlag, Berlin, Germany, 1988.

[Ito90]   Ito, N.
                 "Practical Method of Improving the Turnability of Terrain Vehicles."
                 Journal of Terramechanics, Vol. 27, No. 4, pp. 331-341, 1990.

[Jones70]   Jones, J., C.
                 Design Methods.
                 Council of Industrial Design, John Wiley & Sons Ltd., London, UK, 1970.

[JPL87]   Jet Propulsion Laboratory Report.
                 Proceedings of Mars Rover Technology Workshop, Volume #3: Mobility, Pasadena, CA,
                 April 1987.

[Kannapan87a]   Kannapan, S., Marshek, K., M.
                 "Design Methodologies: A New Perspective on Approaches and Tasks,"
                 Mechanical Systems and Design, Technical Report 201, University of Texas, Austin, TX,
                 August 1987.

[Kannapan87b]   Kannapan, S., Marshek, K., M.
                 "Design Synthetic Reasoning: A Program for Search."
                 Mechanical Systems and Design, Technical Report 202, University of Texas, Austin, TX,
                 August 1987.

[Katragadda98]   Katragadda, L.
                 Synergy: A Language and Framework for Robot Design.
                 Ph.D. Dissertation in Robotics, Carnegie Mellon University, 1998.

[Keller71]   Keller, R., E.
                 Statics and Dynamics of Components and Systems.
                 John Wiley & Sons, Inc., New York, NY, 1971.

[Kelly94]   Kelly, A.
                 "Essential Kinematics for Autonomous Vehicles."
                 Technical Report CMU-RI-TR-94-14, The Robotics Institute, Carnegie Mellon University,
                 Pittsburgh, PA, May 1994.

[Kelly95]   Kelly, A.
                 *An Intelligent, Predictive Control Approach to the High Speed Cross Country Autonomous
                 Navigation Problem.*
                 Ph.D. Dissertation in Robotics, Carnegie Mellon University, 1995.

[Kemp90]   Kemp, H. R.
                 "Climbing Ability of Four-Wheel-Drive Vehicles."
                 Journal of Terramechanics, Vol. 27, No. 1, pp. 7-23, 1990.

[Kemp91]   Kemp, H. R.
                 "Relative Contributions of Different Wheels of Four-Wheel-Drive Vehicles."
                 Journal of Terramechanics, Volume 28, No. 4, pp. 393-402, 1991.

[Kemurdjian92]   Kemurdjian, A. L., et al.
                 "Soviet Developments of Planetary Rovers in Period of 1964-1990."
                 Proceedings of the Conference on Missions, Technologies and Design of Planetary Mobile
                 Vehicles, pp. 25-43, Toulouse, France, September 1992.

[Kemurdjian95]   Kemurdjian, A. L., Potemkin, E. K.
                 "Mobility of Planetary Vehicles: Problems and Reality."
                 Proceedings of the American Nuclear Society Conference, pp. 433-442, 1995.

[Klarer93]   Klarer, P. R., Purvis, J., W.
                 "A Highly Agile Mobility Chassis Design for a Robotic All-Terrain Lunar Exploration
                 Rover."
                 ASCE proceedings, 1992.

[Koller76]   Koller, R.
                 Konstruktionsmethode fur den Maschinen-, Gerate- und Apparatebau.
                 Springer Verlag, Berlin, 1976.

[Kozin62]   Kozin., F., Bogdanoff, J. L.
                 "On the Statistical Properties of the Ground Contour and its Relation to Land Locomotion."
                 Proceedings of the 1st International Conference on the Mechanics of Soil-Vehicle Systems,
                 pp. 224-241, Edizoni, Minerva Tecnica, Italy, June 1962.

[Krotkov94]   Krotkov, E. P., and Hebert, M.
               "Design Considerations on the Stereo System for the 1994 Lunar Rover Demonstration."
               Design Report, The Robotics Institute, Carnegie Mellon University, Pittsburgh, PA,
               February 1994.

[Kusiak95]   Kusiak, A., and larson, N.
               "Decomposition and Representation Methods in Mechanical design."
               Transactions of the ASME, Journal of Mechanical Design: Special 50th Anniversary
               Design Issue, Vol. 117, pp. 17-24, June 1995.

[Larminie88]   Larminie, J. C.
               "Standards for Mobility Requirements of Military Vehicles."
               Journal of Terramechanics, Vol. 25, No. 3, pp. 171-189, 1988.

[Leger99]   Leger, C.
               *Automated Synthesis and Optimization of Robot Configurations: An Evolutionary
               Approach.*
               Ph.D. Dissertation in Robotics, Carnegie Mellon University, 1999.

[Lindemann92] Lindemann, R. A., Eisen, H. J.
               "Mobility Analysis, Simulation and Scale Model Testing for the Design of Wheeled
               Planetary Rovers."
               Proceedings of the Conference on Missions, Technologies and Design of Planetary Mobile
               Vehicles, pp. 531-536, Toulouse, France, September 1992.

[Littmann92]   Littmann, F., Villedieu, E., Idasiak, J. M.
               "Mechanical Design of a Planetary Rover."
               Proceedings of the Conference on Missions, Technologies and Design of Planetary Mobile
               Vehicles, pp. 345-359, Toulouse, France, September 1992.

[Madhusudan95]Madhusudan, T., N.
               "A Review of Bond-Graph Representation Based Design Methodologies."
               Technical Report CMU-RI-TR-95-28, The Robotics Institute, Carnegie Mellon University,
               Pittsburgh, PA, July 1995.

[McKerrow91]   McKerrow, P. J.
               Introduction to Robotics.
               Addison-Wesley Publishing Company, Inc., Sydney, Australia, 1991.

[MMSSC88]   Martin Marietta Space Systems Company.
               "Mars Rover/Sample Return (MRSR) Rover Mobility and Surface Rendezvous Studies."
               JPL Contract 958073, October 1988.

[Muro94]   Muro, T., and Fukagawa, R.
               "The Optimum Height of Application of Force and Eccentricity of a Wheeled Vehicle
               Running on a Loose Sandy Soil."
               Journal of Terramechanics, Vol. 31, No. 5, pp. 313-328, 1994.

[Oomichi86]   Oomichi, T., and Ibe, T.
               "Development of Vehicles With Legs and Wheels."
               Journal of Advanced Robotics RSJ, Vol. 1, No. 4, pp. 343-356, 1986.

[Pahl84]   Pahl, G., and Beitz, W.
               Engineering Design.
               The Design Council, Springer-Verlag, London, UK, 1984.

[Pandey78]   Pandey, K. P., and Ojha, T. P.
               "Effect of Design Parameters on the Performance of Rigid Traction Wheels on Saturated
               Soils.
               Journal of Terramechanics, Vol. 15, No. 3, pp. 145-156, 1978.

[Price90]   Price, S., et al.
               "Wheeled Planetary Rover Testbed."
               SPIE The International Society of Optical Engineering, Vol. 1388, pp. 550-559, 1990.

[Roston94]   Roston, G.
               Genetic Methodology for Configuration Design.
               Ph.D. Dissertation in Mechanical Engineering, Carnegie Mellon University, 1999.

[Ruff92]   Ruff, T., Rao, N., and Doll, S.
               "A Parametric Analysis of Transportation Systems for Use on the Lunar Surface."
               1992 AIAA Space Programs and Technologies Conference, Huntsville, AL, March 1992.

[Shamah98]   Shamah, B.
               Experimental Comparison of Slid Steering vs. Explicit Steering for a Wheeled Mobile Robot.
               M.S. Thesis in Robotics, Carnegie Mellon University, 1998.

[Shigley89]   Shigley, J. E., Mischke, C. R.
               Mechanical Engineering Design.
               McGraw-Hill, Inc., New York, NY, 1989.

[Shishko95]   Shishko, R.
               NASA Systems Engineering Handbook.
               National Aeronautics and Systems Administration, SP-6105, June 1995.

[Spiessbach87] Spiessbach, A., et al.
               "Issues and Options for a Mars Rover."
               SPIE The International Society of Optical Engineering, Vol. 852, Mobile Robots, pp. 163-171, 1987.

[Söhne76]   Söhne, W.
               "Terramechanics and its Influence on the Concepts of Tractors, Tractor Power Development, and Energy Consumption"
               Journal of Terramechanics, Vol. 13, No. 1, pp. 27-43, 1976.

[Sukhatme95]   Sukhatme, G. S., Lewis, M. A., Bekey, G. A.
               "Mission Reachability for Extraterrestrial Rovers."
               Proceedings of the 1995 IEEE Conference on Robotics and Automation (ICRA), pp. 1964-1969, Nagoya, Japan, May 1995.

[Tani89]   Tani, K., Shirai, N.
               "Active Suspension for a Terrain Robot."
               Proceedings of the IEEE/RSJ International Workshop on Intelligent Robots and Systems (IROS), pp. 408-413, Tsukuba, Japan, September 1989.

[Thomson62]   Thomson, J. G.
               "Vehicle Design from Field Test Data."
               Proceedings of the 1st International Conference on the Mechanics of Soil-Vehicle Systems, pp. 171-182, Edizoni, Minerva Tecnica, Italy, June 1962.

[Todd85]   Todd, D.
               Walking Machines: An Introduction to Legged Robots.
               Chapman and Hall, New York, NY, 1985.

[Turnage89]   Turnage, G. W., Banks, D. C.
               "Lunar Surface Mobility Studies Past and the Future."
               Miscellaneous Paper Gl-89-26, Geotechnical Laboratory, U. S. Army Engineer Waterways Experiment Station, Vicksburg, Mississippi, 1989.

[VDI87]   Verein Deutcher Ingenieure.
              Systematic Approach to the Design of Technical Systems and Products.
              VDI Guidelines 2221, August 1987.

[Waldron84]   Waldron, K. J., et al.,
              "Configuration Design of the Adaptive Suspension Vehicle."
              The International Journal of Robotics Research, Vol. 3, No. 2, Summer 1984.

[Waldron85a] Waldron, K. J.
              "The Mechanics of Mobile Robots."
              Proceedings of the 1985 IEEE International Conference on Advanced Robotics, pp. 533-544, Tokyo, Japan, September 1985.

[Waldron85b] Waldron, K. J.
              "Mobility and Controllability Characteristics of Mobile Robotic Platforms."
              Proceedings of the 1985 IEEE International Conference on Robotics and Automation, St. Louis, Missouri, March 1985.

[Waldron95]   Waldron, K. J.
              "Terrain Adaptive Vehicles."
              Transactions of the ASME, Journal of Mechanical Design: Special 50th Anniversary Design Issue, Vol. 117, pp. 107-112, June 1995.

[Wallace92]   Wallace, B. E., Thrasher, D. L.
              "A Preliminary Design Tool for Planetary Rover Subsystems."
              1992 AIAA Aerospace Design Conference, AIAA 92-1109, Irvine, CA, February 1992.

[Wallace93]   Wallace, B., Rao, N.
              "Engineering Elements for Transportation on the Lunar Surface."
              Applied Mechanics Review, Vol. 46, No. 6, June 1993.

[Whittaker95] Whittaker, W. L., et al.
              "Design of a Day/Night Lunar Rover."
              Robotics Institute Technical Report CMU-RI-TR-95-24, Carnegie Mellon University, Pittsburgh, PA, 1995.

[Wismer73]   Wismer, R. D., Luth, H. J.
              "Off-Road Traction Prediction for Wheeled Vehicles."
              Journal of Terramechanics, Vol. 10, No. 2, pp. 49-61, 173.

[Wong68]   Wong, R., E.
              "Surface Mobility Systems for Lunar Exploration."
              Transactions of the Society of Automotive Engineers, Vol.?, pp. 1196-1212, 1968.

[Wong93]   Wong, J., Y.
              Theory of Ground Vehicles.
              John Wiley & Sons, Inc., New York, NY, 1993.

[Yoshioka95] Yoshioka, N., Nishio, Y., Wakabayashi, Y.
              "Integrated Test System for a Six-Powered-Wheel Lunar Rover"
              Proceedings of the 1995 IEEE International Conference on Advanced Robotics, pp. 285-291, Summer 1995.

[Young89]   Young, W., C.
              Roark's Formulas for Stress and Strain.
              McGraw Hill, Inc., New York, NY, 1989.

[Yu91]   Yu, J. C., Waldron, K. J.
              "Design of Wheeled Actively Articulated Vehicle."
              Proceedings of the 1991 National Applied Mechanics and Robotics Conference, pp. VIB. 1.1-1.6, Cincinnati, OH, November 1991.

Appendix: Parametric Configuration for Trafficability

This Appendix summarize the results of parametric configuration based on LocSyn's analytical models of trafficability. These analyses quantify the expected performance of four and six-wheel locomotion configurations and should be considered along with those in Section 4.3.

<u>List of Symbols</u>

a	linear acceleration	ft/sec^2
b'	corrected width of loading area	in
b_w or B_w	tire width, wheel/soil contact width	in
c	cohesion of soil	lbf/in^2 (psi)
d_w or D	wheel diameter	in
f_r	coefficient of rolling friction	-
i	drivetrain reduction ratio	-
j	soil deformation	in
k_c	cohesive modulus of soil deformation	lbf/in^{n+1}
k_ϕ	frictional modulus of soil deformation	lbf/in^{n+2}
l_w	length of the loading area	in
l'	corrected length of loading area	in
m	vehicle mass	lbm or lbf.sec^2/ft
n	exponent of sinkage	-
p	ground pressure	lbf/in^2 (psi)
r	wheel radius	in
z	wheel sinkage	in
A	ground contact area	in^2
B_v	total vehicle width	in or ft
H	soil thrust	lbf
DP	drawbar pull	lbf
J	moment of inertia	lbf.ft.sec^2
K	slip coefficient	in
L_v	total vehicle length	in or ft
R_x	motion resistance due to x	lbf
V	traveling speed	m/sec
W_w	wheel loading	lbf
τ	shear stress of soil	lbf/in.^{2} (psi)
θ	slope angle	deg
ϕ	angle of internal friction of soil	deg

The following values of geophysical properties were used as control parameters in the parametric configuration studies.

Property	Lunar Soil	Desert Dry Sand
Exponent of sinkage (n)	1.0	1.1
Cohesive modulus of soil deformation (k_c)	0.20 lb/in^{n+1}	0.10 lb/in^{n+1}
Frictional modulus of soil deformation (k_f)	3.0 lb/in^{n+2}	3.9 lb/in^{n+2}
Cohesion of soil (c)	0.025 psi	0.151 psi
Coefficient of slip (K)	0.7 in	0.4 in (firm), 1.0 in (loose)
Angle of internal friction (f)	40 deg	28 - 38 deg

Table A1: Geophysical properties of the lunar regolith and dry sand [Wallace93][Bekker60/69].

2. Parametric Configuration from Wheel Sinkage / Equation [4]

(1) θ= 30 deg   (a) Ww= 100 lbf
(2) θ= 25 deg   (b) Ww= 200 lbf
(3) θ= 15 deg   (c) Ww= 275 lbf
(4) θ= 0 deg   (d) Ww= 300 lbf
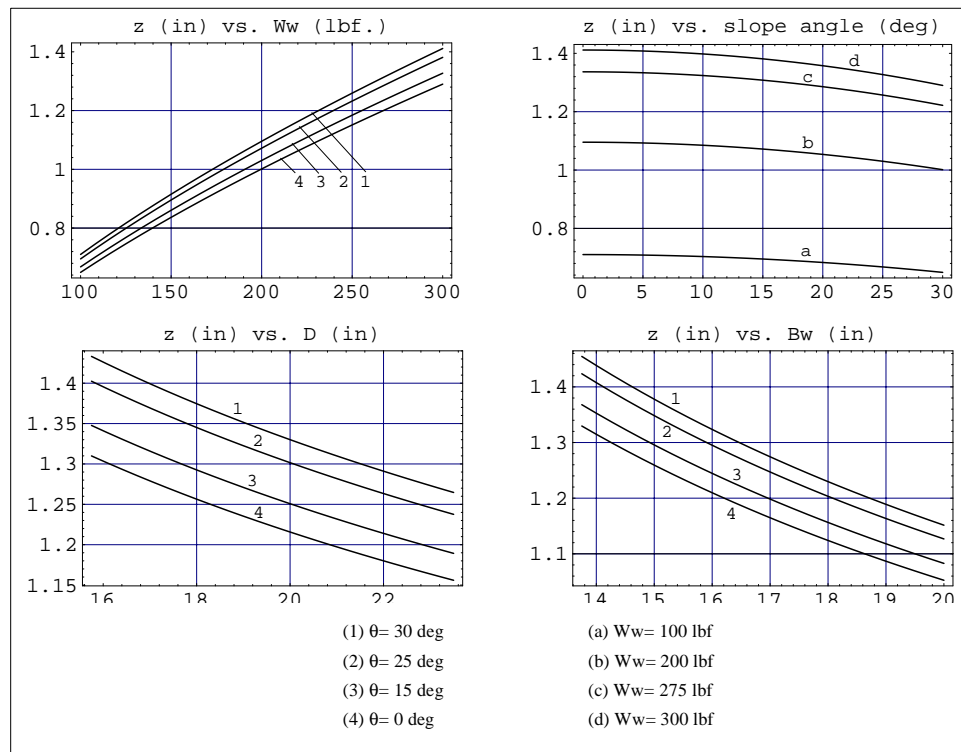
Figure A1: Wheel sinkage z (in) in dry sand as a function of wheel loading W_w (lbf) and the slope angle θ (deg) in the upper row (in both cases D= 20", B_w= 15.75"), and wheel diameter D (in) and tire width B_w (in) in the lower row (in both cases wheel load W_w= 275 lbf).
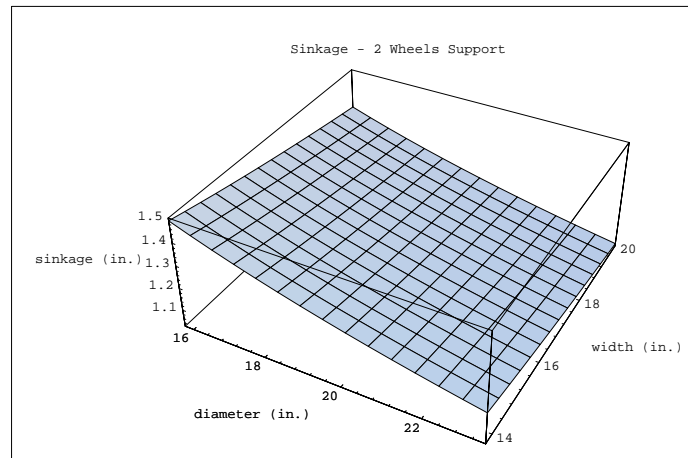
Figure A2: **Wheel sinkage z (in) of a rigid wheel as a function of wheel diameter D (in) and tire width B_w (in) (wheel loading W_w= 275 lbf).**

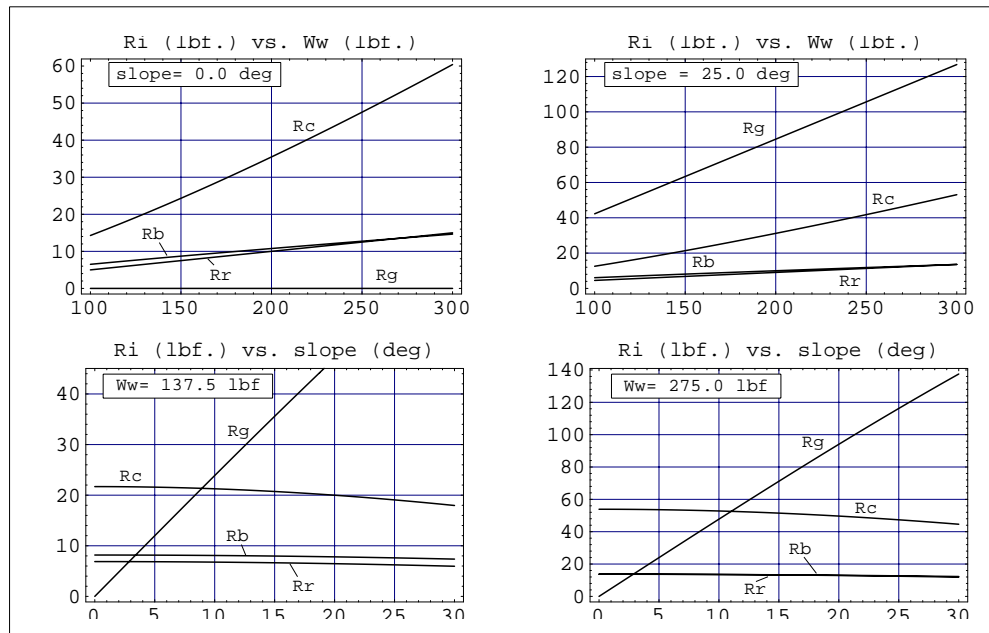## 3. Parametric Configuration from Motion Resistance

2.1 Compaction Resistance / Equation [19]
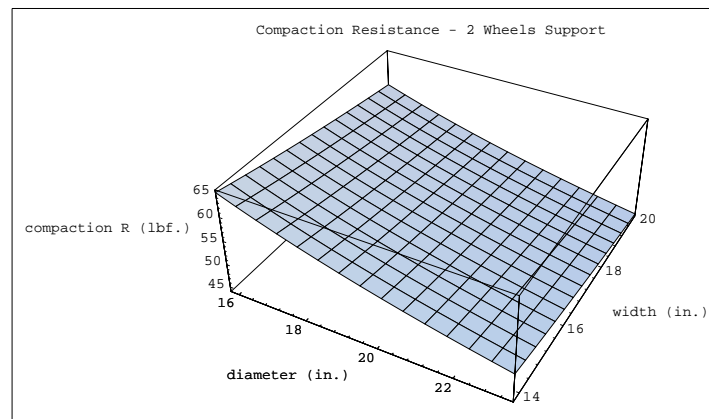
Figure A3: **Compaction resistance R_c of a rigid wheel as a function of wheel diameter D (in) and tire width B_w (in) (wheel loading W_w= 275 lb).**

2.2 Bulldozing Resistance / Equation [20]
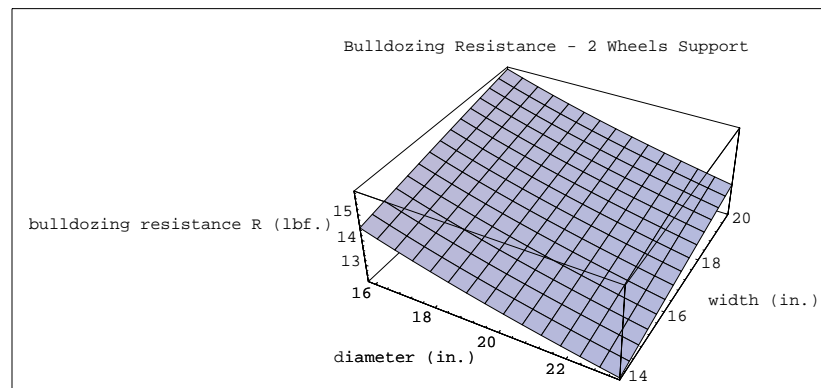
Figure A4: **Bulldozing resistance R_b (lbf) of a rigid wheel as a function of wheel diameter D (in) and tire width B_w (in) (wheel loading W_w= 275 lbf).**

2.3 Rolling Resistance / Equation [21]
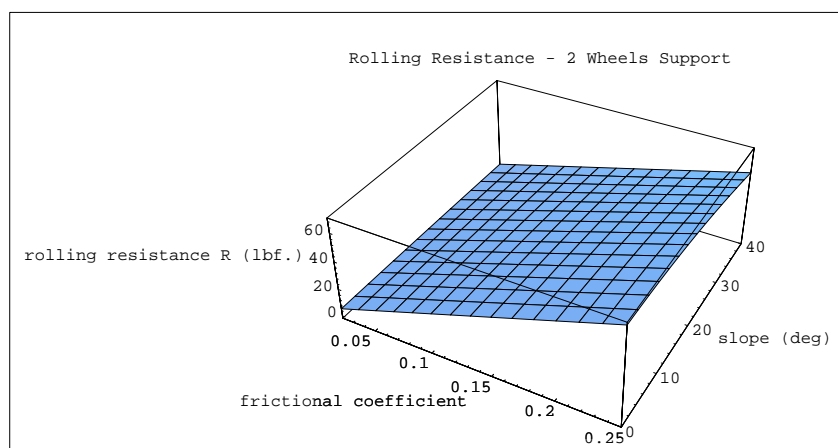
Figure A5: **Rolling resistance as a function of an empirical coefficient of friction f_r and the slope angle θ (deg) (wheel loading W_w= 275 lbf).**

2.4 Gravitational Resistance / Equation [22]
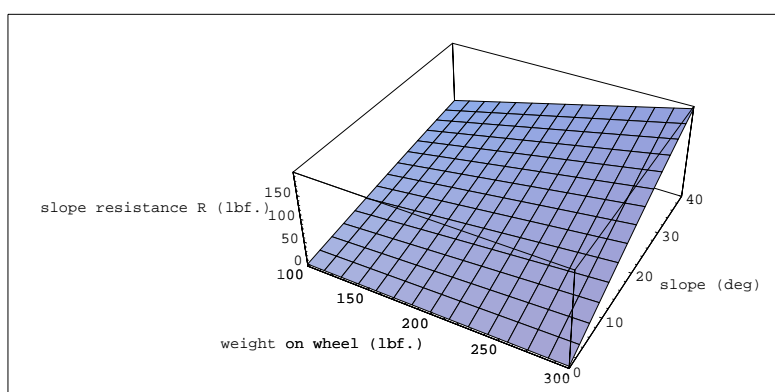
Figure A6: **Resistance due to the gravitational component as a function of wheel loading W_w (lbf) and the slope angle θ (deg).**

2.5 Total Motion Resistance / Equation [34]
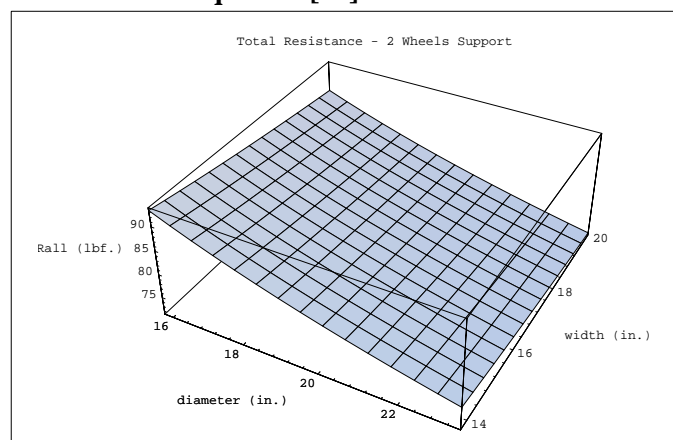
Figure A7: **Total motion resistance Rall (lbf) of a rigid wheel as a function of wheel diameter D (in) and tire width B_w (in) (θ= 0 deg, f_r= 0.05, W_w= 275 lbf).**
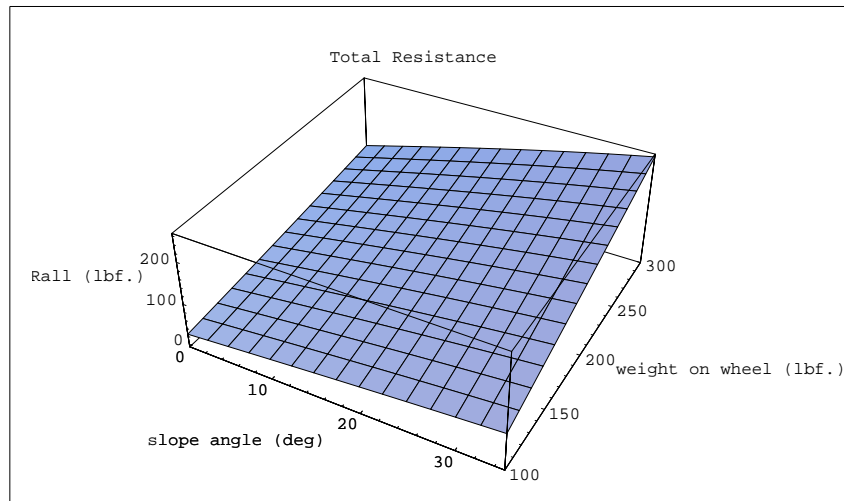
Figure A8: Total resistance R_{all} (lbf) as a function of slope angle θ (deg) and wheel loading W_w (lbf) (D= 20", B_w= 15.75', f_r= 0.05).

Figure A9: Compaction R_c (lbf) / Bulldozing R_b (lbf) / Rolling R_r (lbf) / Gravitational R_g (lbf) resistance as a function of wheel loading W_w (lbf) in the upper row (θ= 0 deg and θ= 25 deg) and slope angle θ (deg) in the lower row (W_w= 137.5 lbf and W_w= 275 lbf). In all cases: D= 20", B_w= 15.75", f_r= 0.05.

4. Parametric Configuration from Drawbar Pull / Equation [35]
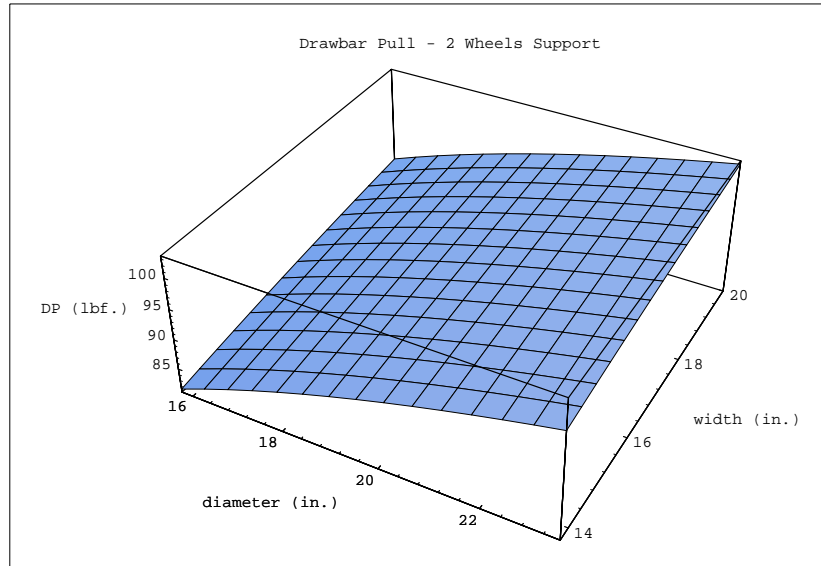
Figure A10: Drawbar pull DP (lbf) developed by a rigid wheel as a function of wheel diameter D (in) and tire width B_w (in) (θ= 0 deg, f_r= 0.05, A= 250 in^2, W_w= 275 lbf).
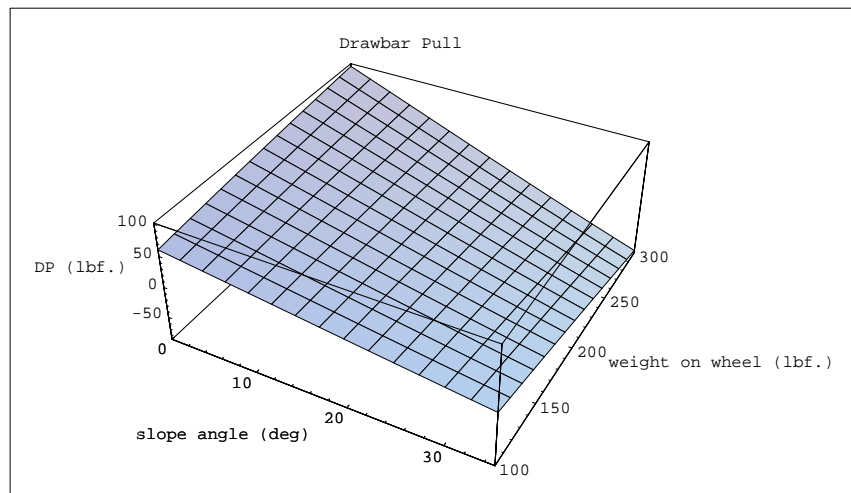
Figure A11: Drawbar pull DP (lbf) as a function of the slope angle θ (deg) and wheel loading W_w (lbf) (D= 20", B_w= 15.75", f_r= 0.05).
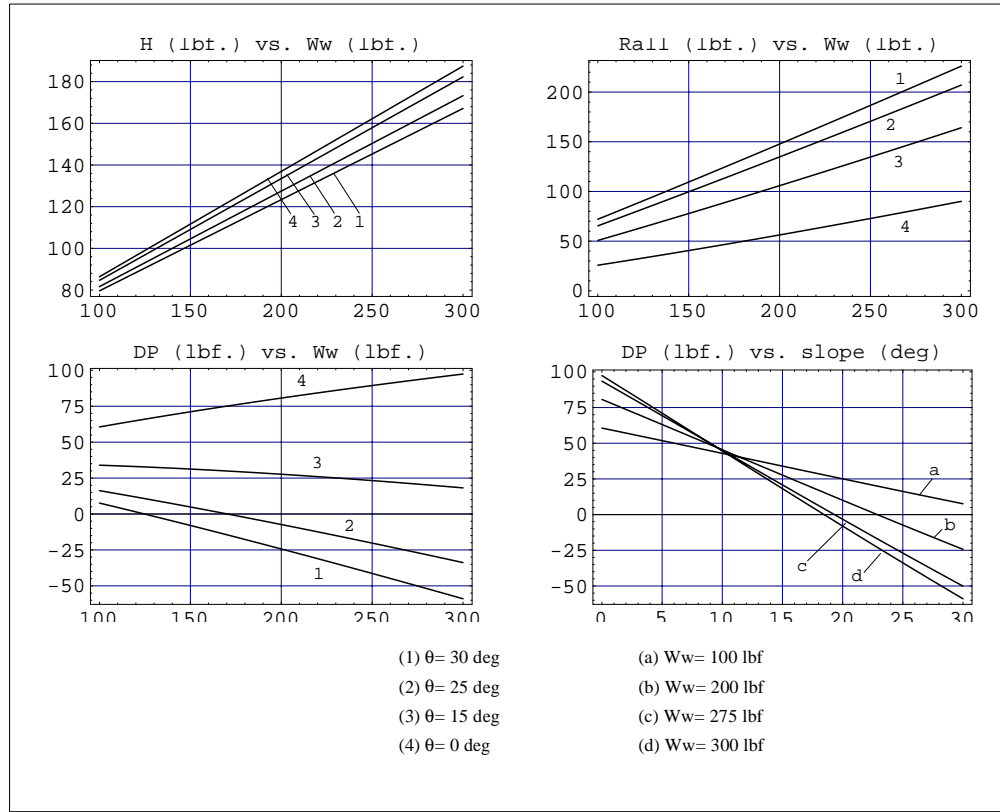
Figure A12: Soil thrust H (lbf) and total motion resistance R_{all} (lbf) as functions of wheel loading W_w (lbf) in the upper row and drawbar pull DP (lbf) as a function of wheel loading W_w (lbf) and the slope angle θ (deg) in the lower row. In all cases: D= 20", B_w= 15.75", f_r= 0.05.

5. Parametric Configuration from Drive Torque
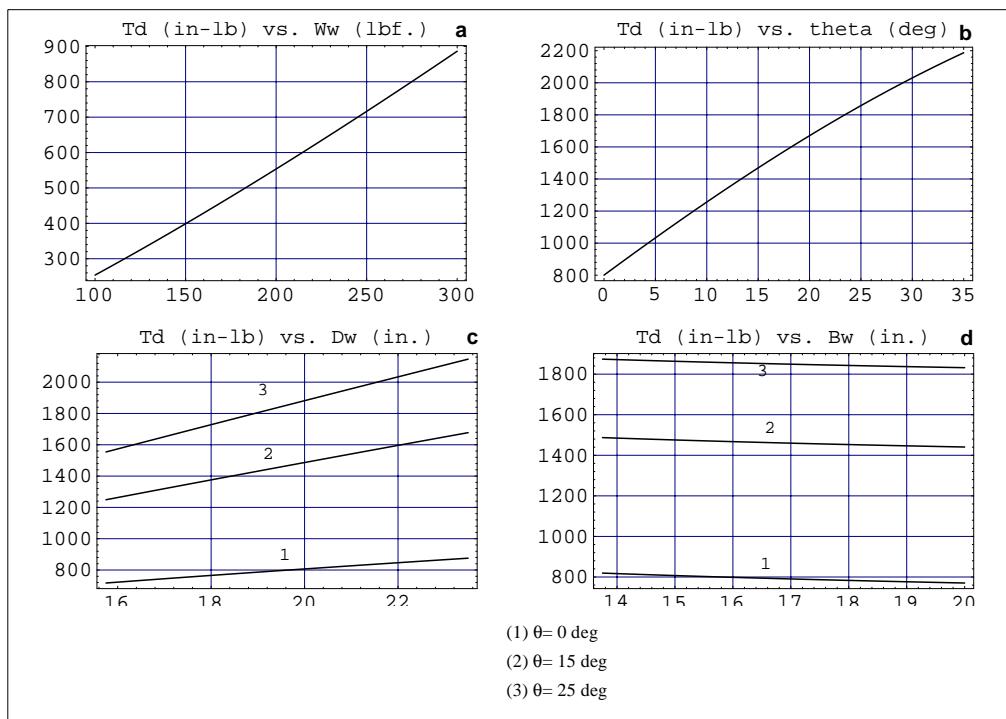
4.1 Torque for Driving on Flat Terrain / Equation [36]
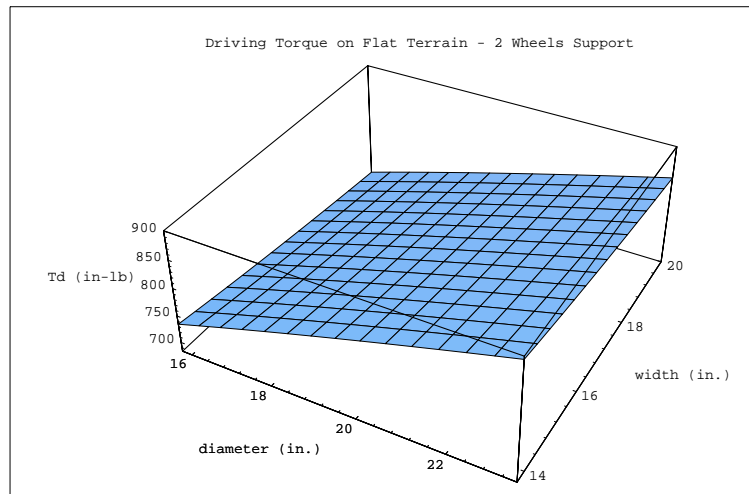
Figure A13: Drive torque T_d (in-lb) as a function of wheel diameter D (in) and tire width B_w (in) (θ= 0 deg, f_r= 0.05, A= 250 in^2, W_w= 275 lbf).

4.2 Torque for Driving on Inclined Terrain / Equation [37]
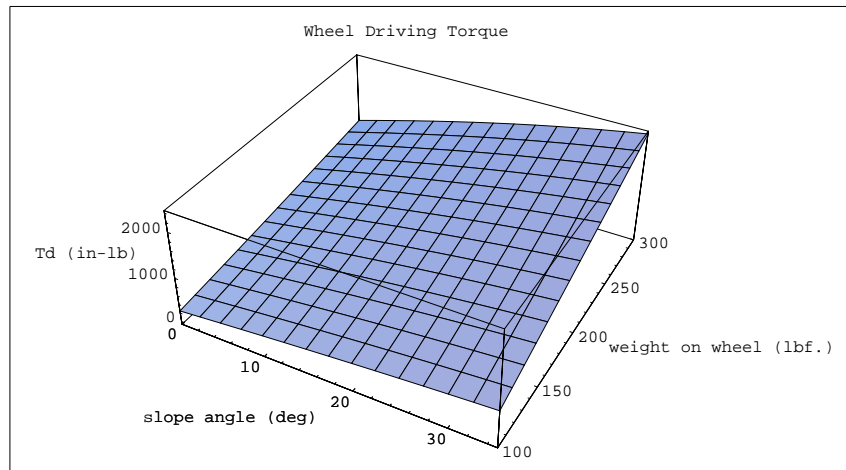
Figure A14: Drive torque T_d (in-lb) as a function of the slope angle θ (deg) and wheel loading W_w (lbf) (D= 20", B_w= 15.75", f_r= 0.05).

Figure A15: Drive torque T_d (in-lb) as a function of: (a) wheel loading Ww (lbf) (θ= 0 deg, D= 20", B_w= 15.75", f_r= 0.05), (b) the slope angle q (deg) (D= 20" (50 cm), B_w= 15.75", f_r= 0.05, W_w= 275 lbf), (c) wheel diameter D (in), and (d) tire width B_w (in).

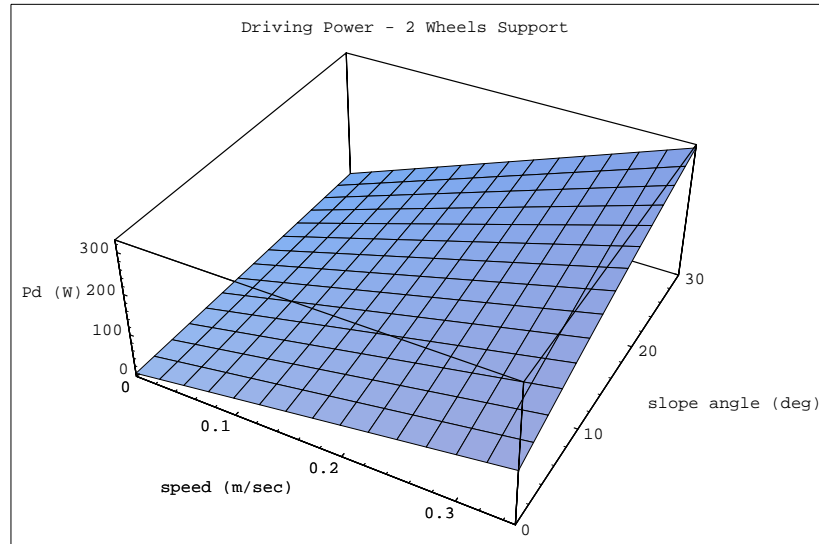## 6. Parametric Configuration from Drive Power / Equation [38]

Figure A16: Output drive power P_d (W) as a function of traveling speed V (m/sec) and the slope angle θ (deg) (D= 20", B_w= 15.75", W_w= 275 lbf, f_r= 0.05).
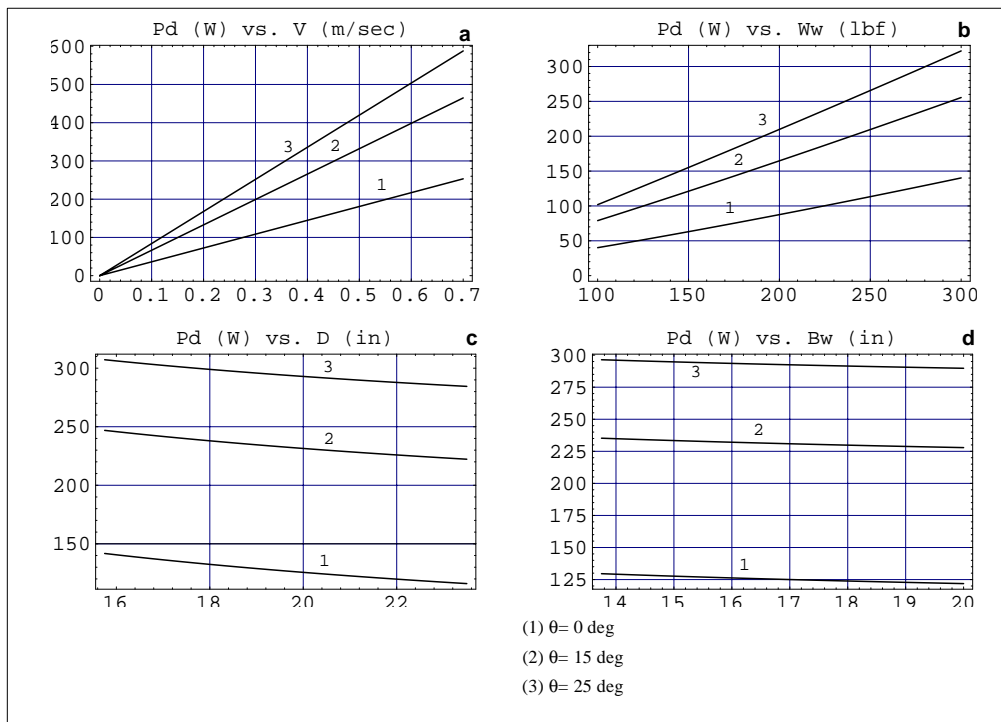

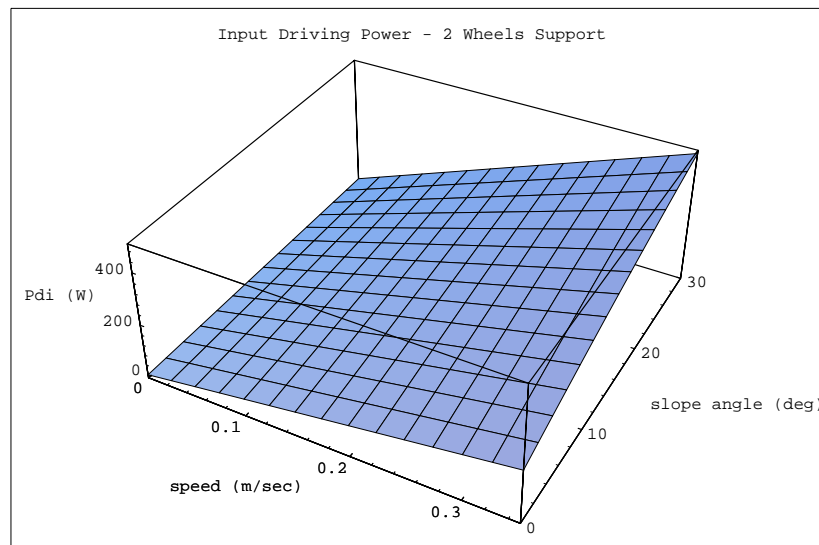**Figure A17:** Output drive power P_d (W) as a function of: (a) traveling speed V (m/sec) (D= 20", B_w= 15.75", f_r= 0.05, W_w= 275 lbf), (b) wheel loading W_w (lbf) (D= 20", B_w= 15.75", f_r= 0.05), (c) wheel diameter D (in), and (d) tire width B_w (in).

Figure A18: **Input drive power P$_{di}$ (W) as a function of traveling speed V (m/sec) and the slope angle θ (deg) (D= 20", B$_w$= 15.75", W$_w$= 275 lbf., f$_r$= 0.05, drivetrain efficiency: 0.85, motor efficiency: 0.80, drive electronics efficiency: 0.90).**